Electronic Supplementary Material (ESI) for RSC Advances.

Fluorescent Phenanthridine-based Calix[4]arene Derivatives: Synthesis, Thermodynamic and Computational studies of their Complexation with Alkali-Metal Cations

ELECTRONIC SUPPLEMENTARY INFORMATION

Marina Tranfić Bakić,[a,b,c] Dijana Jadreško,[c] Tomica Hrenar,[b] Gordan Horvat,[b] Josip Požar,[b] Nives Galić,[b] Vesna Sokol,[d] Renato Tomaš,[d] Sulejman Alihodžić,[e] Mladen Žinić,[f] Leo Frkanec,*[c] and Vladislav Tomišić,*[b]

[a] *Department of Chemistry and Biochemistry, Faculty of Food Technology and Biotechnology. University of Zagreb, Pierottijeva 6, 10000 Zagreb, Croatia*

[b] *Department of Chemistry, Faculty of Science, University of Zagreb, Horvatovac 102a, 10 000 Zagreb, Croatia, Tel: +385 1 4606 136; E-mail: vtomisic@chem.pmf.hr*

[c] *Ruđer Bošković Institute, Bijenička cesta 54, 10000 Zagreb, Croatia; Tel: +385 1 4571 328; E-mail: frkanec@irb.hr*

[d] *Division of Chemistry, Faculty of Chemistry and Technology, University of Split, Teslina 10/V, 21 000 Split, Croatia*

[e] *Fidelta Ltd., Prilaz baruna Filipovića 29, 10 000 Zagreb, Croatia*

[f] *Croatian Academy of Sciences and Arts, Trg Nikole Šubića Zrinskog 11, 10000, Zagreb and Baltazar University of Applied Sciences, Vladimira Novaka 23, 10 290 Zaprešić*

Contents

Synthesis – Analytical data

5,11,17,23-tetra-tert-butyl-25,26,27,28-tetrakis-((phenanthridine-6-yl)methoxy)calix[4]arene (1) and 5,11,17,23-tetra-*tert*-butyl-25,27-bis-((phenanthridine-6-yl)methoxy)-26,28-dihydroxycalix[4]arene (2)

Compound **1**:

R_f (MeOH:CH_2Cl_2 = 10:90) = 0.26.

M_p = (210–212) °C.

Elemental analysis calculated for $C_{100}H_{92}N_4O_4$ (1413.82): % C 84.95, % H 6.56, % N 3.96; %. Found: 85.24 % C, 6.51 % H, 3.94 % N.

HRMS: *m/z* $[M+H]^+$ calcd for: $C_{100}H_{92}N_4O_4$ (1413.7190); found: 1413.7220.

IR (KBr) ν/cm^{-1}: 3067, 2958, 2865, 1615, 1580, 1530, 1478, 1460, 1450, 1392, 1303, 1238, 1195, 1126, 1068, 1037, 995, 947, 870, 820, 759, 727.

^{1}H-NMR ($CDCl_3$) δ/ppm: 0.98 (s, 36H, C–$(CH_3)_3$), 2.49 (d, 4H, J_{AB} = 12.93 Hz, Ar–CH_2–Ar, H_a), 4.09 (d, 4H, J_{AB} = 12.69 Hz, Ar–CH_2–Ar, H_b), 5.41 (s, 8H, F–CH_2), 6.54 (s, 8H, Ar), 7.35 (t, 4H, J = 7.62 Hz, F–H8), 7.55 (m, 4H, F–H2), 7.57 (m, 4H, F–H3), 7.63 (t, 4H, J = 7.69 Hz, F–H9), 8.00 (m, 4H, F–H4), 8.41 (d, 4H, J = 8.18 Hz, F–H7), 8.49 (m, 4H, F–H1), 8.53 (d, 4H, J = 8.24 Hz, F–H10).

^{13}C-NMR ($CDCl_3$, 150 MHz) δ/ppm: 31.40, 31.76, 33.73, 75.59, 121.86, 121.89, 124.08, 124.96, 125.60, 126.74, 127.04, 127.84, 128.36, 130.19, 130.24, 132.74, 133.59, 143.62, 144.20, 153.46, 158.1.

Compound **2**:

R_f (MeOH:CH_2Cl_2 = 5:95) = 0.28.

M_p = (205–207) °C.

Elemental analysis calculated for $C_{72}H_{74}N_2O_4$ (1031.39): % C 83.85, % H 7.32, % N 2.72; Found: 83.67 % C, 7.20 % H, 2.88 % N.

HRMS: *m/z* $[M+H]^+$ calcd for: $C_{72}H_{74}N_2O_4$ (1031.5721); found: 1031.5729.

IR (KBr) ν/cm^{-1}: 3400, 3080, 2960, 2860, 1610, 1590, 1490, 1460, 1390, 1360, 1300, 1200, 1120, 1100, 1010, 980, 870, 820, 756, 750, 730, 720.

^{1}H-NMR ($CDCl_3$) δ/ppm: 0.98 (s, 18H, C–$(CH_3)_3$), 1.23 (s, 18H, C–$(CH_3)_3$), 3.22 (d, 4H, J_{AB} = 13.16 Hz, Ar–CH_2–Ar, H_a), 4.42 (d, 4H, J_{AB} = 13.10 Hz, Ar–CH_2–Ar, H_b), 5.69 (s, 4H, F–CH_2), 6.80 (s, 4H, Ar), 6.97 (s, 4H, Ar), 7.29 (t, 2H, J = 7.51 Hz, F–H9), 7.57 (t, 2H, J = 7.56 Hz, F–H8), 7.61 (m, 4H, F–H2), 7.68 (s, 2H, OH), 8.16 (m, 2H, F–H4), 8.47 (m, 2H, F–H1), 8.51 (d, 2H, J = 8.16 Hz, F–H10).

^{13}C-NMR ($CDCl_3$, 150 MHz) δ/ppm: 30.78, 31.47, 31.96, 33.57, 33.73, 78.10, 121.78, 121.90, 121.20, 124.71, 124.89, 125.60, 126.76, 127.08, 127.43, 127.84, 128.51, 130.22, 130.50, 132.72, 132.75, 141.10, 143.23, 146.70, 150.77, 151.51, 156.08.

5,11,17,23-tetra-*tert*-butyl-25,27-bis-((phenanthridine-6-yl)methoxy)-26,28-dimethoxycalix[4]arene (3)

Compound **3**:

R_f (MeOH:CH_2Cl_2 = 5:95) = 0.50.

M_p = (223–225) °C.

Elemental analysis calculated for $C_{74}H_{78}N_2O_4$ (1059.42): % C 83.89, % H 7.42, % N 2.64; Found: 83.67 % C, 7.20 % H, 2.88 % N.

HRMS: m/z $[M+H]^+$ calcd for $C_{74}H_{78}N_2O_4$ (1059.6034); found: 1059.6012.

IR (KBr) ν/cm^{-1}: 3067, 2958, 2866, 1614, 1585, 1480, 1462, 1392, 1361, 1304, 1193, 1121, 1100, 1016, 980, 870, 820, 760, 730, 724.

^{1}H-NMR ($CDCl_3$) δ/ppm: 0.39, 0.80, 1.05, 1.30 (4s, 36H, C–$(CH_3)_3$), 2.91, 3.30, 3.39 (3s, 6H, OCH_3), 3.03, 3.61, 3.85, 4.01, 4.29 (5d, 8H, Ar-CH_2-Ar, H_a, H_b), 5.34, 5.43 (2s, 4H, 4H, F-CH_2), 6.41, 6.76, 6.90, 6.99, 7.04 (5s, 8H, Ar), 7.48, 7.70, 7.79, 8.13, 8.37, 8.60 (6m, 16H, F-H).

^{13}C-NMR ($CDCl_3$) δ/ppm: 30.57, 31.08, 31.35, 31.68, 31.51, 33.60, 34.08, 34.11, 37.61, 37.63, 57.83, 60.17, 76.61, 77.03, 121.93, 122.13, 124.38, 124.65, 125.23, 126.33, 126.99, 127.16, 127.33, 128.59, 130.43, 131.77, 132.03, 132.87, 133.03, 133.10, 133.25, 135.93, 143.66, 143.71, 144.12, 144.36, 144.53, 145.11, 154.79, 154.83, 157.31.

NMR data

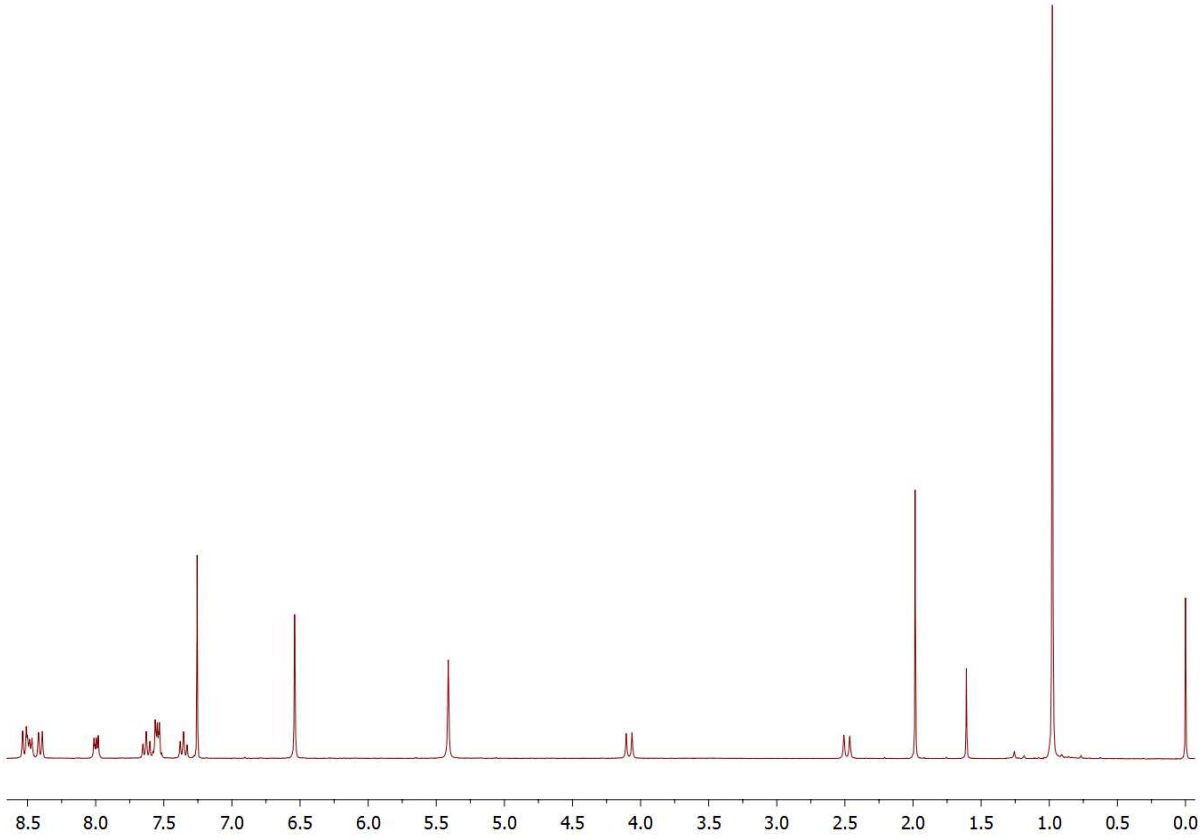

Figure S1. ^{1}H NMR spectrum of compound **1** in $CDCl_3$.

COSY and NOESY spectra were recorded to enable complete assignment of the compound **1** signals. The most important information for the assignment of the chemical shifts was provided by NOE interactions. More exactly, for unambiguous assignment of phenanthridine protons the NOE interaction between methylene group (position 6) and phenanthridine proton at position 7 is the most important. The other signals are then relatively easy assigned using COSY spectrum.

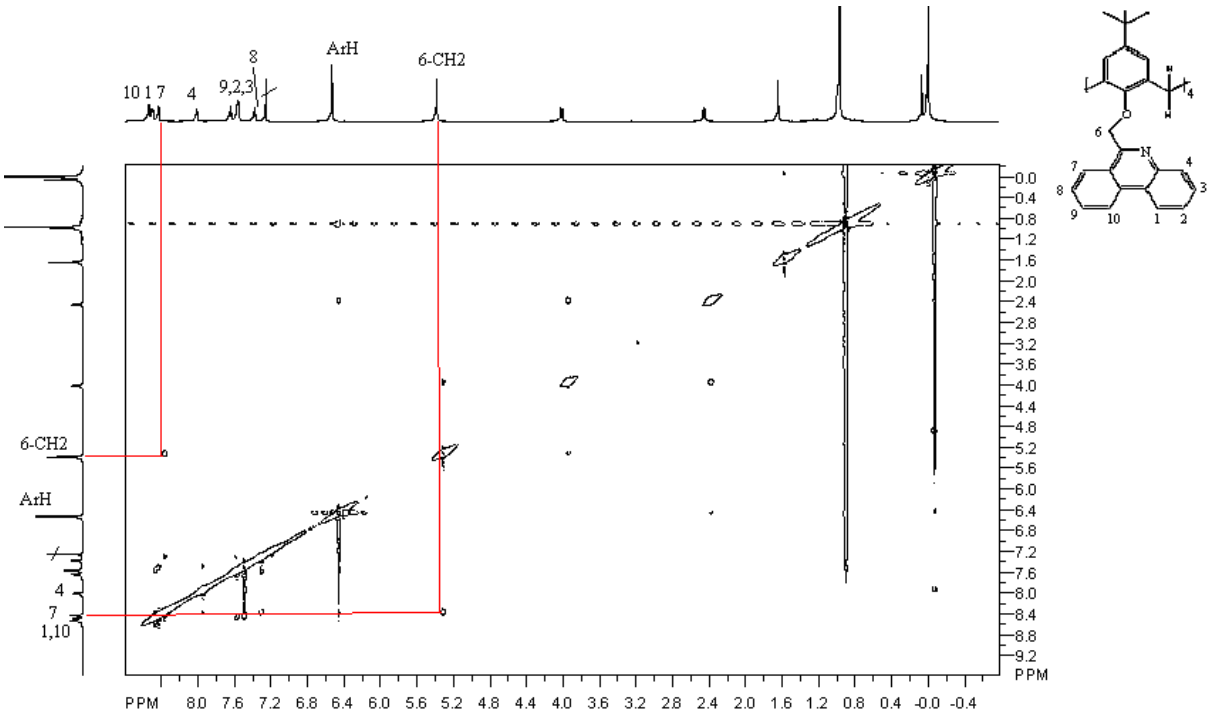

Figure S2. NOESY (600 MHz) of compound **1** in $CDCl_3$.

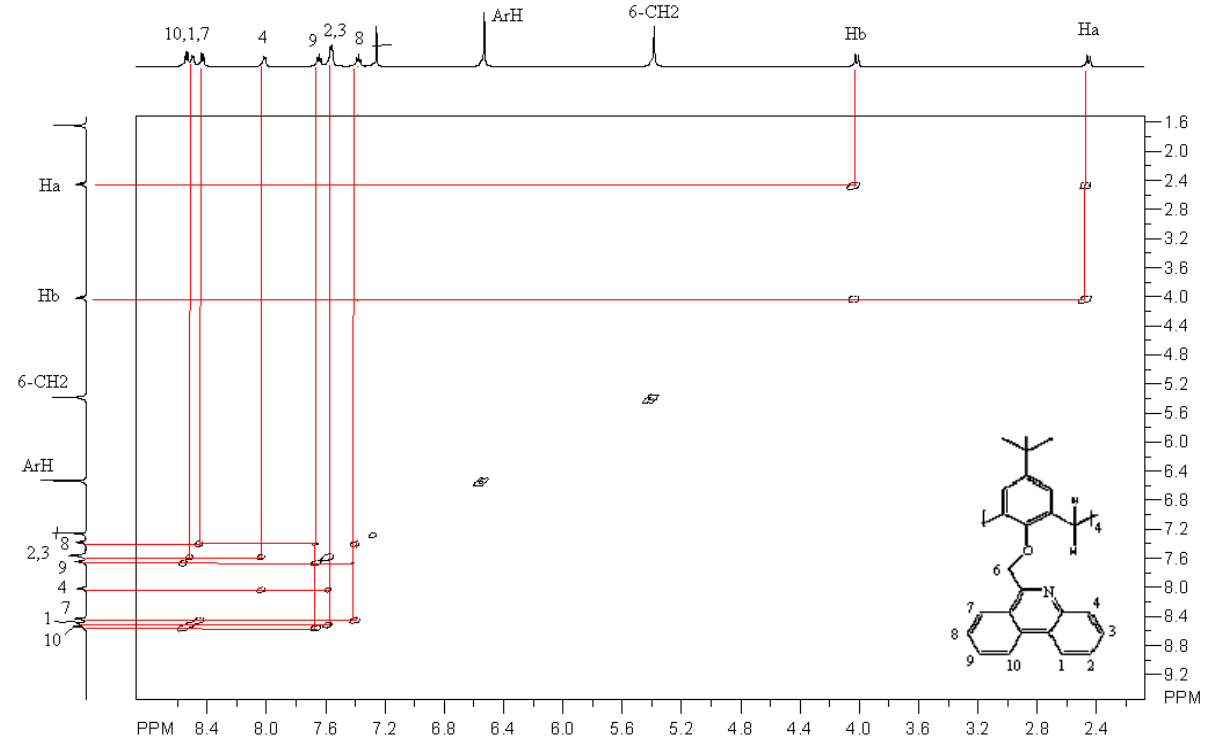

Figure S3. COSY (600 MHz) of compound **1** in $CDCl_3$.

Table S1. Assignment of ^{1}H NMR spectrum of compound **1** in $CDCl_3$.

Group	δ / ppm	$J_{a,b}$ / Hz
s, 36H, $C(CH_3)_3$	0.98	
d, 4H, Ar-CH_2-Ar, H_a	2.49	12.93
d, 4H, Ar-CH_2-Ar, H_b	4.09	12.69
s, 8H, F-CH_2	5.41	
s, 8H, Ar	6.54	
t, 4H, F-H8	7.35	7.62
m, 4H, F-H2	7.55	
m, 4H, F-H3	7.57	
t, 4H, F-H9	7.63	7.69
m, 4H, F-H4	8.00	
d, 4H, F-H7	8.41	8.18
m, 4H, F-H1	8.49	
d, 4H, F-H10	8.53	8.24

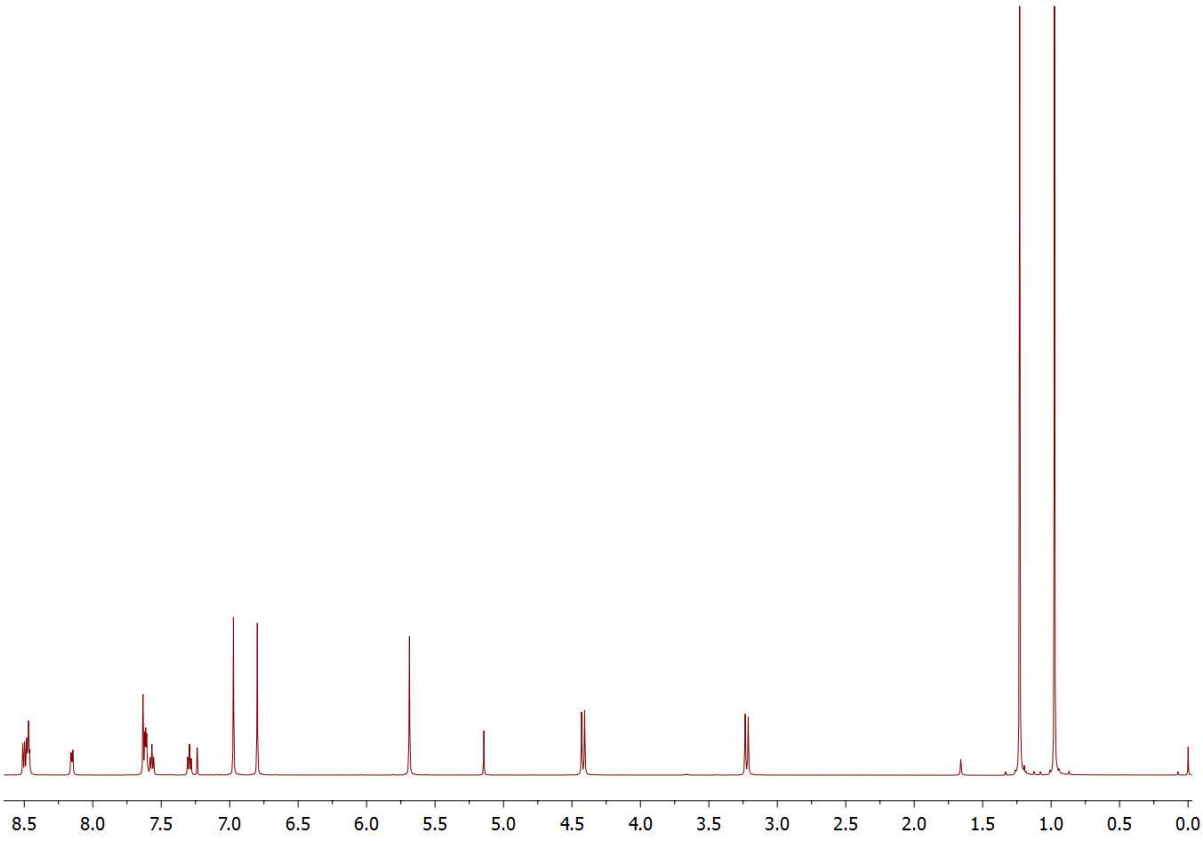

Figure S4. ^{1}H NMR spectrum of compound **2** in $CDCl_3$.

Table S2. Assignment of ^{1}H NMR spectrum of compound **2** in $CDCl_3$.

Group	δ / ppm	$J_{a,b}$ / Hz
2s, 18H, $C(CH_3)_3$	0.98, 1.23	
d, 4H, Ar-CH_2-Ar, H_a	3.22	13.16
d, 4H, Ar-CH_2-Ar, H_b	4.42	13.10
s, 4H, F-CH_2	5.69	
s, 4H, Ar	6.80	
s, 4H, Ar	6.97	
t, 2H, F-H9	7.29	7.51
t, 2H, F-H8	7.57	7.56
m, 4H, F-H2, F-H3	7.61	
s, 2H, OH	7.63	
m, 2H, F-H4	8.16	
m, 4H, F-H1, F-H7	8.47	
d, 2H, F-H10	8.51	8.16

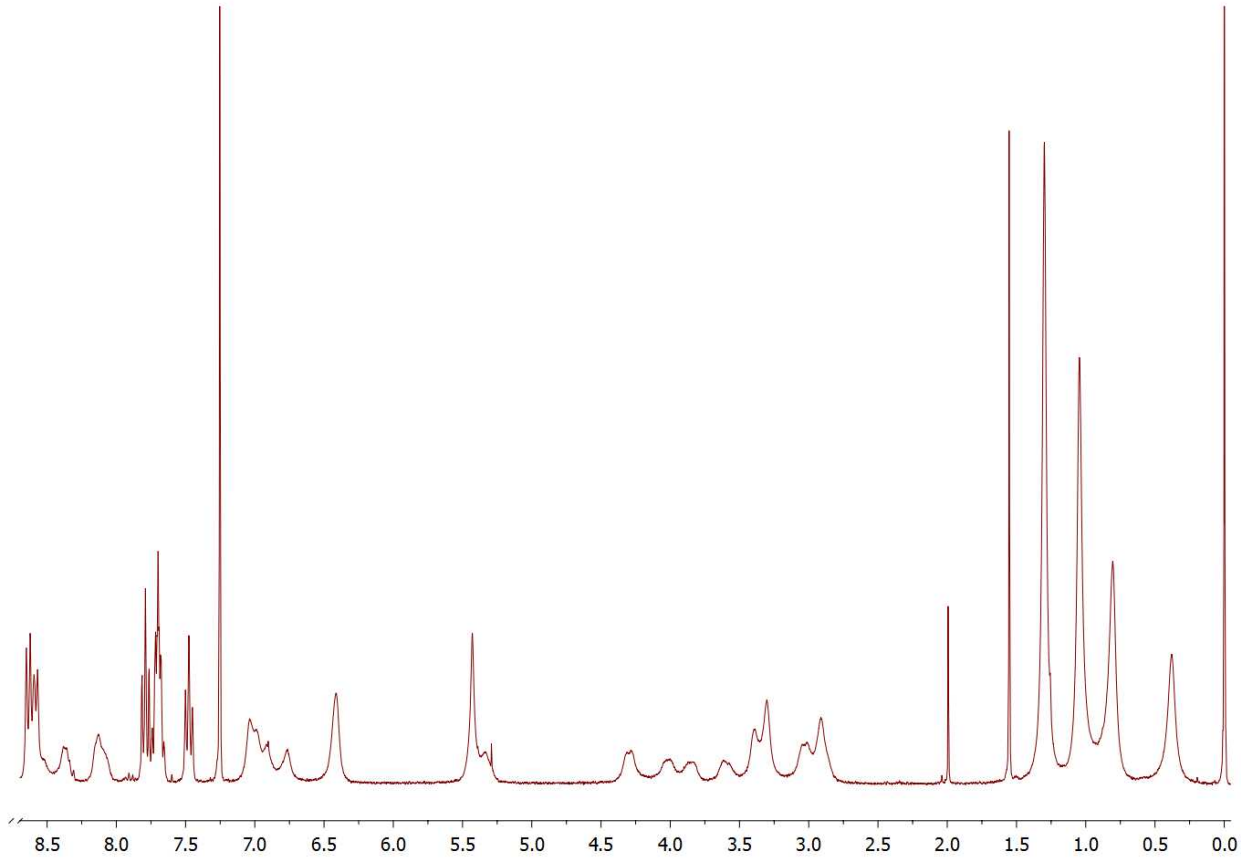

Figure S5. ^{1}H NMR spectrum of compound **3** in $CDCl_3$.

Table S3. Assignment of ^{1}H NMR spectrum of compound **3** in $CDCl_3$.

Group	δ / ppm
4s, 36H, $C(CH_3)_3$	0.38, 0.80, 1.05,1.30
3s, 6H, OCH_3	2.91, 3.30, 3.39
5d, 8H, Ar-CH_2-Ar, H_a, H_b	3.03, 3.61, 3.85, 4.01, 4.29
2s, 4H, F-CH_2	5.34, 5.43
5s, 8H, Ar	6.41, 6.76, 6.90, 6.99, 7.04
6m, 16H, F-H	7.48, 7.70, 7.79, 8.13, 8.37, 8.60

[Na1$^+$]SCN$^-$ (Na$^+$[5,11,17,23-tetra-*tert*-butyl-25,26,27,28-tetrakis-((phenanthridine-6-yl)methoxy)calix[4]arene]SCN$^-$)

^{1}H NMR ($CDCl_3$, 300 MHz, δ/ppm): 1.11 (s, 36H), 2.28 (d, 2H), 4.19 (d, 2H), 5.68 (s, 8H), 6.94 (t, 4H), 6.94 (d, 4H), 7.46 (t, 4H), 7.46 (d, 4H), 7.88 (t, 4H), 7.88 (t, 4H), 8.53 (d, 4H), 8.70 (d, 4H).

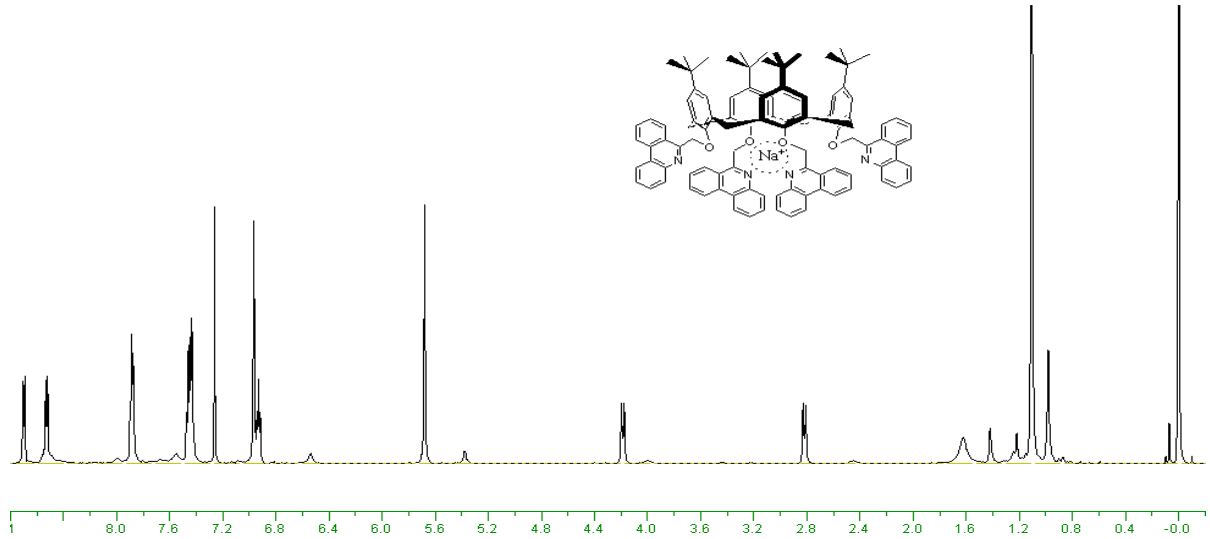

Figure S6. ^{1}H NMR (300 MHz) of compound [Na**1**$^+$]SCN$^-$ in $CDCl_3$.

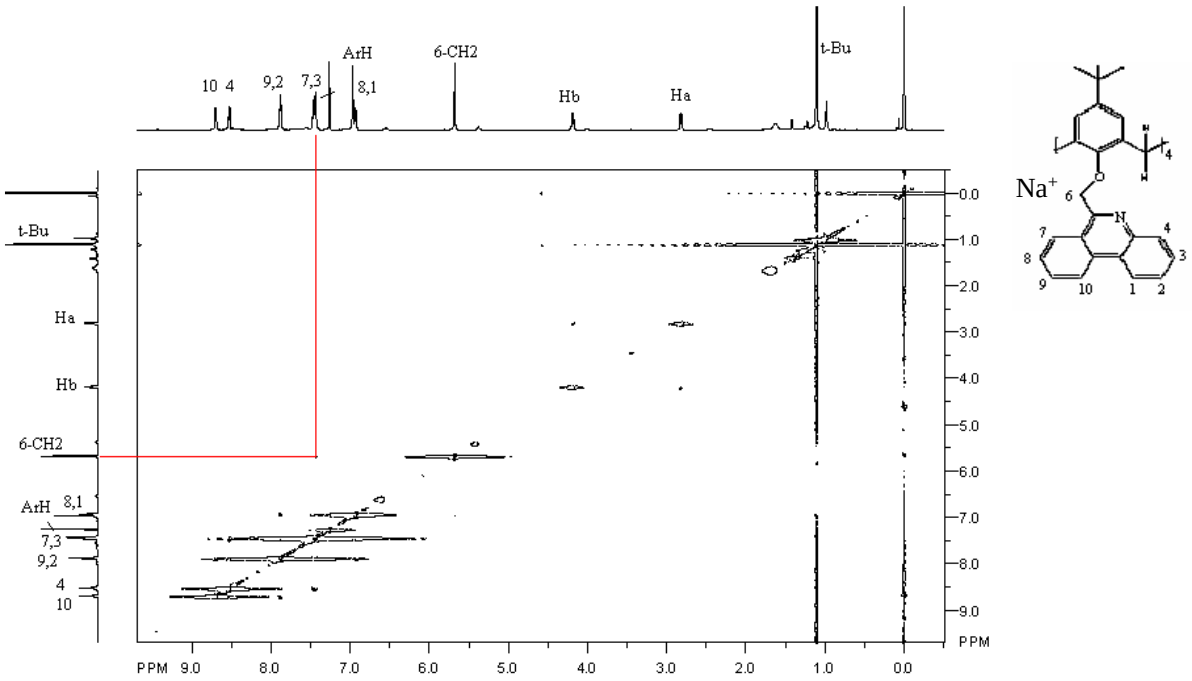

Figure S7. NOESY (600 MHz) of compound [Na**1**$^{+}$]SCN^{-} in $CDCl_3$.

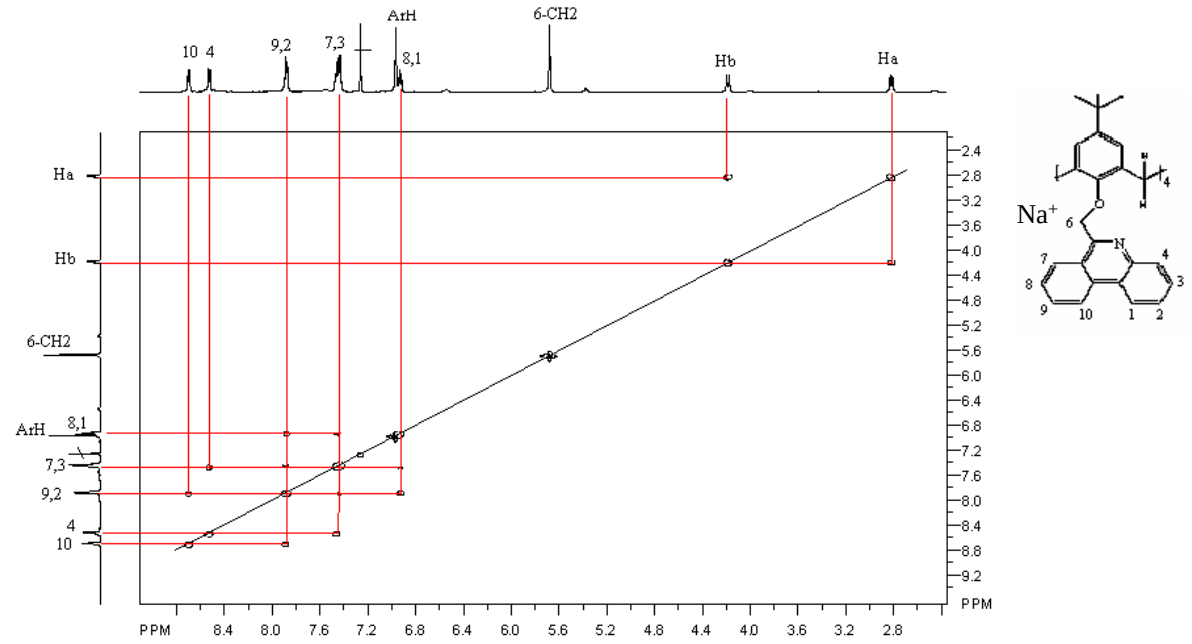

Figure S8. COSY (600 MHz) of compound [Na**1**$^{+}$]SCN^{-} in $CDCl_3$.

Table S4. Assignment of ^{1}H NMR spectrum of compound [Na**1**$^{+}$]SCN^{-} in $CDCl_3$.

Group	δ / ppm	$J_{a,b}$ / Hz
s, 36H, $C(CH_3)_3$	1.11	
d, 2H, Ar-CH_2-Ar, H_a	2.82	12.27
d, 2H, Ar-CH_2-Ar, H_b	4.19	12.24
s, 8H, F-CH_2	5.68	
t, 4H, F-H8	6.94	
d, 4H, F-H1	6.94	
s, 8H, Ar	6.97	
t, 4H, F-H3	7.46	
d, 4H, F-H7	7.46	
t, 4H, F-H2	7.88	
t, 4H, F-H9	7.88	
d, 4H, F-H4	8.53	
d, 4H, F-H10	8.70	

[K1$^+$]SCN$^-$ (K$^+$[5,11,17,23-tetra-*tert*-butyl-25,26,27,28-tetrakis-((phenanthridine-6-yl)methoxy)calix[4]arene]SCN$^-$)

^{1}H NMR ($CDCl_3$, 300 MHz, δ/ppm): 1.11 (s, 36H), 2.78 (d, 2H), 3.87 (d, 2H), 5.49 (s, 8H), 6.86 (t, 4H), 6.94 (s, 8H), 7.18 (d, 4H), 7.38 (t, 4H), 7.46 (t, 4H), 7.90 (t, 4H), 8.07 (d, 4H), 8.62 (d, 4H), 8.74 (d, 4H).

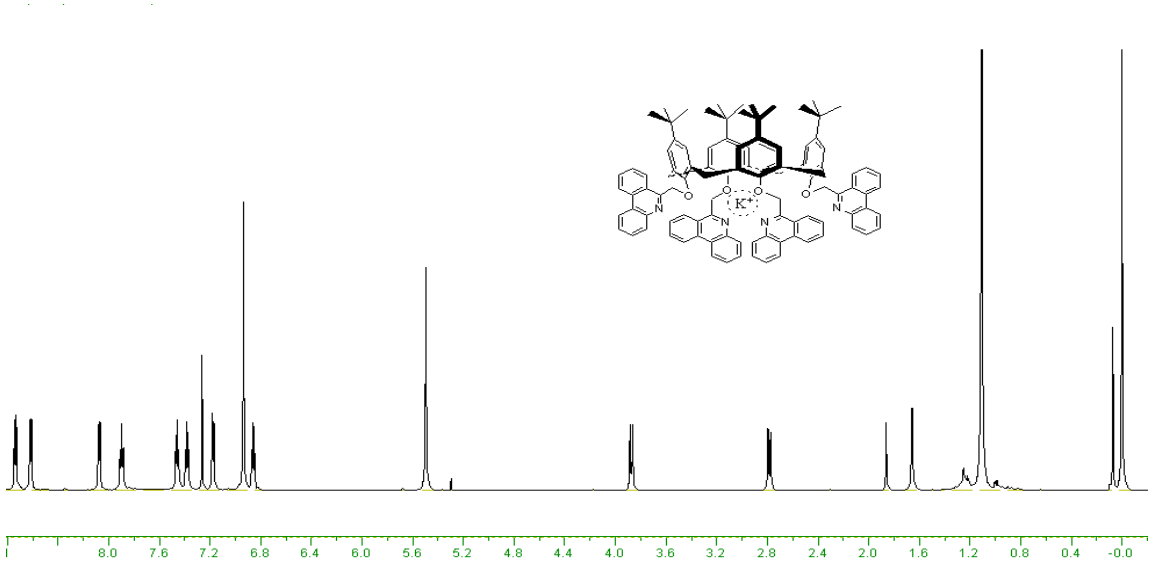

Figure S9. ^{1}H NMR (300 MHz) of compound [K**1**$^+$]SCN$^-$ in $CDCl_3$.

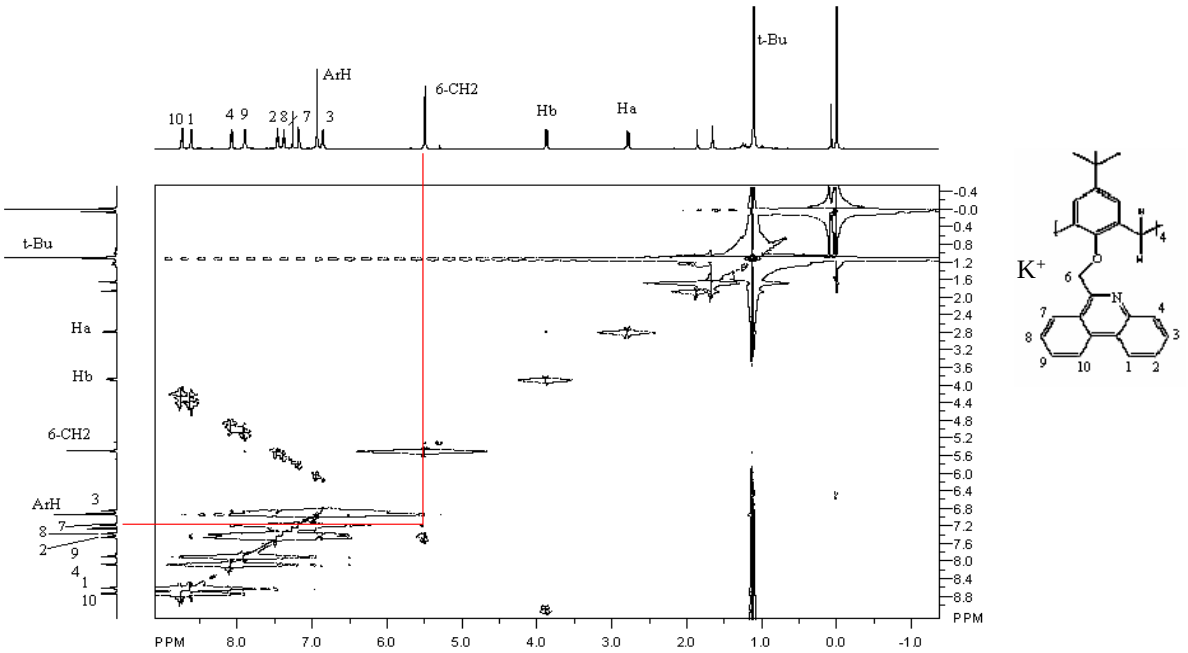

Figure S10. NOESY (600 MHz) of compound [K**1**$^{+}$]SCN^{-} in $CDCl_3$.

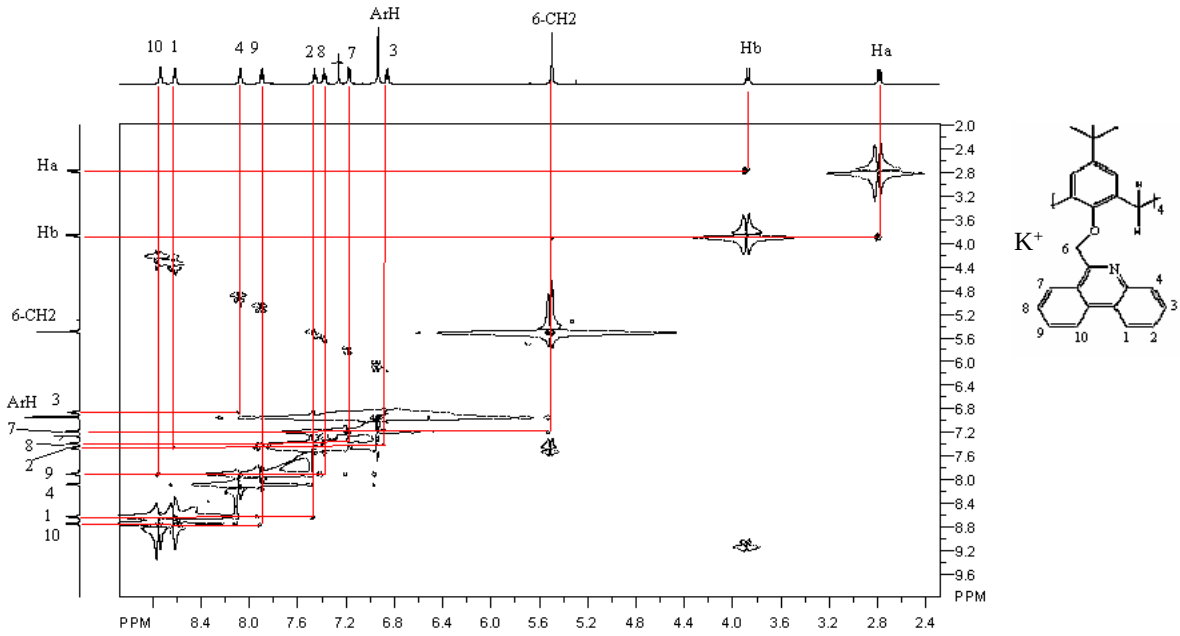

Figure S11. COSY (600 MHz) of compound [K**1**$^{+}$]SCN^{-} in $CDCl_3$.

Table S5. Assignment of ^{1}H NMR spectrum of compound [K**1**$^{+}$]SCN^{-} in $CDCl_3$.

Group	δ / ppm	$J_{a,b}$ / Hz
s, 36H, $C(CH_3)_3$	1.11	
d, 2H, Ar-CH_2-Ar, H_a	2.78	12.42
d, 2H, Ar-CH_2-Ar, H_b	3.87	12.48
s, 8H, F-CH_2	5.49	
t, 4H, F-H3	6.86	
s, 8H, Ar	6.94	
d, 4H, F-H7	7.18	
t, 4H, F-H8	7.38	
t, 4H, F-H2	7.46	
t, 4H, F-H9	7.90	
d, 4H, F-H4	8.07	
d, 4H, F-H1	8.62	
d, 4H, F-H10	8.74	

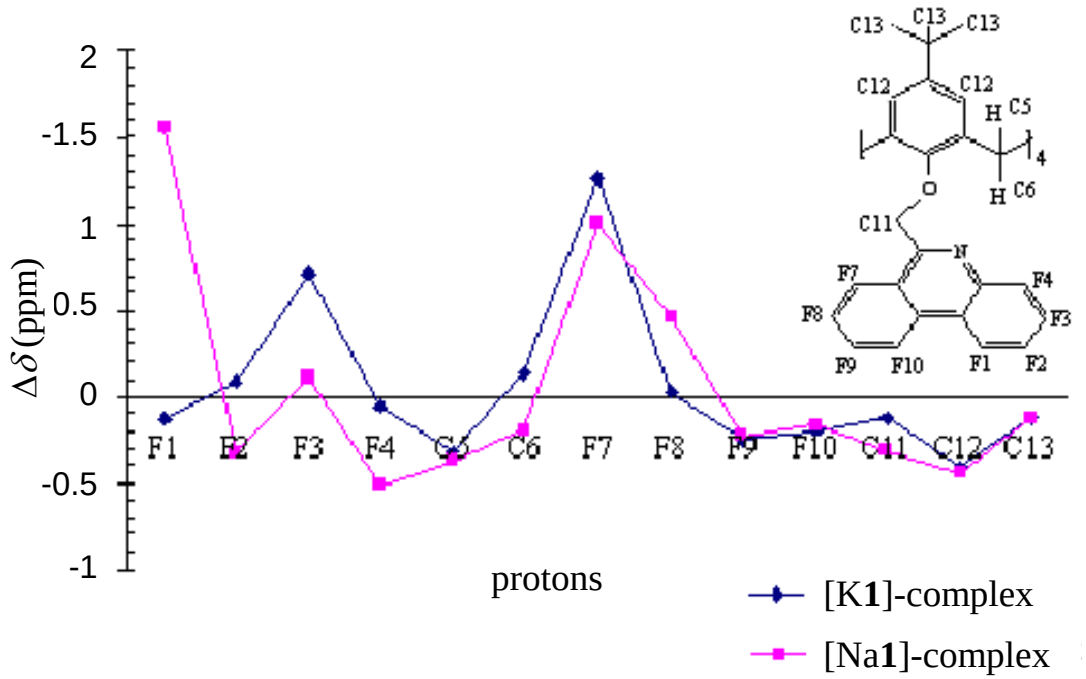

Figure S12. Shift changes of all protons of compound **1** as a result of complexation of Na^+ and K^+ ions, obtained by equation: $\Delta\delta = \delta_{Hi\mathbf{1}} - \delta_{HiM\mathbf{1}^+}$.

Table S6. Complexation-induced shifts of calixarene protons of metal-ion complex $[Na(K)\mathbf{1}^+]SCN^-$, obtained by equation: $\Delta\delta = \delta_{Hi\mathbf{1}} - \delta_{HiM\mathbf{1}^+}$.

Group	**1** δ/ppm	$[Na\mathbf{1}^+]SCN^-$ δ/ppm	$[K\mathbf{1}^+]SCN^-$ δ/ppm	$\Delta\delta_{(Hi\mathbf{1}-Hi\mathbf{1}Na^+)}$ /ppm	$\Delta\delta_{(Hi\mathbf{1}-Hi\mathbf{1}K^+)}$ /ppm
$C(CH_3)_3$	0.99	1.11	1.11	–0.12	–0.12
Ar-CH_2-Ar H_a	2.45	2.82	2.78	–0.37	–0.33
Ar-CH_2-Ar H_b	4.00	4.19	3.87	–0.19	0.13
F-CH_2-O-	5.37	5.68	5.49	–0.31	–0.12
Ar	6.53	6.97	6.94	–0.44	–0.41

Conductometric Measurements

Table S7. The density, viscosity and permittivity values of binary solvent mixtures $MeCN/CH_2Cl_2$ (φ = 0.5) and $MeOH/CH_2Cl_2$ (φ = 0.5) at 25.0 °C.

	$MeCN/CH_2Cl_2$	$MeOH/CH_2Cl_2$
ρ / g cm^{-3}	1.0505	1.0600
η / mPa s	0.356	0.506
ε_r	24.6	23.2

Table S8. Limiting molar conductivities (Λ_0) and ion-association constants (K_A) obtained by the LWPT model for alkali-metal salts in $MeCN/CH_2Cl_2$ and $MeOH/CH_2Cl_2$ solvent mixtures (φ = 0.5) at (25.0 ± 0.1) °C. Uncertainties are given in parentheses as standard deviations.

Salt	$MeCN/CH_2Cl_2$		$MeOH/CH_2Cl_2$	
	$\frac{\Lambda_0}{\text{S cm}^2\ \text{mol}^{-1}}$	K_A	$\frac{\Lambda_0}{\text{S cm}^2\ \text{mol}^{-1}}$	K_A
$LiClO_4$	140.71(7)	110.6(5)	96.88(7)	51.1(9)
$NaClO_4$	139.09(8)	123.6(6)	103.5(1)	93(2)
KCl	– [a]	– [a]	91.72(8)	195(3)
$RbNO_3$	– [a]	– [a]	99.5(2)	390(5)
RbCl	– [a]	– [a]	94.7(1)	251(2)

[a] not determined because of the low salt solubility

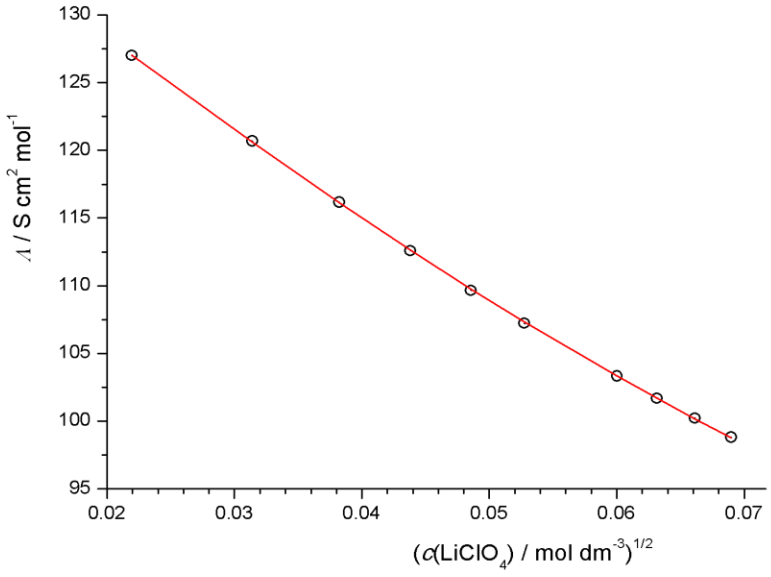

Figure S13. Dependence of molar conductivity of $LiClO_4$ in $MeCN/CH_2Cl_2$ mixture (φ = 0.5) on its concentration at (25.0 ± 0.1) °C. ○ experimental; – calculated.

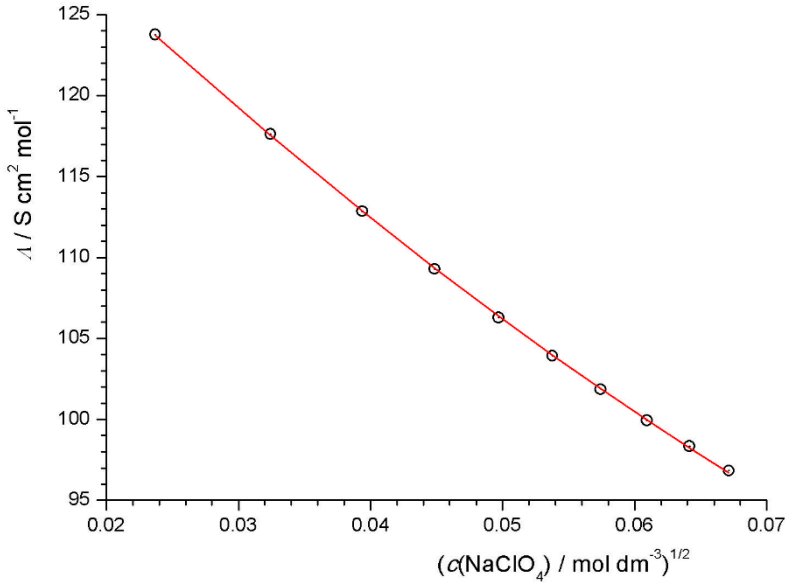

Figure S14. Dependence of molar conductivity of $NaClO_4$ on its concentration in $MeCN/CH_2Cl_2$ mixture (φ = 0.5) at (25.0 ± 0.1) °C. ○ experimental; – calculated.

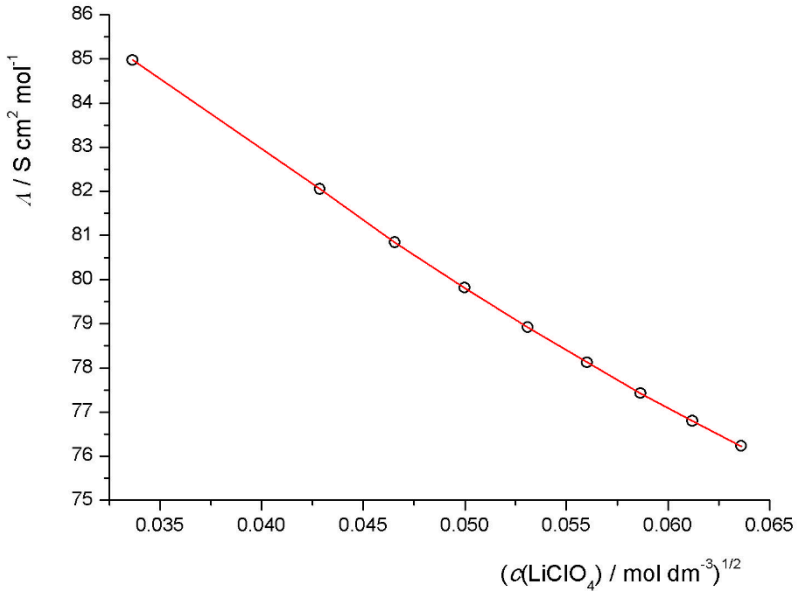

Figure S15. Dependence of molar conductivity of $LiClO_4$ on its concentration in $MeOH/CH_2Cl_2$ mixture (φ = 0.5) at (25.0 ± 0.1) °C. ○ experimental; – calculated.

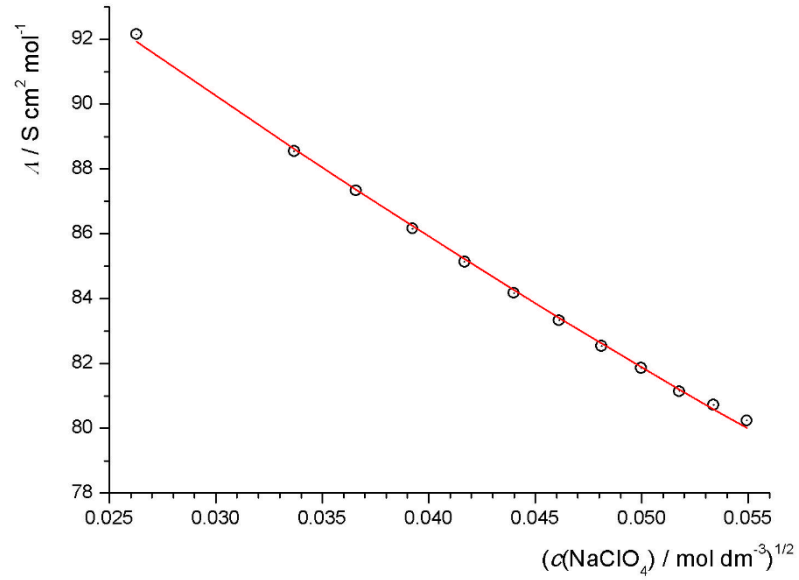

Figure S16. Dependence of molar conductivity of $NaClO_4$ on its concentration in $MeOH/CH_2Cl_2$ mixture (φ = 0.5) at (25.0 ± 0.1) °C. ○ experimental; – calculated.

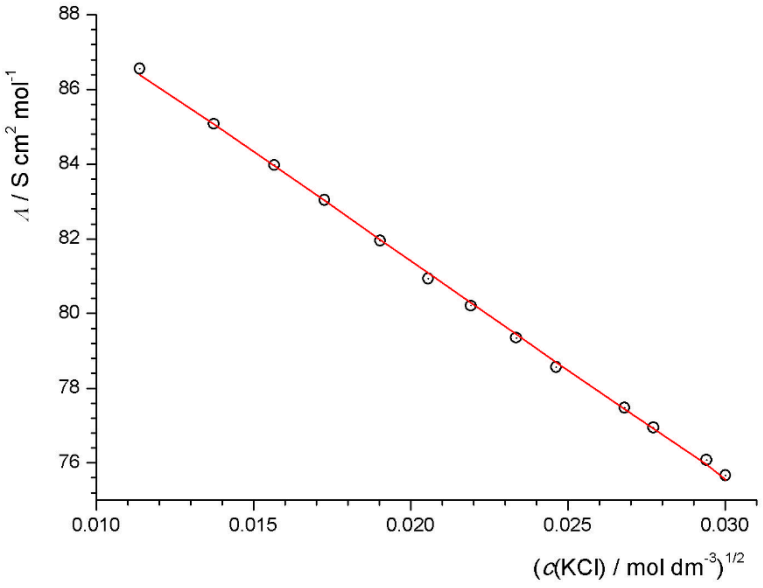

Figure S17. Dependence of molar conductivity of KCl on its concentration in MeOH/CH_2Cl_2 mixture (φ = 0.5) at (25.0 ± 0.1) °C. ○ experimental; – calculated.

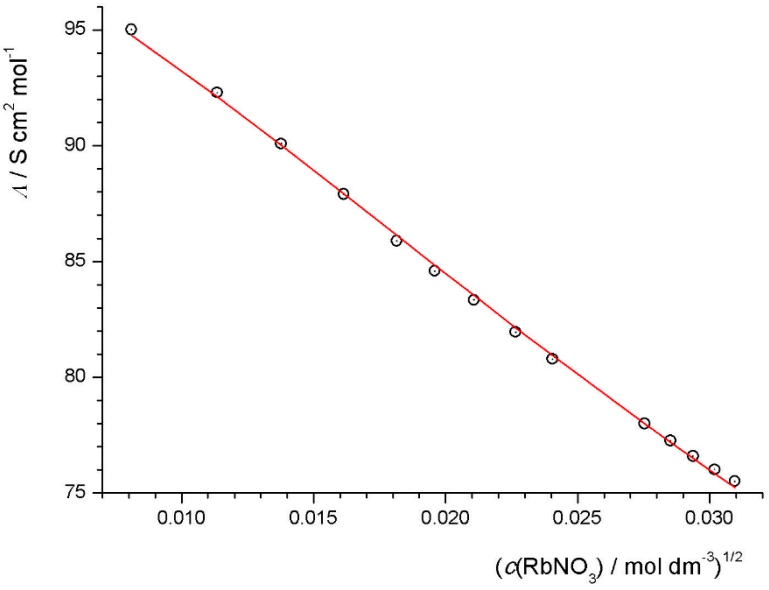

Figure S18. Dependence of molar conductivity of $RbNO_3$ on its concentration in MeOH/CH_2Cl_2 mixture (φ = 0.5) at (25.0 ± 0.1) °C. ○ experimental; – calculated.

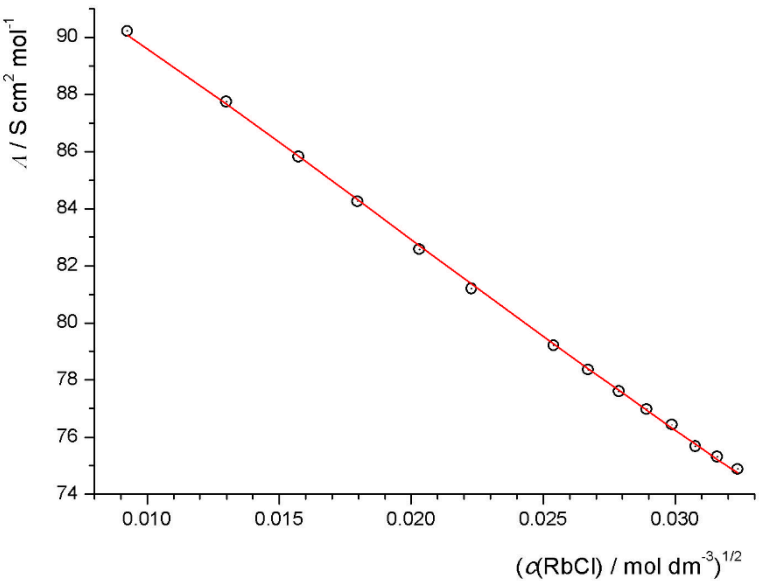

Figure S19. Dependence of molar conductivity of RbCl on its concentration in MeOH/CH_2Cl_2 mixture (φ = 0.5) at (25.0 ± 0.1) °C. ○ experimental; – calculated.

Titrations

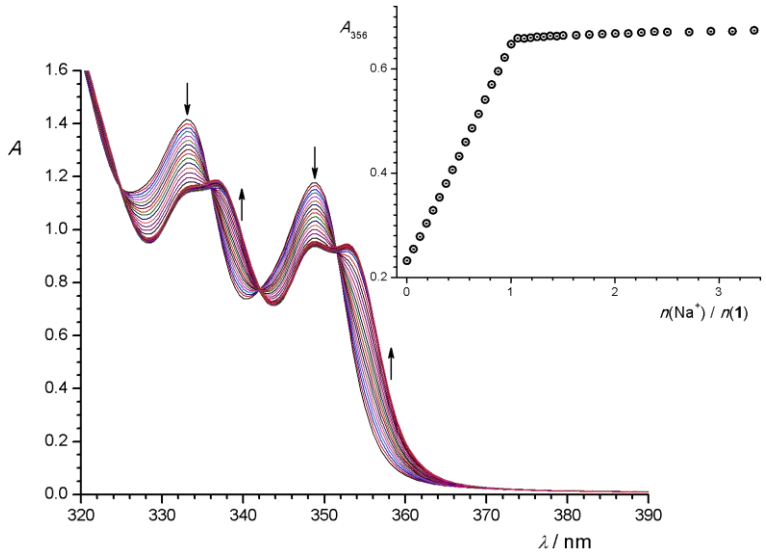

Figure S20. Spectrophotometric titration of **1** ($c = 1.51 \times 10^{-4}$ mol dm^{-3}) with $NaClO_4$ ($c = 2.51 \times 10^{-3}$ mol dm^{-3}) in $MeCN/CH_2Cl_2$ mixture ($\varphi = 0.5$) at (25.0 ± 0.1) °C. Spectra are corrected for dilution. Inset: absorbance at 356 nm as a function of cation to ligand molar ratio; ○ experimental; – calculated.

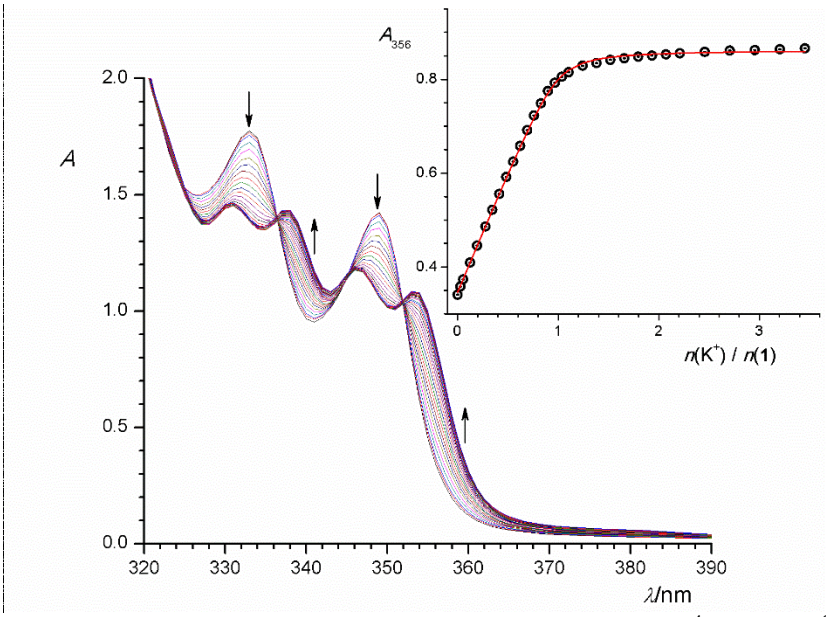

Figure S21. Spectrophotometric titration of **1** ($c = 1.79 \times 10^{-4}$ mol dm^{-3}) with $KClO_4$ ($c = 9.90 \times 10^{-4}$ mol dm^{-3}) in $MeCN/CH_2Cl_2$ mixture ($\varphi = 0.5$) at (25.0 ± 0.1) °C. Spectra are corrected for dilution. Inset: absorbance at 356 nm as a function of cation to ligand molar ratio; ○ experimental; – calculated.

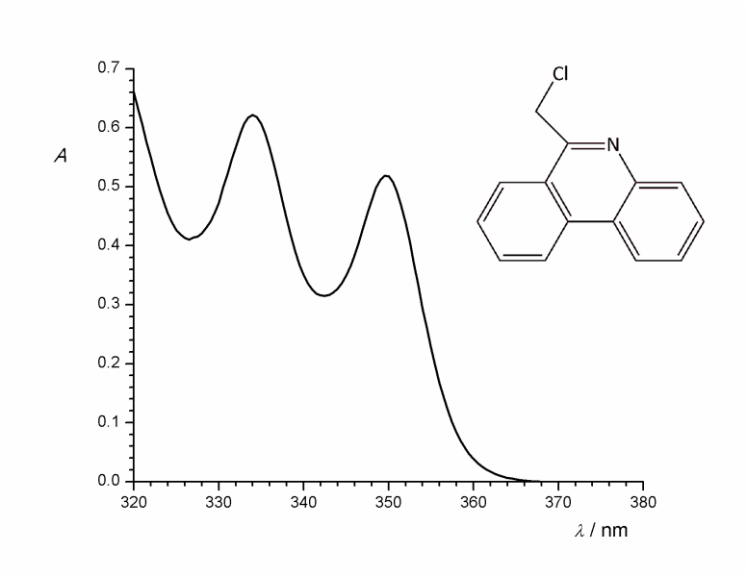

Figure S22. UV absorption spectrum of 6-(chloromethyl)phenanthridine (c = 4.34 × 10^{-4} mol dm^{-3}) in MeCN/CH_2Cl_2 mixture (φ = 0.5) at (25.0 ± 0.1) °C.

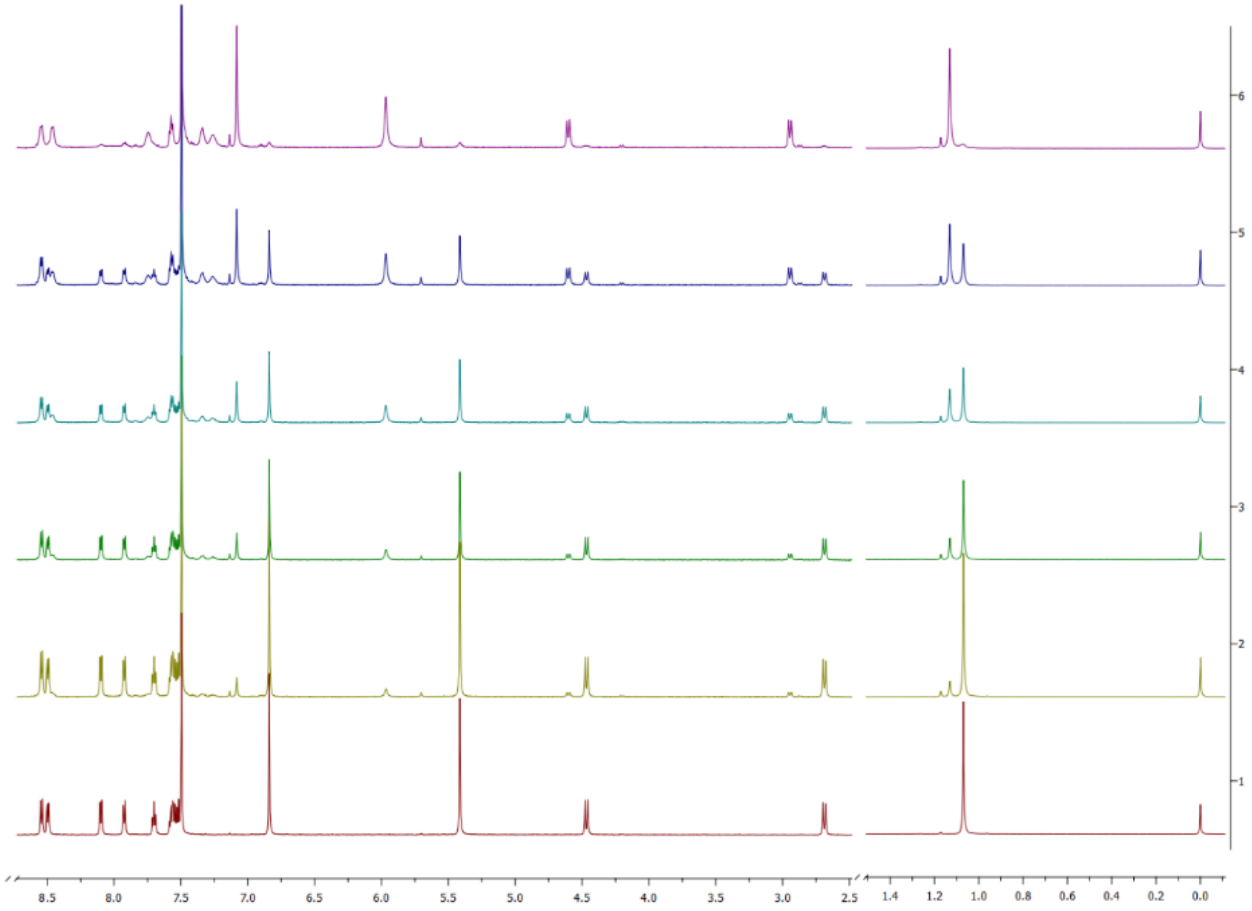

Figure S23. ^{1}H NMR titration of ligand **1** (c = 2.26 × 10^{-3} mol dm^{-3}) with $LiClO_4$ (c = 3.20 × 10^{-2} mol dm^{-3}) in $CD_3CN/CDCl_3$ mixture (φ = 0.5) at 25.0 °C. $n(Li^+)$ / n(**1**) = 0 (1); 0.25 (2); 0.5 (3); 0.75 (4); 1 (5); 1.5 (6).

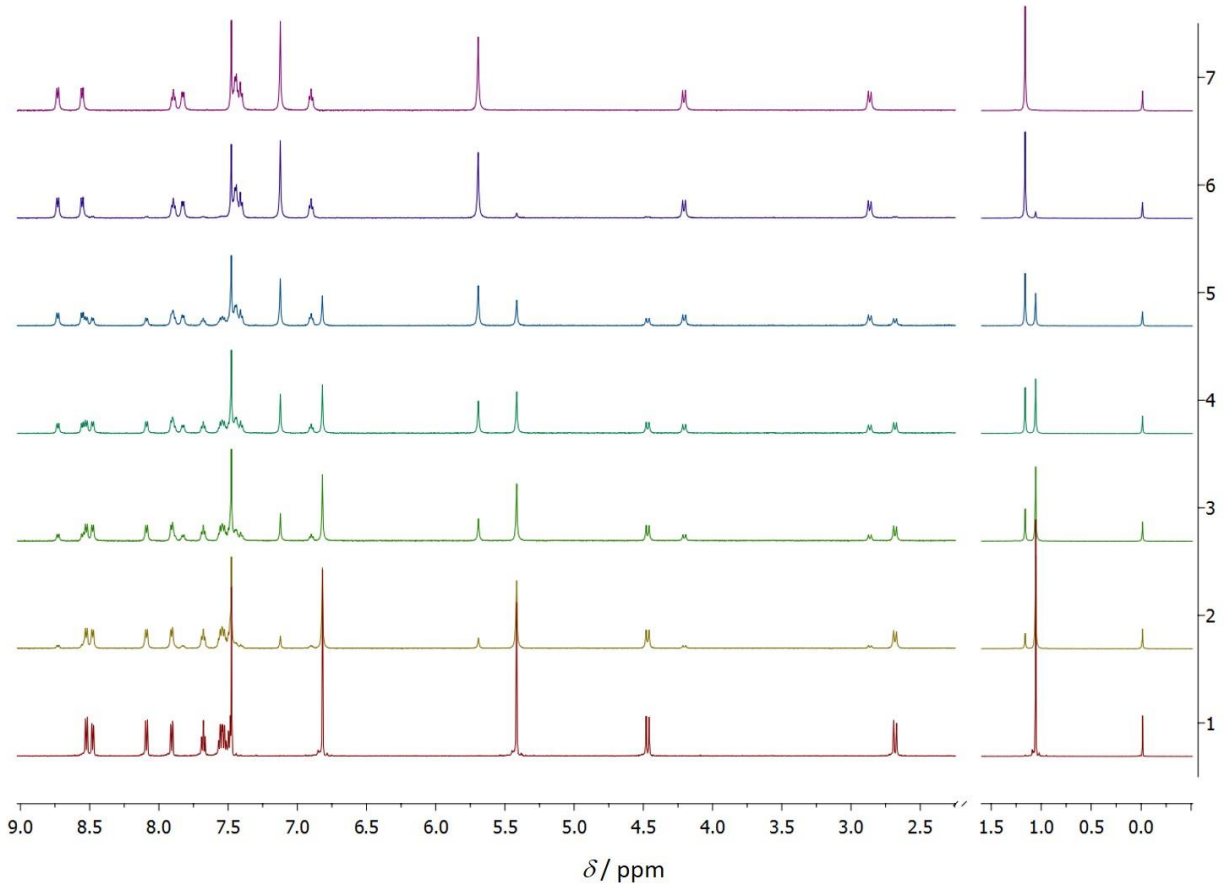

Figure S24. ^{1}H NMR titration of **1** ($c = 3.35 \times 10^{-3}$ mol dm^{-3}) with $NaClO_4$ ($c = 3.675 \times 10^{-2}$ mol dm^{-3}) in $CDCl_3/CD_3CN$ solvent mixture ($\varphi = 0.5$) at 25.0 °C. $n(Na^+) / n(\mathbf{1}) = 0$ (1); 0.25 (2); 0.5 (3); 0.75 (4); 1 (5); 1.5 (6); 2(7).

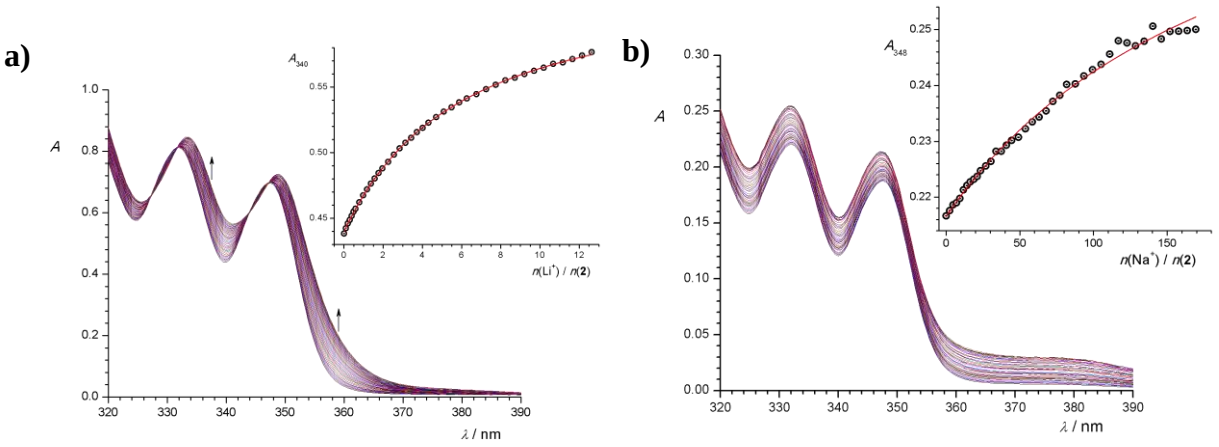

Figure S25. Spectrophotometric titration of **a) 2** ($c = 2.42 \times 10^{-4}$ mol dm^{-3}) with $LiClO_4$ ($c = 9.49 \times 10^{-3}$ mol dm^{-3}) and **b) 2** ($c = 9.45 \times 10^{-5}$ mol dm^{-3}) with $NaClO_4$ ($c = 3.153 \times 10^{-2}$ mol dm^{-3}) in $MeCN/CH_2Cl_2$ mixture ($\varphi = 0.5$) at (25.0 ± 0.1) °C. Spectra are corrected for dilution. Insets: absorbances at 340 nm and 348 nm, respectively, as a function of cation to ligand molar ratio. ○ experimental; – calculated.

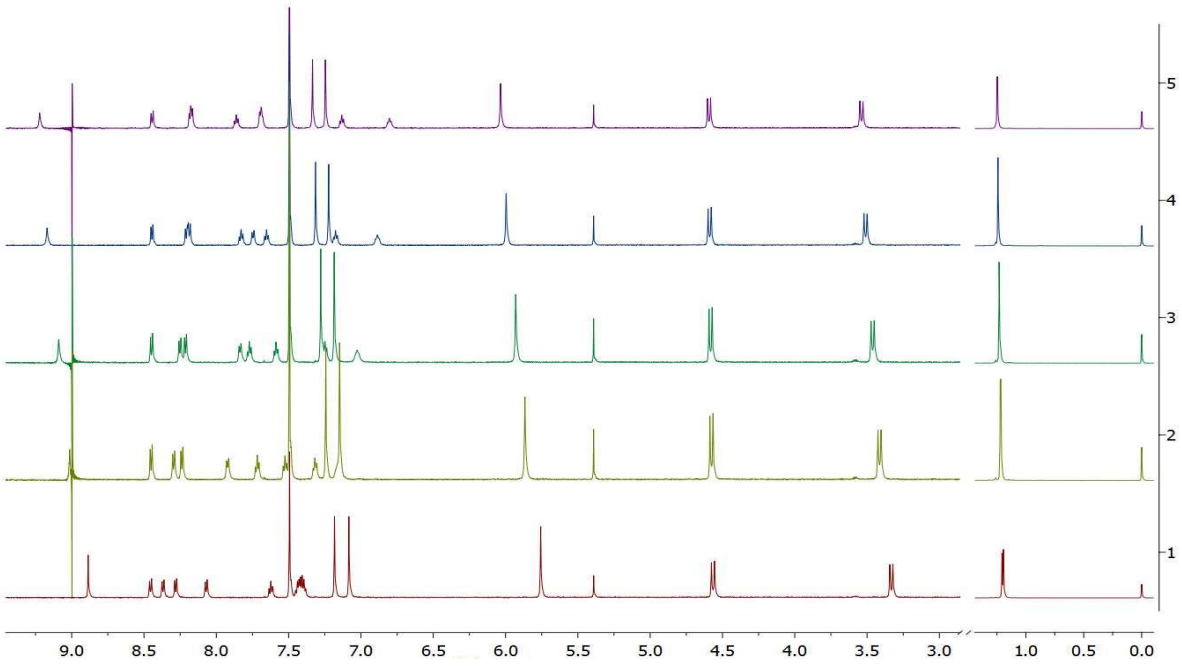

Figure S26. ^{1}H NMR titration of ligand **2** ($c = 2.71 \times 10^{-3}$ mol dm^{-3}) with $LiClO_4$ ($c = 7.52 \times 10^{-2}$ mol dm^{-3}) in $CD_3CN/CDCl_3$ mixture ($\varphi = 0.5$) at 25.0 °C. $n(Li^+) / n(\mathbf{2})$ = 0 (1); 2 (2); 4 (3); 7 (4); 10 (5); 2 (6).

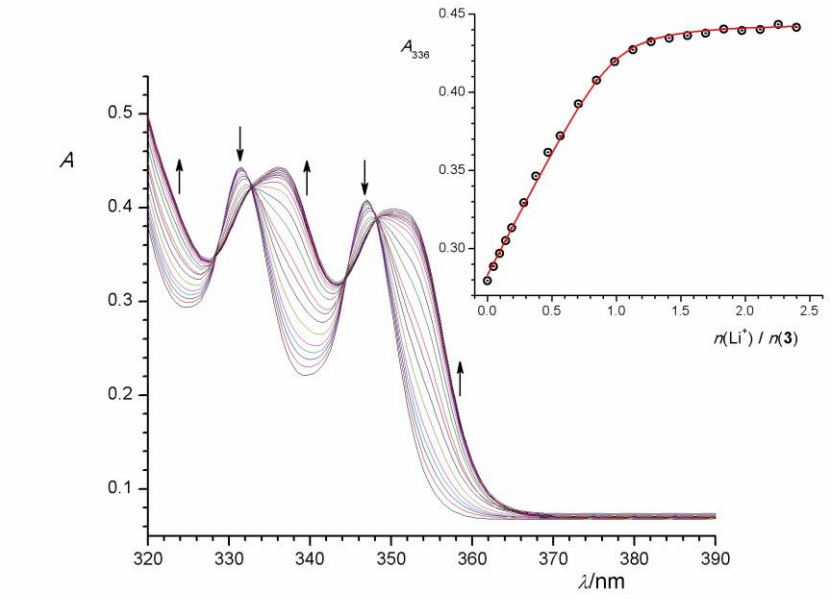

Figure S27. Spectrophotometric titration of **3** ($c = 1.0 \times 10^{-4}$ mol dm^{-3}) with $LiClO_4$ ($c = 3.76 \times 10^{-4}$ mol dm^{-3}) in $MeCN/CH_2Cl_2$ mixture ($\varphi = 0.5$) at (25.0 ± 0.1) °C. Spectra are corrected for dilution. Inset: absorbance at 336 nm as a function of cation to ligand molar ratio; ○ experimental; – calculated.

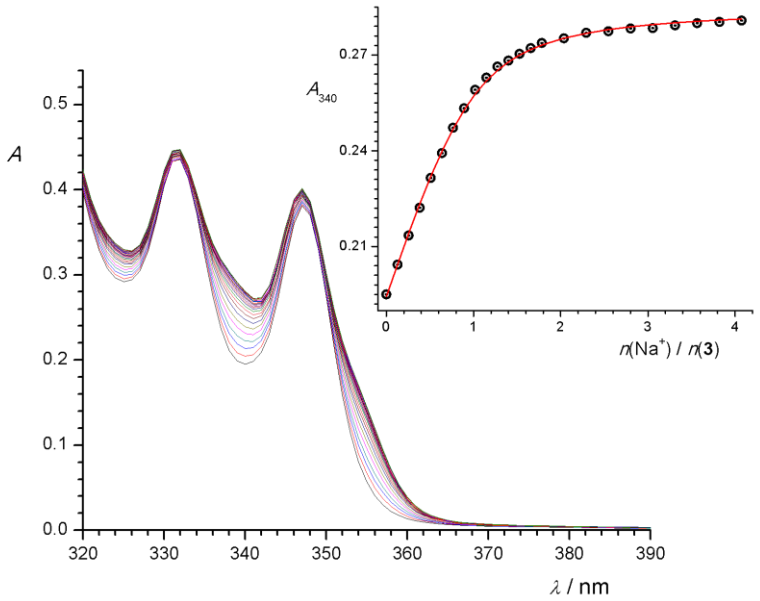

Figure S28. Spectrophotometric titration of **3** ($c = 9.933 \times 10^{-5}$ mol dm^{-3}) with $NaClO_4$ ($c = 2.53 \times 10^{-3}$ mol dm^{-3}) in $MeCN/CH_2Cl_2$ mixture ($\varphi = 0.5$) at (25.0 ± 0.1) °C. Spectra are corrected for dilution. Inset: absorbance at 340 nm as a function of cation to ligand molar ratio; ○ experimental; – calculated.

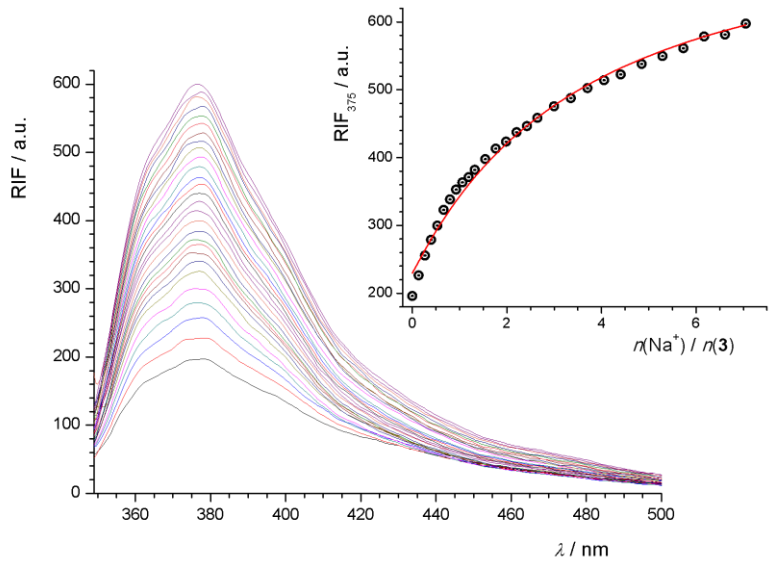

Figure S29. Fluorimetric titration of **3** ($c = 1.945 \times 10^{-6}$ mol dm^{-3}) with $NaClO_4$ ($c = 4.288 \times 10^{-5}$ mol dm^{-3}) in $MeCN/CH_2Cl_2$ solvent mixture ($\varphi = 0.5$) at (25.0 ± 0.1) °C; $\lambda_{ex} = 333$ nm, excitation slit 10, emission slit 10 nm. Spectra are corrected for dilution. Inset: fluorescence intensity at 375 nm as a function of cation to ligand molar ratio; ○ experimental; – calculated.

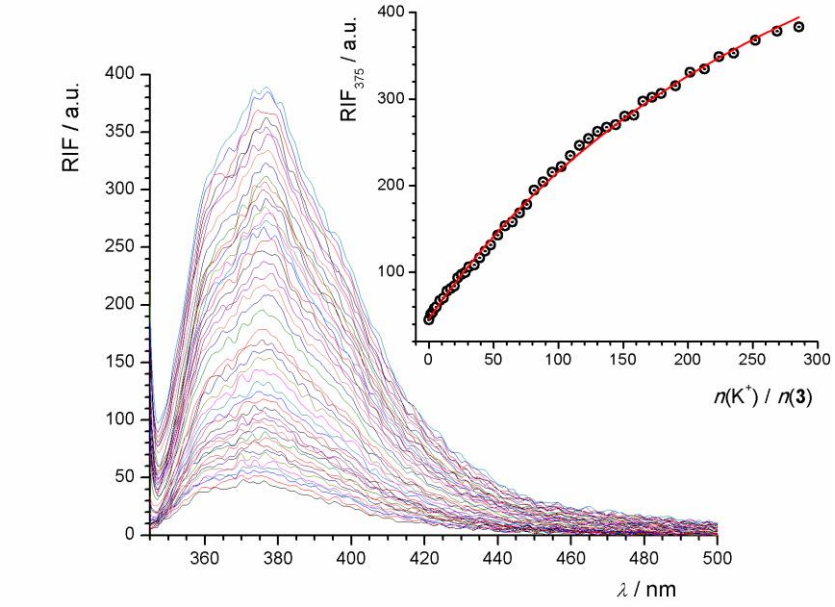

Figure S30. Fluorimetric titration of **3** ($c = 1.69 \times 10^{-6}$ mol dm^{-3}) with $KClO_4$ ($c = 1.184 \times 10^{-3}$ mol dm^{-3}) in $MeCN/CH_2Cl_2$ solvent mixture ($\varphi = 0.5$) at (25.0 ± 0.1) °C; $\lambda_{ex} = 333$ nm, excitation slit 5, emission slit 7.5 nm. Spectra are corrected for dilution. Inset: fluorescence intensity at 375 nm as a function of cation to ligand molar ratio; ○ experimental; – calculated.

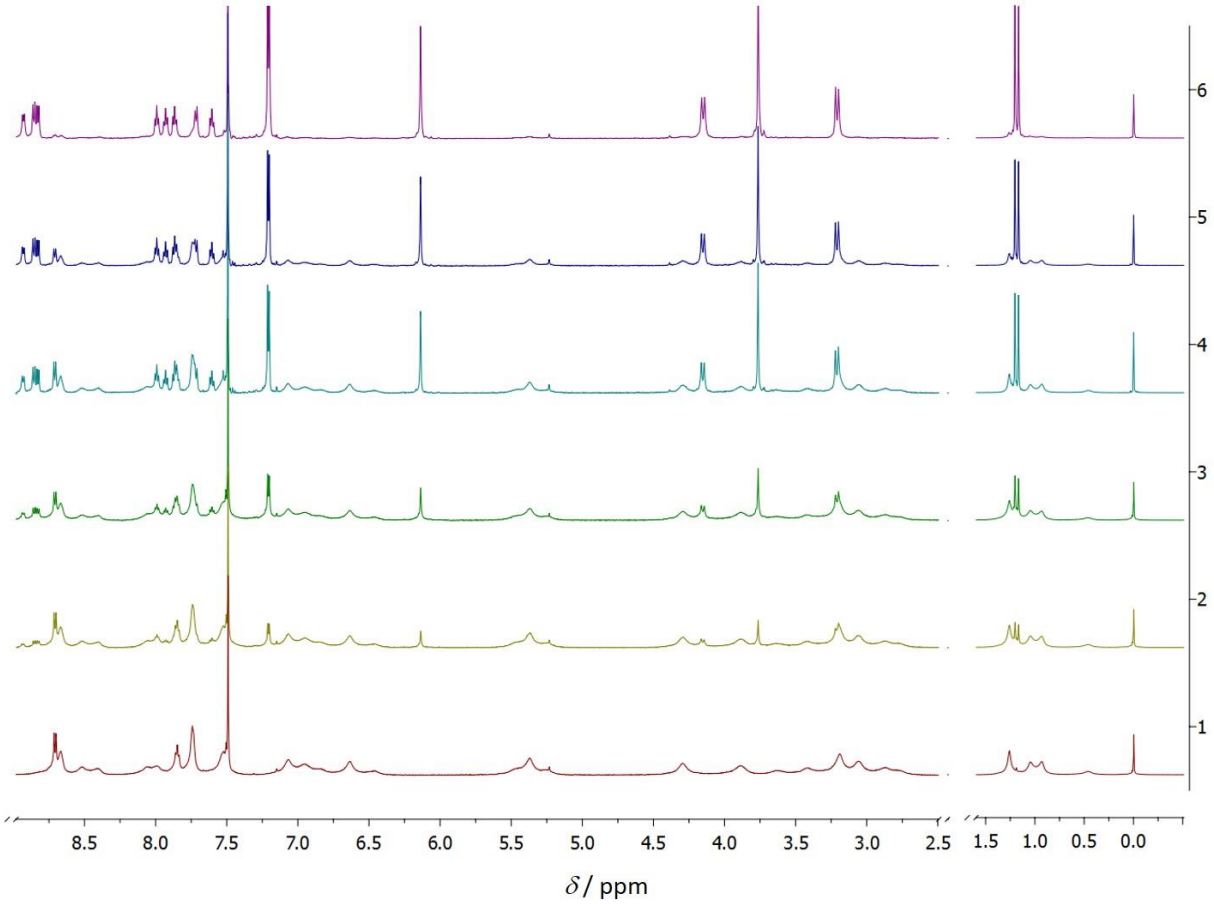

Figure S31. ^{1}H NMR titration of **3** ($c = 4.83 \times 10^{-3}$ mol dm^{-3}) with $LiClO_4$ ($c = 4.813 \times 10^{-2}$ mol dm^{-3}) in $CD_3CN/CDCl_3$ solvent mixture ($\varphi = 0.5$) at 25.0 °C. $n(Li^+) / n(\mathbf{3}) = 0$ (1); 0.25 (2); 0.5 (3); 0.75 (4); 1 (5); 1.5 (6).

Table S9. Standard Gibbs energies of transfer of alkali-metal cations from dichloromethane to acetonitrile and methanol at (25.0 ± 0.1) °C.[a]

cation	$\Delta_t G^o(CH_2Cl_2 \rightarrow MeCN)$/kJ mol^{-1}	$\Delta_t G^o(CH_2Cl_2 \rightarrow MeOH)$/kJ mol^{-1}
Na^+	–43	–50
K^+	–24	–22
Rb^+	–16	–14
Cs^+	–16	–13

[a] Calculated by combining Gibbs energy of transfer of cations from water to dichloromethane, acetonitrile, or methanol tabulated in ref. 1:

$$\Delta_t G(CH_2Cl_2 \rightarrow MeCN) = \Delta_t G(H_2O \rightarrow MeCN) - \Delta_t G(H_2O \rightarrow CH_2Cl_2);$$

$$\Delta_t G(CH_2Cl_2 \rightarrow MeOH) = \Delta_t G(H_2O \rightarrow MeOH) - \Delta_t G(H_2O \rightarrow CH_2Cl_2).$$

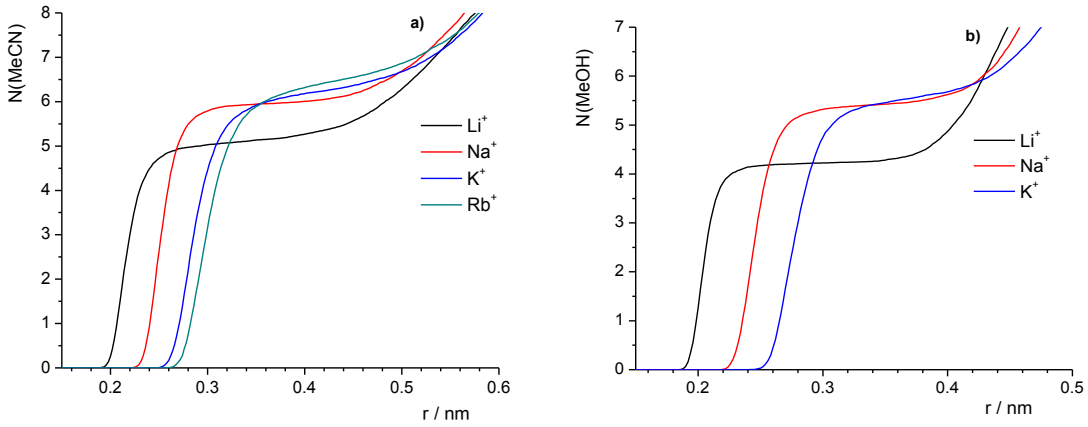

Figure S32. The cumulative average number of solvent molecules as a function of distance from alkali-metal cation in **a)** MeCN/CH_2Cl_2 and **b)** MeOH/CH_2Cl_2 mixtures ($\varphi = 0.5$) obtained by MD simulations at 25 °C.

[1] Marcus, Y. *Ion Properties*; CRC Press: Boca Raton, FL, 1997.

Table S10. Energies of interactions of alkali-metal cations with acetonitrile and dichloromethane obtained by MD simulations in MeCN/CH_2Cl_2 mixture (φ = 0.5) at 25 °C; t_{tot} = 1 ns.

Ion	E(MeCN) / kJ mol^{-1}	E(CH_2Cl_2) / kJ mol^{-1}
Li^+	–582 ± 41	–7 ± 15
Na^+	–471 ± 27	–4 ± 10
K^+	–351 ± 33	–7 ± 17
Rb^+	–324 ± 29	–5 ± 14

Table S11. Energies of interactions of alkali-metal cations with methanol and dichloromethane obtained by MD simulations in MeOH/CH_2Cl_2 mixture (φ = 0.5) at 25 °C; t_{tot} = 1 ns.

Ion	E(MeOH) / kJ mol^{-1}	E(CH_2Cl_2) / kJ mol^{-1}
Li^+	–564 ± 37	–6 ± 12
Na^+	–464 ± 35	–8 ± 14
K^+	–342 ± 38	–14 ± 21

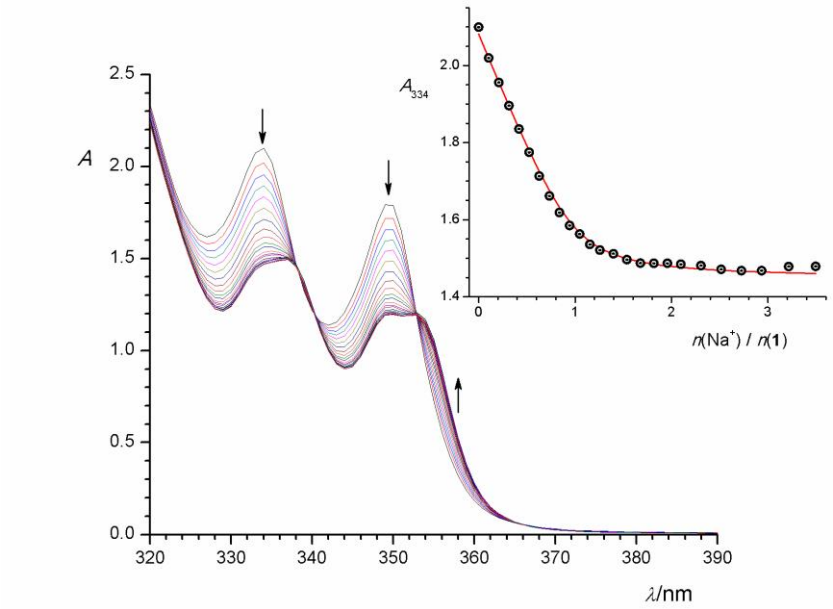

Figure S33. Spectrophotometric titration of **1** ($c = 1.79 \times 10^{-4}$ mol dm^{-3}) with $NaClO_4$ ($c = 2.51 \times 10^{-3}$ mol dm^{-3}) in MeOH/CH_2Cl_2 mixture ($\varphi = 0.5$) at (25.0 ± 0.1) °C. Spectra are corrected for dilution. Inset: absorbance at 350 nm as a function of cation to ligand molar ratio; ○ experimental; – calculated.

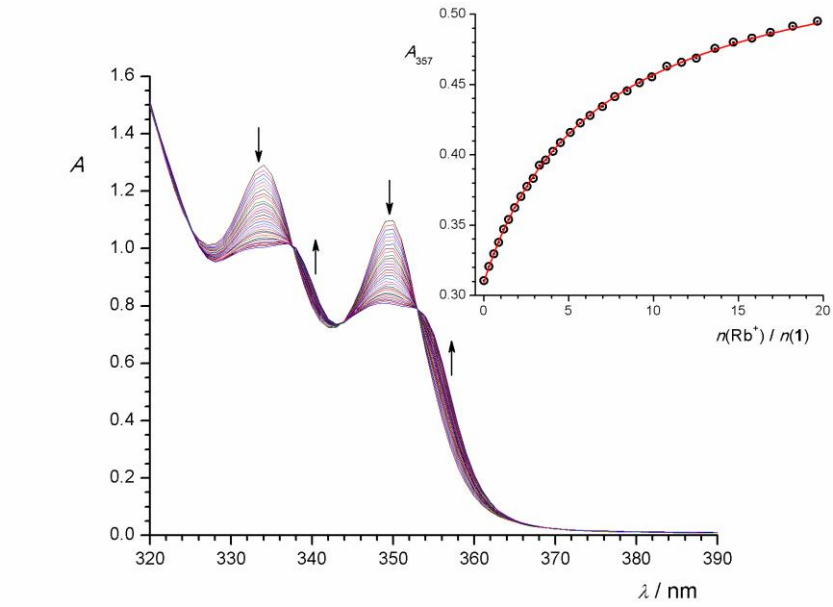

Figure S34. Spectrophotometric titration of **1** ($c = 1.19 \times 10^{-4}$ mol dm^{-3}) with $RbNO_3$ ($c = 3.45 \times 10^{-3}$ mol dm^{-3}) in MeOH/CH_2Cl_2 mixture ($\varphi = 0.5$) at (25.0 ± 0.1) °C. Spectra are corrected for dilution. Inset: absorbance at 357 nm as a function of cation to ligand molar ratio; ○ experimental; – calculated.

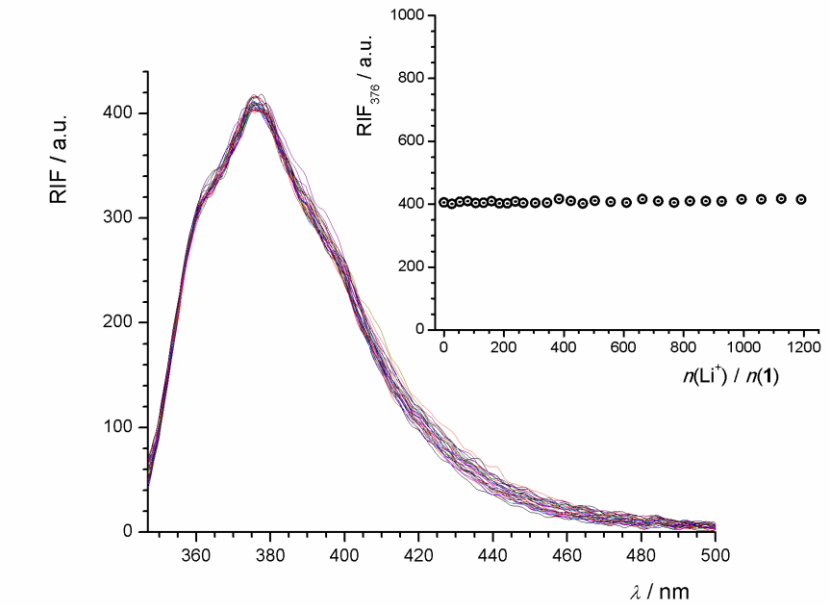

Figure S35. Fluorimetric titration of **1** ($c = 1.45 \times 10^{-6}$ mol dm^{-3}) with $LiClO_4$ ($c = 4.79 \times 10^{-3}$ mol dm^{-3}) in MeOH/CH_2Cl_2 solvent mixture ($\varphi = 0.5$) at (25.0 ± 0.1) °C; λ_{ex} = 333 nm, excitation slit 5, emission slit 10 nm. Spectra are corrected for dilution. Inset: fluorescence intensity at 375 nm as a function of cation to ligand molar ratio; ○ experimental; – calculated.

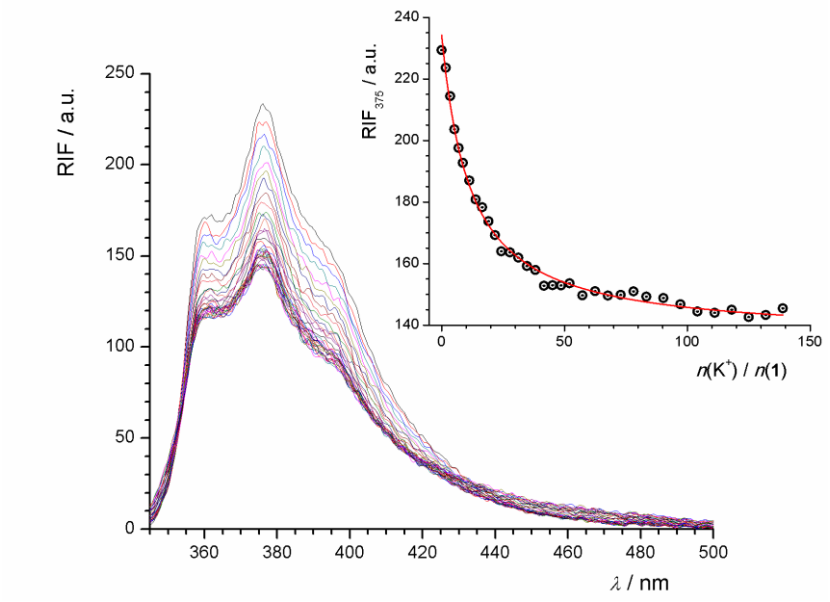

Figure S36. Fluorimetric titration of **1** ($c = 3.83 \times 10^{-6}$ mol dm^{-3}) with KCl ($c = 1.66 \times 10^{-3}$ mol dm^{-3}) in MeOH/CH_2Cl_2 solvent mixture ($\varphi = 0.5$) at (25.0 ± 0.1) °C; λ_{ex} = 333 nm, excitation slit 5, emission slit 5 nm. Spectra are corrected for dilution. Inset: fluorescence intensity at 375 nm as a function of cation to ligand molar ratio; ○ experimental; – calculated.

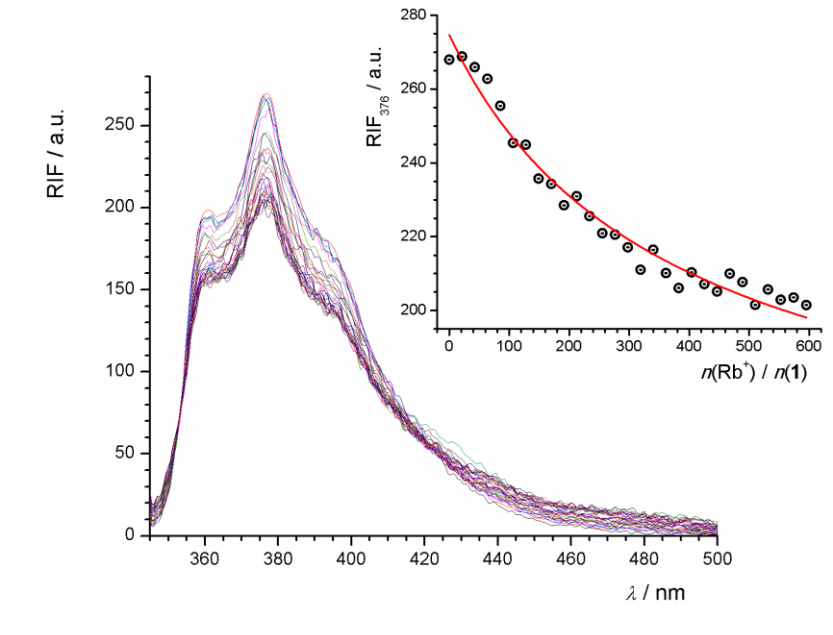

Figure S37. Fluorimetric titration of **1** ($c = 3.734 \times 10^{-6}$ mol dm^{-3}) with RbCl ($c = 3{,}970 \times 10^{-3}$ mol dm^{-3}) in MeOH/CH_2Cl_2 solvent mixture ($\varphi = 0.5$) at (25.0 ± 0.1) °C; $\lambda_{ex} = 333$ nm, excitation slit 5, emission slit 5 nm. Spectra are corrected for dilution. Inset: fluorescence intensity at 376 nm as a function of cation to ligand molar ratio; ○ experimental; – calculated.

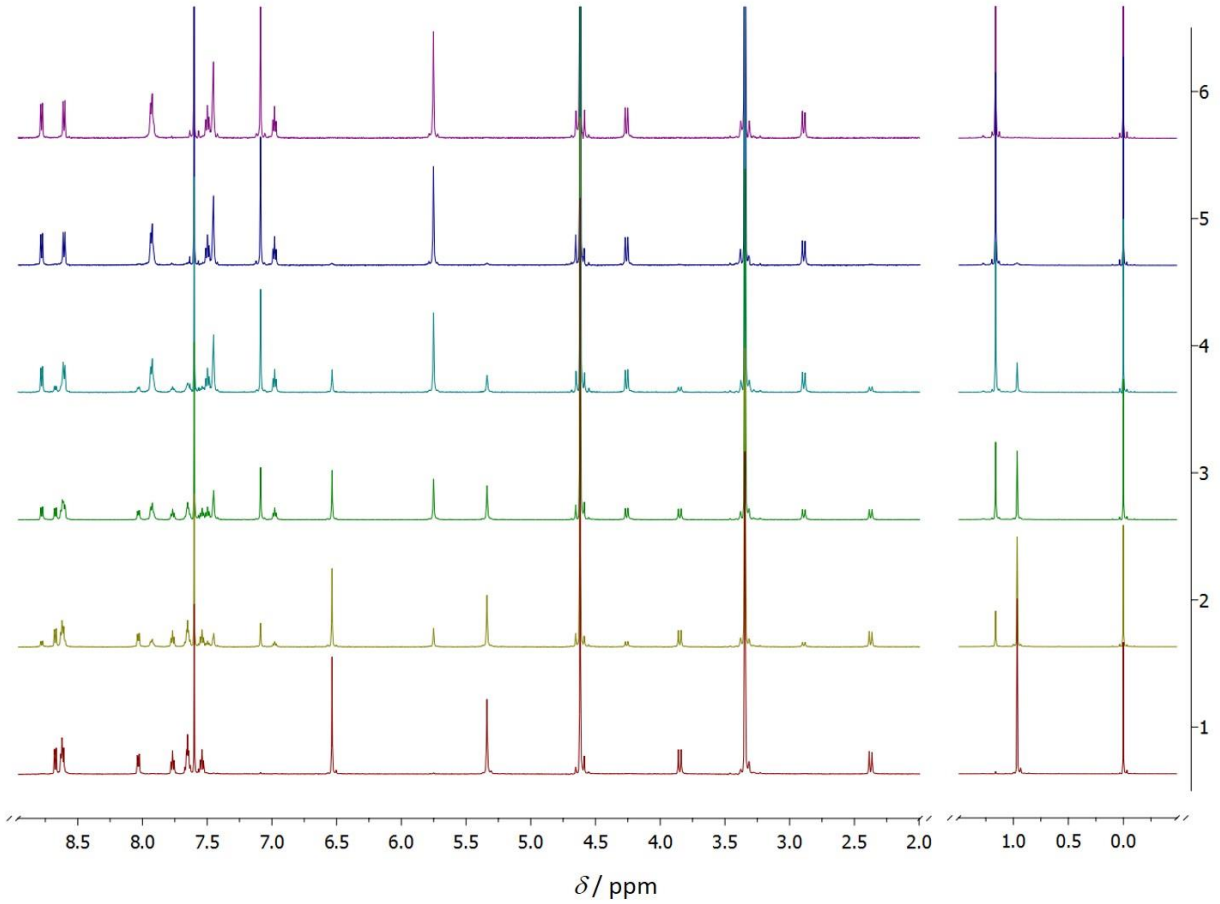

Figure S38. ^{1}H NMR titration of **1** ($c = 2.55 \times 10^{-3}$ mol dm^{-3}) with $NaClO_4$ ($c = 2.336 \times 10^{-2}$ mol dm^{-3}) in $CD_3OD/CDCl_3$ solvent mixture ($\varphi = 0.5$) at 25.0 °C. $n(Na^+) / n(\mathbf{1}) = 0$ (1); 0.5 (2); 1 (3); 1.5 (4); 2 (5); 2.5 (6).

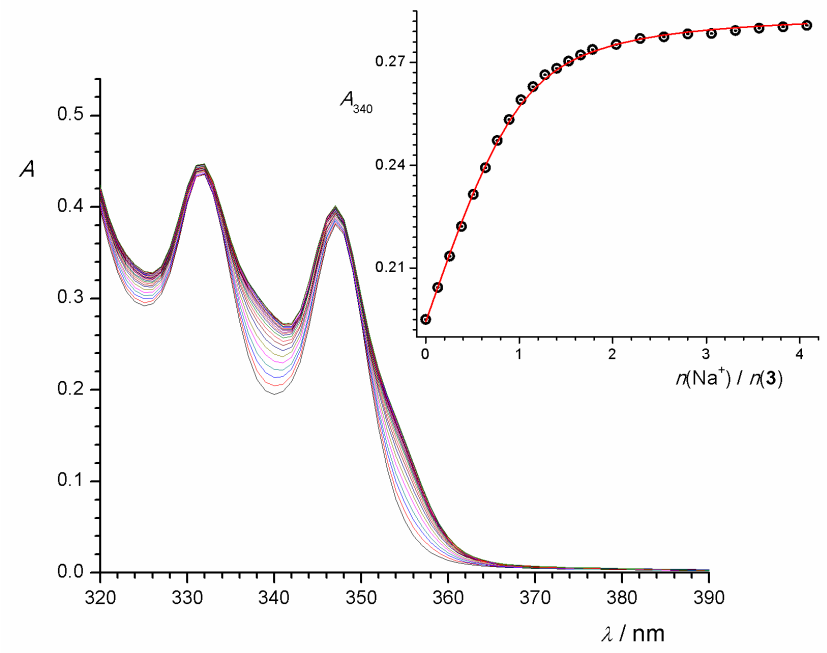

Figure S39. Spectrophotometric titration of **3** ($c = 1.0 \times 10^{-4}$ mol dm^{-3}) with $NaClO_4$ ($c = 3.34 \times 10^{-2}$ mol dm^{-3}) in MeOH/CH_2Cl_2 mixture ($\varphi = 0.5$) at (25.0 ± 0.1) °C. Spectra are corrected for dilution. Inset: absorbance at 350 nm as a function of cation to ligand molar ratio. ○ experimental; – calculated.

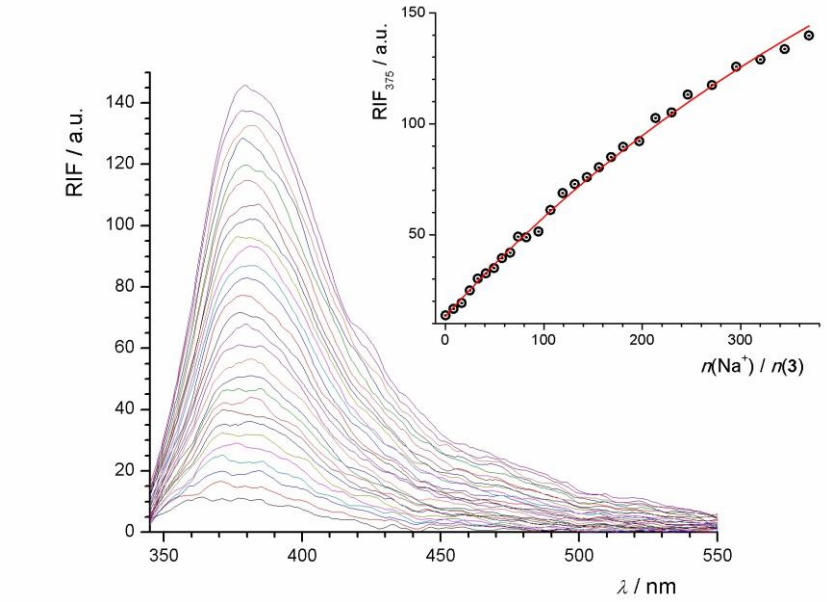

Figure S40. Fluorimetric titration of **3** ($c = 1.5 \times 10^{-6}$ mol dm^{-3}) with $NaClO_4$ ($c = 3.02 \times 10^{-3}$ mol dm^{-3}) in MeOH/CH_2Cl_2 mixture ($\varphi = 0.5$) at (25.0 ± 0.1) °C; $\lambda_{ex} = 333$ nm, excitation slit 5 nm, emission slit 7.5 nm. Spectra are corrected for dilution. Inset: relative fluorescence intensity at 375 nm as a function of cation to ligand molar ratio; ○ experimental; – calculated.

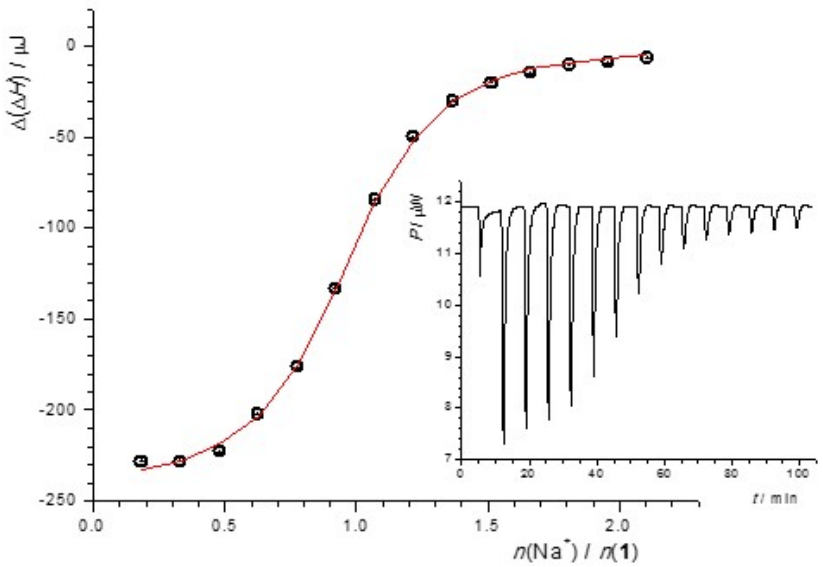

Figure S41. Microcalorimetric titration of **1** ($c = 2.41 \times 10^{-4}$ mol dm^{-3}, $V = 1.4182$ cm^3) with Na[B(Ph)$_4$] ($c = 2.52 \times 10^{-3}$ mol dm^{-3}) in MeOH/CH_2Cl_2 mixture ($\varphi = 0.5$) at (25.0 ± 0.1) °C; dependence of successive enthalpy change on $n(Na^+)$ / n(**1**) ratio; ○ experimental; – calculated. Inset: raw calorimetric data.

MD results

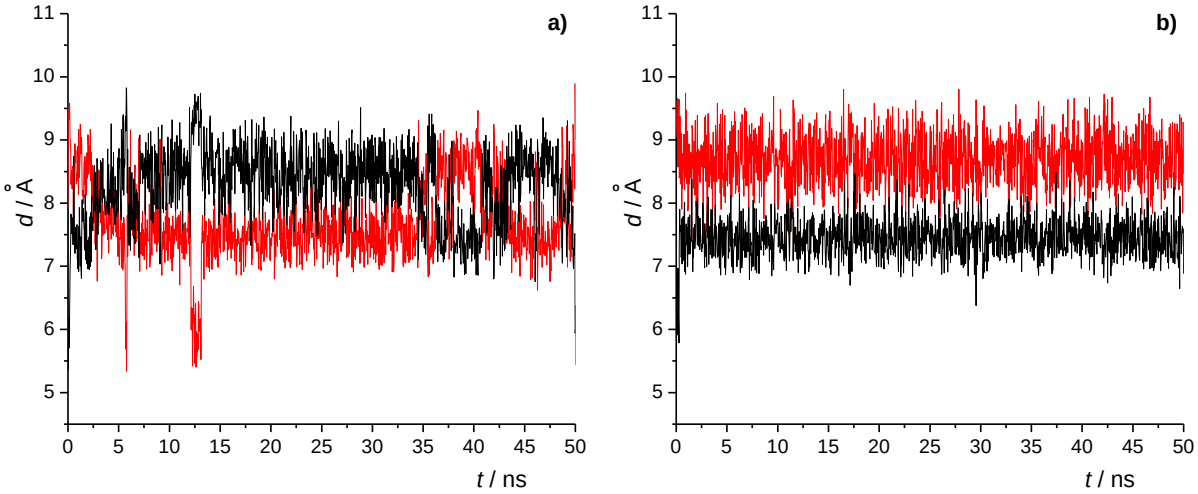

Figure S42. Distances between the opposing phenyl carbon atoms that are directly connected to the *tert*-butyl group during the MD simulations of **a)** ligand **1** and **b)** ligand **3** in MeCN/CH_2Cl_2 mixture (φ = 0.5) at 25 °C.

Table S12. Average distances ($\bar{d}$) between the opposing phenyl carbon atoms that are directly connected to the *tert*-butyl group during the MD simulations of ligand **1** and **3** in MeCN/CH_2Cl_2 and MeOH/CH_2Cl_2 mixtures (φ = 0.5) at 25 °C (σ denotes standard deviation); t_{tot} = 50 ns.

	MeCN/CH_2Cl_2			MeOH/CH_2Cl_2		
	t / t_{tot}	$\bar{d}$ / Å	$\sigma(\bar{d})$ / Å	t / t_{tot}	$\bar{d}$ / Å	$\sigma(\bar{d})$ / Å
1	0.080	5.86 9.28	0.43 0.34	0.449	5.96 9.17	0.49 0.42
1–MeCN	0.862	7.78 8.03	0.34 0.36	–	–	–
1–MeOH	–	–	–	0.474	7.70 8.11	0.30 0.31
1–CH_2Cl_2	0.058	7.79 8.20	0.34 0.35	0.085	7.94 8.08	0.37 0.37
3	0.012	6.08 9.46	0.44 0.33	0.131	6.05 9.48	0.31 0.44
3–MeCN	0.983	7.45 8.69	0.29 0.41	–	–	–
3–MeOH	–	–	–	0.832	7.54 8.55	0.27 0.37
3–CH_2Cl_2	0.005	7.49 8.95	0.37 0.43	0.037	7.52 8.88	0.36 0.42

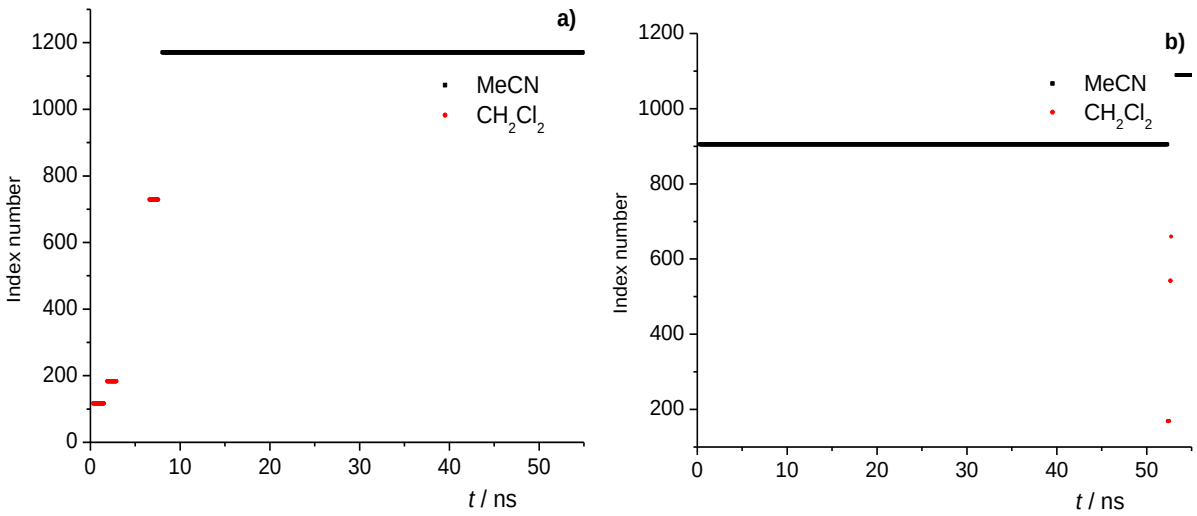

Figure S43. Index numbers of acetonitrile and dichloromethane molecules that occupied hydrophobic cavity of **a)** ligand **1** and **b)** ligand **3** during MD simulations in MeCN/CH_2Cl_2 mixture (φ = 0.5) at 25 °C.

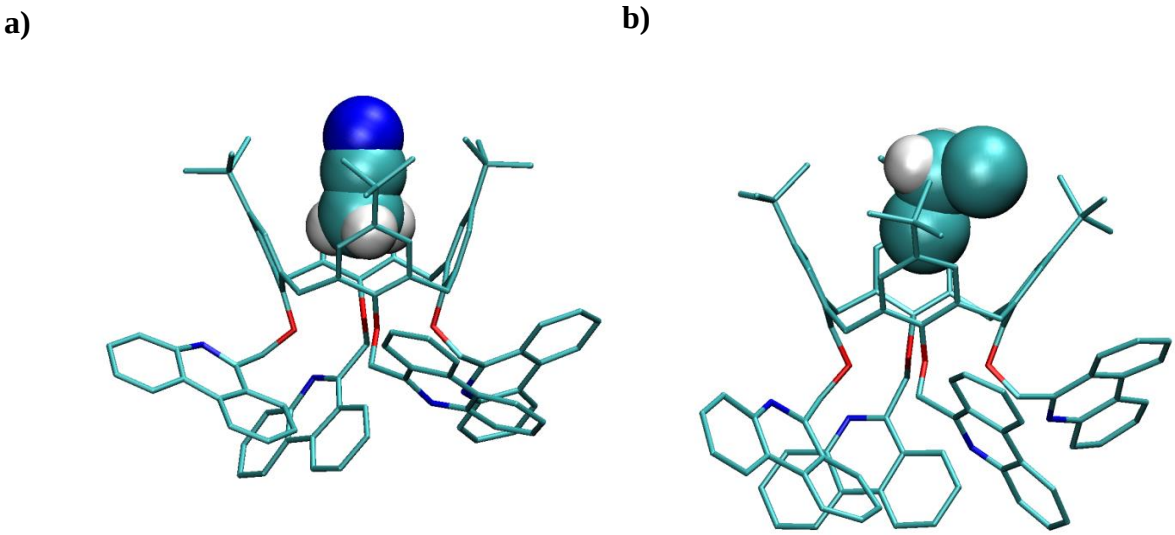

Figure S44. Molecular structures of **a)** **1**MeCN and **b)** **1**CH_2Cl_2 adducts obtained by MD simulation of **1** in MeCN/CH_2Cl_2 mixture (φ = 0.5) at 25 °C. Hydrogen atoms bound to carbon atoms of **1** have been omitted for clarity.

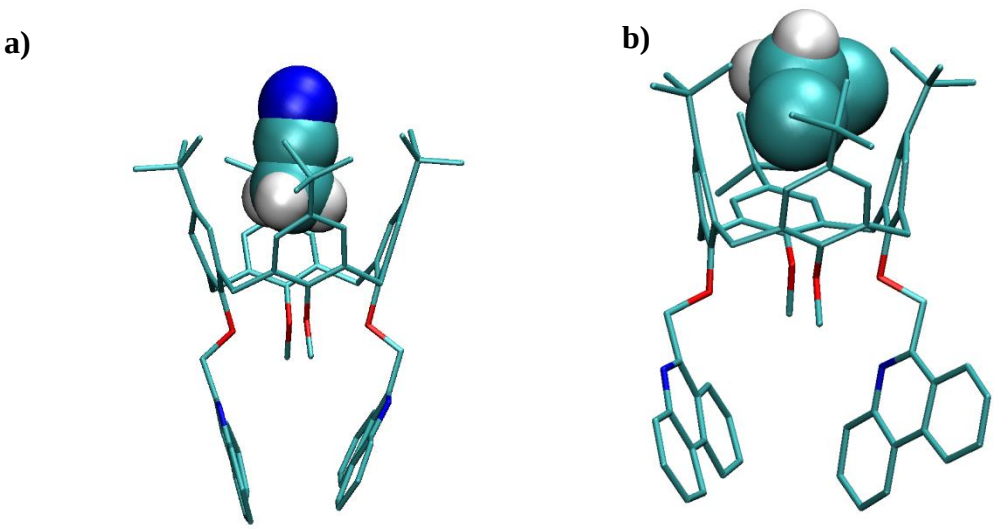

Figure S45. Molecular structures of **a) 3**MeCN and **b) 3**CH_2Cl_2 adducts obtained by MD simulation of **3** in MeCN/CH_2Cl_2 mixture (φ = 0.5) at 25 °C. Hydrogen atoms bound to carbon atoms of **3** have been omitted for clarity.

Table S13. Energies of interactions of **1** and **3** with solvent molecules obtained by MD simulations in MeCN/CH_2Cl_2 and MeOH/CH_2Cl_2 mixtures (φ = 0.5) at 25 °C; t_{tot} = 50 ns.

	MeCN/CH_2Cl_2			MeOH/CH_2Cl_2		
	$\frac{E(\mathbf{L}-\mathrm{MeCN})}{\mathrm{kJ\ mol^{-1}}}$	$\frac{E(\mathbf{L}-\mathrm{CH_2Cl_2})}{\mathrm{kJ\ mol^{-1}}}$	$\frac{E(\mathbf{L}-\mathrm{SOLV_{incl}})}{\mathrm{kJ\ mol^{-1}}}$	$\frac{E(\mathbf{L}-\mathrm{MeOH})}{\mathrm{kJ\ mol^{-1}}}$	$\frac{E(\mathbf{L}-\mathrm{CH_2Cl_2})}{\mathrm{kJ\ mol^{-1}}}$	$\frac{E(\mathbf{L}-\mathrm{SOLV_{incl}})}{\mathrm{kJ\ mol^{-1}}}$
1	–172 ± 44	–381 ± 52	–	–180 ± 44	–412 ± 50	–
1–MeCN	–226 ± 39	–386 ± 50	–52 ± 5	–	–	–
1–MeOH	–	–	–	–230 ± 44	–393 ± 49	–49 ± 5
1–CH_2Cl_2	–182 ± 39	–412 ± 49	–50 ± 7	–188 ± 46	–442 ± 53	–50 ± 7
3	–130 ± 27	–311 ± 40	–	–147 ± 39	–315 ± 46	–
3–MeCN	–200 ± 33	–291 ± 41	–52 ± 5	–	–	–
3–MeOH	–	–	–	–191 ± 37	–306 ± 42	–49 ± 5
3–CH_2Cl_2	–160 ± 36	–310 ± 41	–51 ± 6	–135 ± 40	–358 ± 43	–50 ± 7

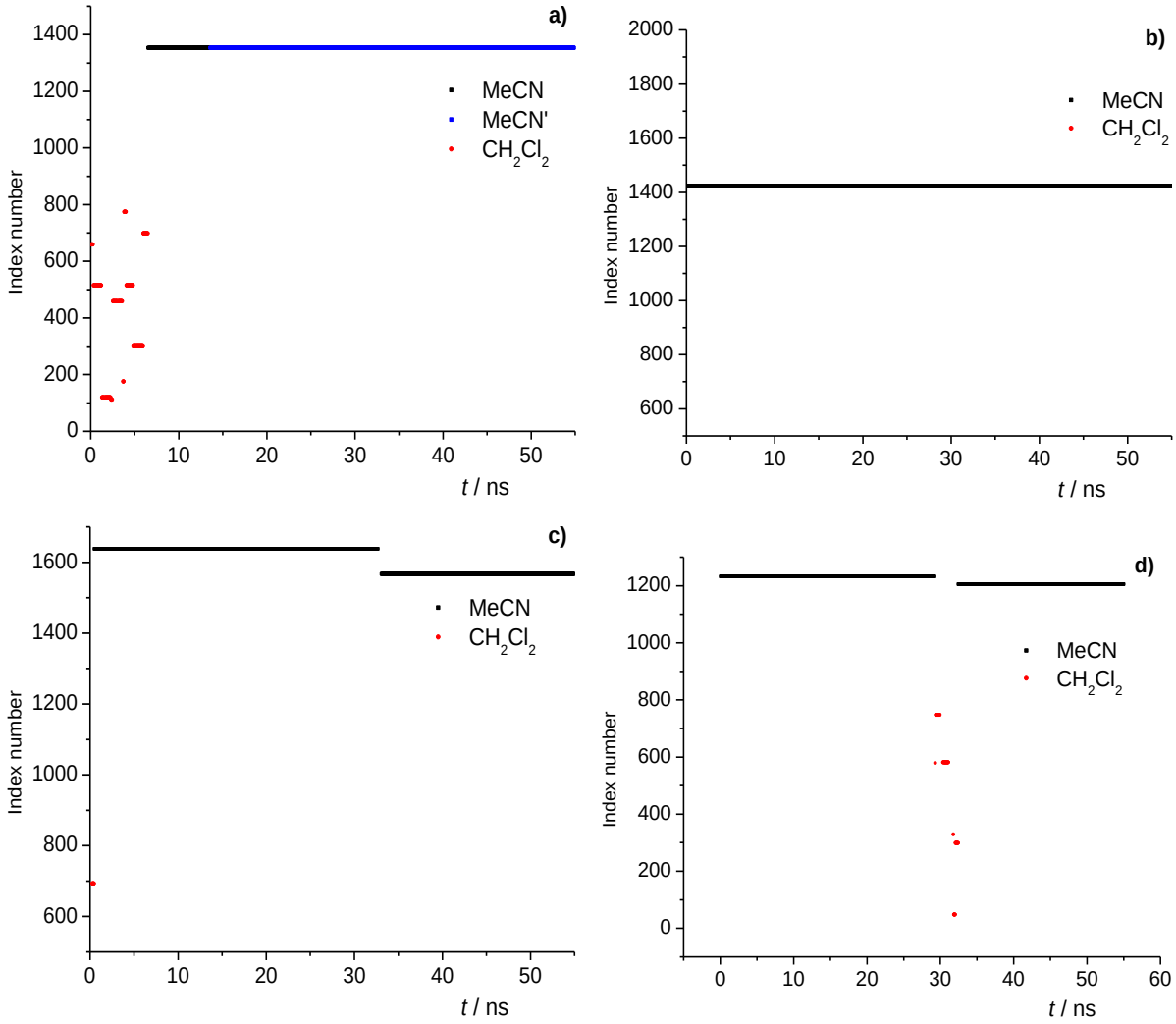

Figure S46. Index numbers of acetonitrile and dichloromethane molecules that occupied hydrophobic cavity of **a)** Li**1**$^+$, **b)** Na**1**$^+$, **c)** K**1**$^+$ and **d)** Rb**1**$^+$ complexes during MD simulations in MeCN/CH_2Cl_2 mixture (φ = 0.5) at 25 °C.

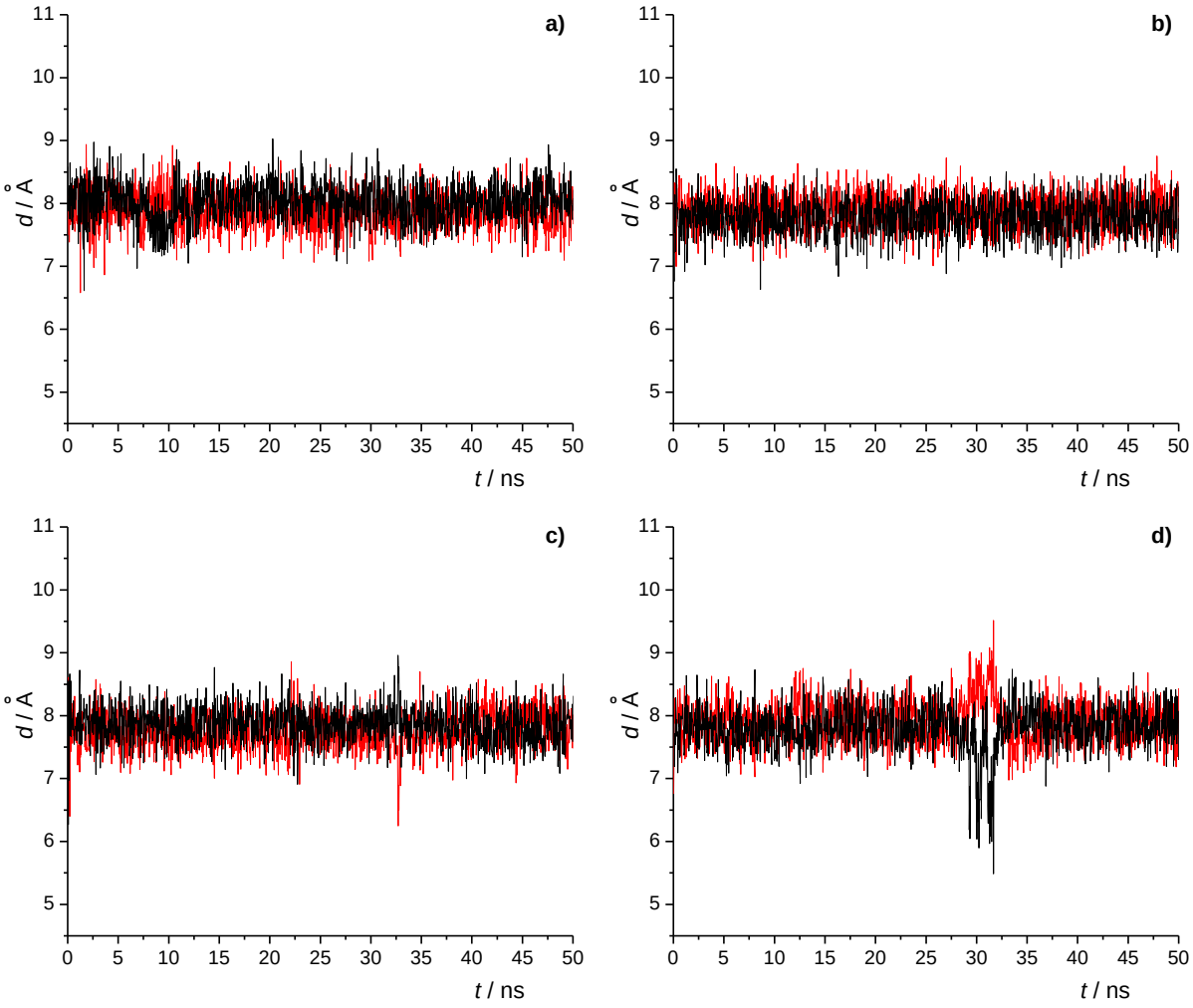

Figure S47. Distances between the opposing phenyl carbon atoms that are directly connected to the *tert*-butyl group during the MD simulations of **a)** Li**1**$^+$, **b)** Na**1**$^+$, **c)** K**1**$^+$ and **d)** Rb**1**$^+$ in MeCN/CH_2Cl_2 (φ = 0.5) mixture at 25 °C.

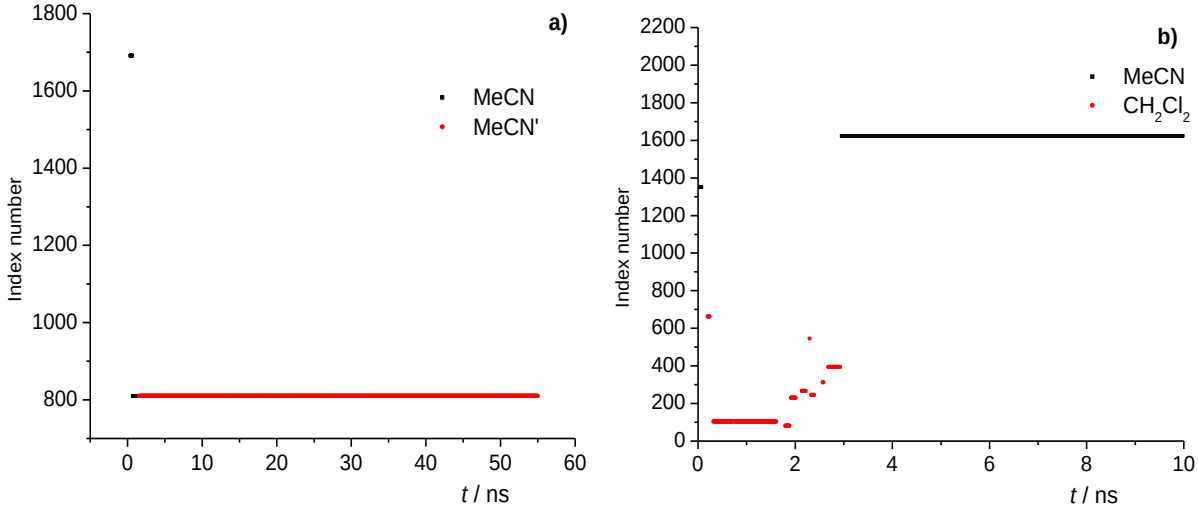

Figure S48. Index numbers of acetonitrile and dichloromethane molecules that occupied hydrophobic cavity of **a)** Li**3**$^+$ and **b)** Na**3**$^+$ complexes during MD simulations in MeCN/CH_2Cl_2 mixture (φ = 0.5) at 25 °C.

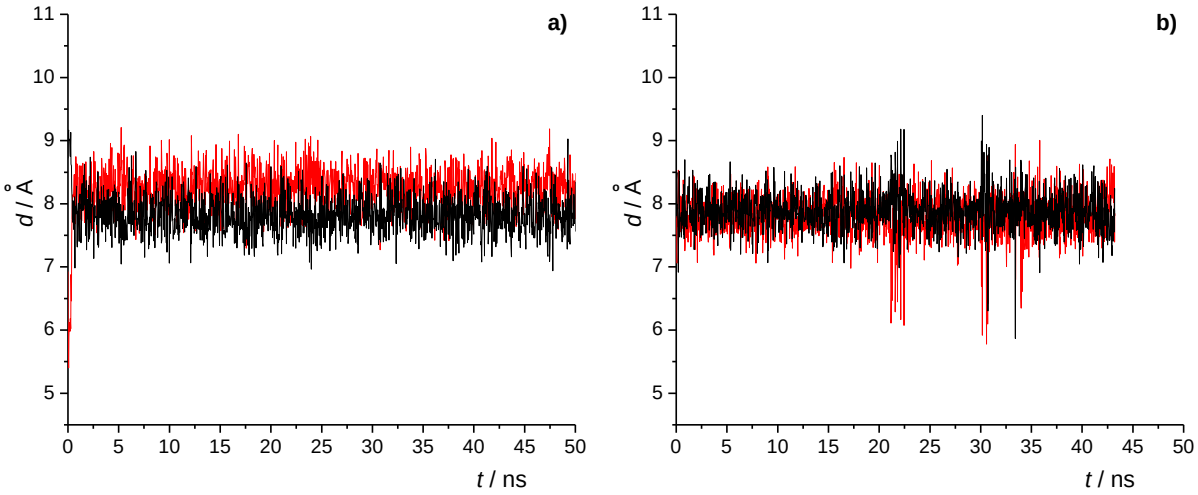

Figure S49. Distances between the opposing phenyl carbon atoms that are directly connected to the *tert*-butyl group during the MD simulations of **a)** Li**3**$^+$, **b)** Na**3**$^+$, in MeCN/CH_2Cl_2 mixture (φ = 0.5) at 25 °C.

Table S14. Energies of interactions of **1** with lithium cation, acetonitrile, and dichloromethane, occurrence time ratio of different chemical species, and the number of phenanthridine nitrogen atoms which coordinate metal cation in the complexes obtained by MD simulations in $MeCN/CH_2Cl_2$ mixture (φ = 0.5) at 25 °C; t_{tot} = 50 ns.

	Li**1**$^+$	Li**1**MeCN$^+$	Li**1**MeCN$'^+$	Li**1**$CH_2Cl_2^+$
E(Li$^+$–**1**) / kJ mol^{-1}	–343 ± 11	–358 ± 17	–303 ± 14	–345 ± 11
E(**1**–MeCN) / kJ mol^{-1}	–176 ± 45	–234 ± 39	–158 ± 38	–179 ± 44
E(**1**–$MeCN_{incl}$) / kJ mol^{-1}	–	–50 ± 6	20 ± 9	–
E(**1**–CH_2Cl_2) / kJ mol^{-1}	–410 ± 58	–380 ± 49	–389 ± 48	–427 ± 60
E(**1**–CH_2Cl_{2incl}) / kJ mol^{-1}	–	–	–	–46 ± 9
E(Li$^+$– MeCN) / kJ mol^{-1}	–10 ± 7	–2 ± 8	–125 ± 9	–10 ± 7
E(Li$^+$– $MeCN_{incl}$) / kJ mol^{-1}	–	10 ± 3	–120 ± 7	–
E(Li$^+$– CH_2Cl_2) / kJ mol^{-1}	–3 ± 6	–7 ± 6	–4 ± 4	–1 ± 6
E(Li$^+$– CH_2Cl_{2incl}) / kJ mol^{-1}	–	–	–	4 ± 3
t / t_{tot}	0.009	0.129	0.760	0.102
N(coordinated nitrogen atoms)	1.00	1.43	0.708	1.00
N($SOLV_{incl}$)	–	1	1	8
$\bar{d}$ / Å[a]	7.81 8.01	7.88 7.93	7,86 8,03	7.86 7.90
$\sigma(\bar{d})$ / Å	0.48 0.47	0.30 0.35	0.27 0.29	0.29 0.29

[a] Average distance between the opposing aromatic carbon atoms directly bound to *tert*-butyl groups.

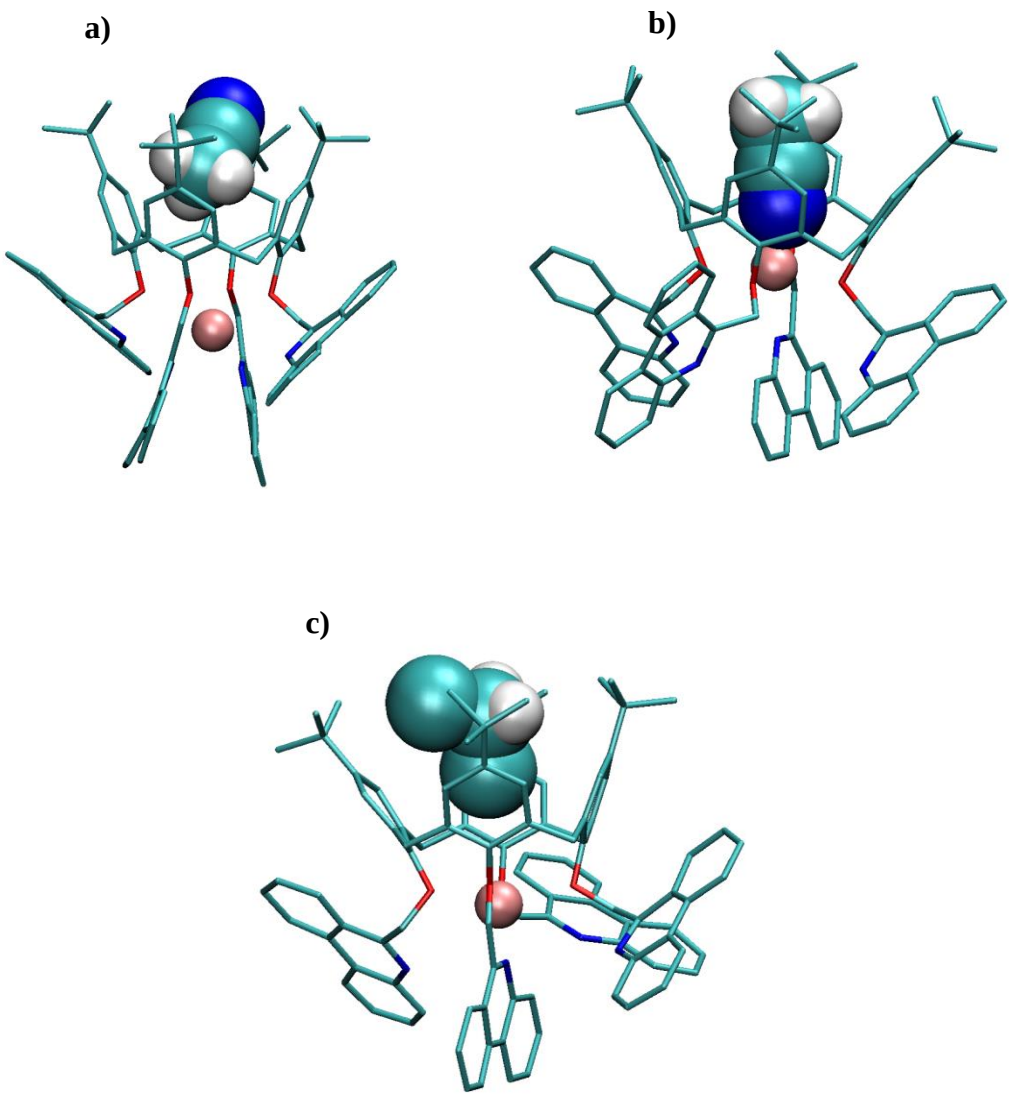

Figure S50. Molecular structures of **a)** Li**1**MeCN$^+$, **b)** Li**1**MeCN'$^+$ and **c)** Li**1**$CH_2Cl_2^+$ adducts obtained by MD simulation of Li**1**$^+$ in MeCN/CH_2Cl_2 mixture ($\varphi = 0.5$) at 25 °C. Hydrogen atoms bound to carbon atoms of **1** have been omitted for clarity.

Table S15. Energies of interactions of **3** with lithium cation, acetonitrile, and dichloromethane, occurrence time ratio of different chemical species, and the number of phenanthridine nitrogen atoms which coordinate metal cation in the complexes obtained by MD simulations in $MeCN/CH_2Cl_2$ mixture (φ = 0.5) at 25 °C; t_{tot} = 50 ns.

	Li**3**$^+$	Li**3**MeCN$^+$	Li**3**MeCN'$^+$
E(Li$^+$–**3**) / kJ mol^{-1}	–332 ± 61	–332 ± 11	–294 ± 12
E(**3**–MeCN) / kJ mol^{-1}	–219 ± 22	–235 ± 28	–138 ± 35
E(**3**–$MeCN_{incl}$) / kJ mol^{-1}	–	–48 ± 12	15 ± 7
E(**3**–CH_2Cl_2) / kJ mol^{-1}	–224 ± 31	–264 ± 34	–306 ± 44
E(Li$^+$– MeCN) / kJ mol^{-1}	–25 ± 8	–20 ± 12	–131 ± 8
E(Li$^+$– $MeCN_{incl}$) / kJ mol^{-1}	–	10 ± 4	–121 ± 6
E(Li$^+$– CH_2Cl_2) / kJ mol^{-1}	–6 ± 5	–8 ± 7	–6 ± 5
t / t_{tot}	0.001	0.019	0.981
N(coordinated nitrogen atoms)	1.00	1.01	0.104
N($SOLV_{incl}$)	–	2	1
$\bar{d}$ / Å	7.37	7.83	7.83
	8.31	8.09	8.25
$\sigma(\bar{d})$ / Å	0.49	0.28	0.29
	0.31	0.31	0.31

[a] Average distance between the opposing aromatic carbon atoms directly bound to *tert*-butyl groups.

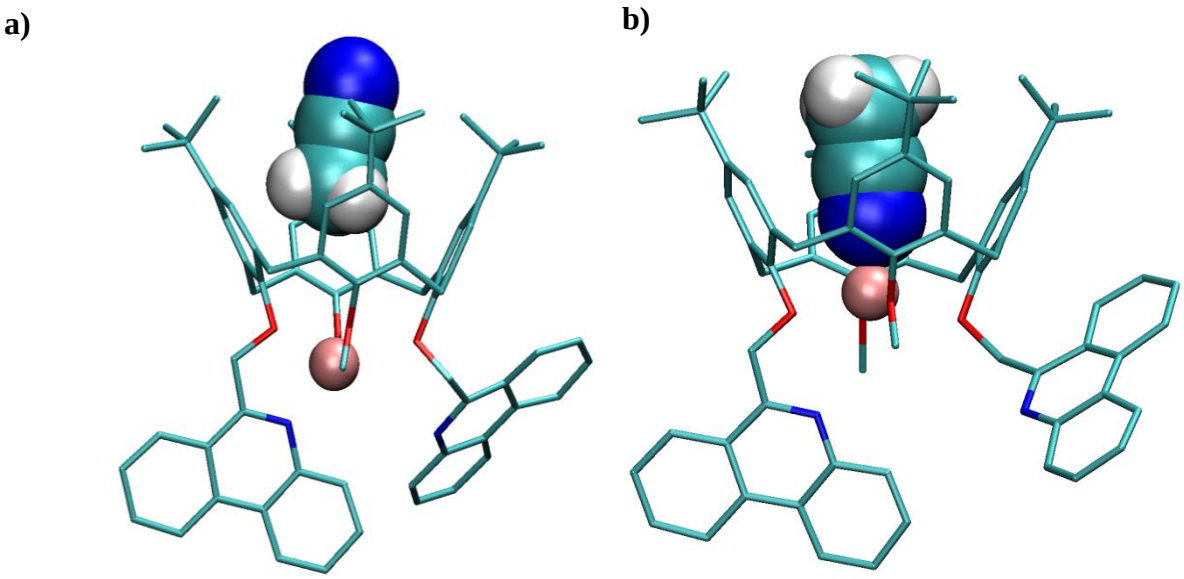

Figure S51. Molecular structures of **a)** Li**3**MeCN^{+} and **b)** Li**3**MeCN'$^{+}$ adducts obtained by MD simulation of Li**3**$^{+}$ in MeCN/CH_2Cl_2 mixture (φ = 0.5) at 25 °C. Hydrogen atoms bound to carbon atoms of **3** have been omitted for clarity.

Table S16. Energies of interactions of **1** with sodium cation, acetonitrile, and dichloromethane, occurrence time ratio of different chemical species, and the number of phenanthridine nitrogen atoms which coordinate metal cation in the complexes obtained by MD simulations in $MeCN/CH_2Cl_2$ mixture (φ = 0.5) at 25 °C; t_{tot} = 50 ns.

	$Na\mathbf{1}MeCN^+$
$E(Na^+–\mathbf{1})$ / kJ mol^{-1}	–304 ± 9
$E(\mathbf{1}–MeCN)$ / kJ mol^{-1}	–234 ± 36
$E(\mathbf{1}–MeCN_{incl})$ / kJ mol^{-1}	–51 ± 5
$E(\mathbf{1}–CH_2Cl_2)$ / kJ mol^{-1}	–386 ± 47
$E(Na^+–MeCN)$ / kJ mol^{-1}	–12 ± 11
$E(Na^+–MeCN_{incl})$ / kJ mol^{-1}	9 ± 2
$E(Na^+–CH_2Cl_2)$ / kJ mol^{-1}	–7 ± 6
t / t_{tot}	1
N(coordinated nitrogen atoms)	1.99
$N(SOLV_{incl})$	1
$\bar{d}$ / Å	7.78 7.89
$\sigma(\bar{d})$ / Å	0.28 0.27

[a] Average distance between the opposing aromatic carbon atoms directly bound to *tert*-butyl groups.

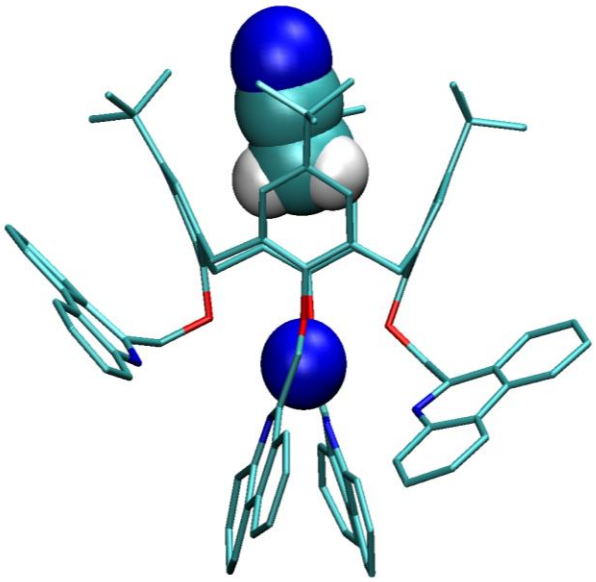

Figure S52. Molecular structure of Na**1**MeCN$^+$ adduct obtained by MD simulation of Na**1**$^+$ in MeCN/CH_2Cl_2 mixture ($\varphi = 0.5$) at 25 °C. Hydrogen atoms bound to carbon atoms of **1** have been omitted for clarity.

Table S17. Energies of interactions of **3** with sodium cation, acetonitrile, and dichloromethane, occurrence time ratio of different chemical species, and the number of phenanthridine nitrogen atoms which coordinate metal cation in the complexes obtained by MD simulations in $MeCN/CH_2Cl_2$ mixture (φ = 0.5) at 25 °C; t_{tot} = 50 ns.

	$Na\mathbf{3}^+$	$Na\mathbf{3}MeCN^+$	$Na\mathbf{3}CH_2Cl_2^+$
$E(Na^+–\mathbf{3})$ / kJ mol^{-1}	–278 ± 17	–280 ± 22	–287 ± 11
$E(\mathbf{3}–MeCN)$ / kJ mol^{-1}	–161 ± 25	–209 ± 34	–167 ± 27
$E(\mathbf{3}–MeCN_{incl})$ / kJ mol^{-1}	–	–51 ± 5	–
$E(\mathbf{3}–CH_2Cl_2)$ / kJ mol^{-1}	–300 ± 32	–300 ± 43	–333 ± 34
$E(\mathbf{3}–CH_2Cl_{2incl})$ / kJ mol^{-1}	–	–	–44 ± 9
$E(Na^+–MeCN)$ / kJ mol^{-1}	–45 ± 16	–33 ± 28	–36 ± 14
$E(Na^+–MeCN_{incl})$ / kJ mol^{-1}	–	9 ± 2	–
$E(Na^+–CH_2Cl_2)$ / kJ mol^{-1}	–7 ± 7	–12 ± 9	–5 ± 7
$E(Na^+–CH_2Cl_{2incl})$ / kJ mol^{-1}	–	–	3 ± 2
t / t_{tot}	0.035	0.891	0.074
N(coordinated nitrogen atoms)	1.73	1.87	1.96
$N(SOLV_{incl})$	–	1	4
$\bar{d}$ / Å	7.57 7.87	7.84 7.87	7.90 7.97
$\sigma(\bar{d})$ / Å	0.69 0.63	0.29 0.28	0.31 0.29

[a] Average distance between the opposing aromatic carbon atoms directly bound to *tert*-butyl groups.

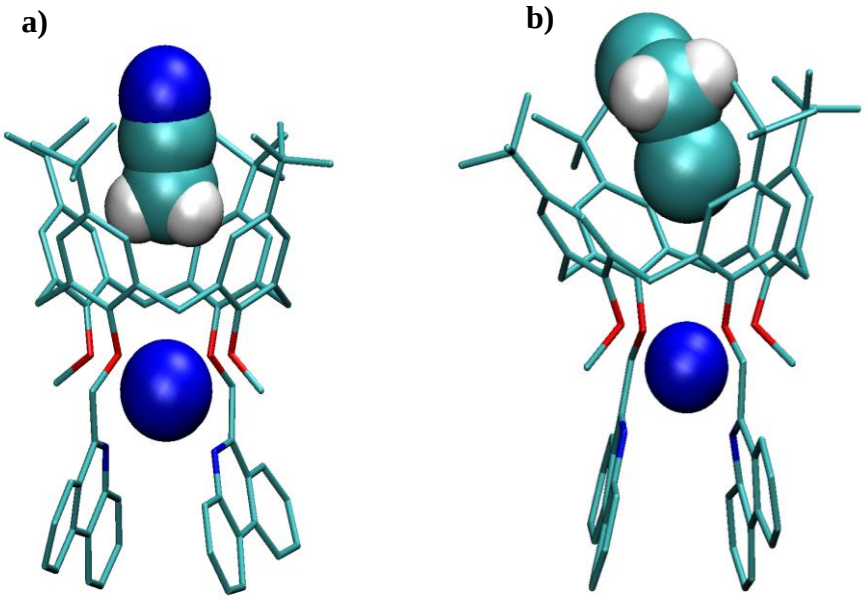

Figure S53. Molecular structures of **a)** Na**3**MeCN$^+$ and **b)** Na**3**$CH_2Cl_2^+$ adducts obtained by MD simulation of Na**3**$^+$ in MeCN/CH_2Cl_2 mixture ($\varphi = 0.5$) at 25 °C. Hydrogen atoms bound to carbon atoms of **3** have been omitted for clarity.

Table S18. Energies of interactions of **1** with potassium cation, acetonitrile, and dichloromethane, occurrence time ratio of different chemical species, and the number of phenanthridine nitrogen atoms which coordinate metal cation in the complexes obtained by MD simulations in $MeCN/CH_2Cl_2$ mixture (φ = 0.5) at 25 °C; t_{tot} = 50 ns.

	$K\mathbf{1}^+$	$K\mathbf{1}MeCN^+$
$E(K^+–\mathbf{1})$ / kJ mol^{-1}	–233 ± 8	–232 ± 9
$E(\mathbf{1}–MeCN)$ / kJ mol^{-1}	–210 ± 40	–231 ± 36
$E(\mathbf{1}–MeCN_{incl})$ / kJ mol^{-1}	–	–51 ± 5
$E(\mathbf{1}–CH_2Cl_2)$ / kJ mol^{-1}	–347 ± 49	–386 ± 46
$E(K^+–MeCN)$ / kJ mol^{-1}	–24 ± 15	–18 ± 17
$E(K^+–MeCN_{incl})$ / kJ mol^{-1}	–	8 ± 2
$E(K^+–CH_2Cl_2)$ / kJ mol^{-1}	–6 ± 6	–8 ± 7
t / t_{tot}	0.008	0.992
N(coordinated nitrogen atoms)	1.98	1.98
$N(SOLV_{incl})$	–	2
$\bar{d}$ / Å	7.26	7.73
	8.11	7.87
$\sigma(\bar{d})$ / Å	0.58	0.26
	0.48	0.27

[a] Average distance between the opposing aromatic carbon atoms directly bound to *tert*-butyl groups.

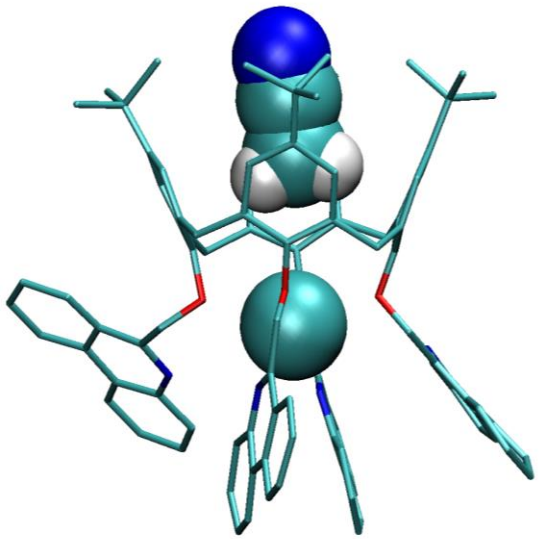

Figure S54. Molecular structure of K**1**MeCN$^+$ adduct obtained by MD simulation of K**1**$^+$ in MeCN/CH_2Cl_2 mixture ($\varphi = 0.5$) at 25 °C. Hydrogen atoms bound to carbon atoms of **1** have been omitted for clarity.

Table S19. Energies of interactions of **1** with rubidium cation, acetonitrile, and dichloromethane, occurrence time ratio of different chemical species, and the number of phenanthridine nitrogen atoms which coordinate metal cation in the complexes obtained by MD simulations in $MeCN/CH_2Cl_2$ mixture (φ = 0.5) at 25 °C; t_{tot} = 50 ns.

	$Rb\mathbf{1}^+$	$Rb\mathbf{1}MeCN^+$	$Rb\mathbf{1}CH_2Cl_2^+$
$E(Rb^+–\mathbf{1})$ / kJ mol^{-1}	–219 ± 10	–193 ± 20	–207 ± 17
$E(\mathbf{1}–MeCN)$ / kJ mol^{-1}	–177 ± 33	–223 ± 37	–178 ± 39
$E(\mathbf{1}–MeCN_{incl})$ / kJ mol^{-1}	–	–52 ± 5	–
$E(\mathbf{1}–CH_2Cl_2)$ / kJ mol^{-1}	–385 ± 44	–378 ± 49	–417± 54
$E(\mathbf{1}–CH_2Cl_{2incl})$ / kJ mol^{-1}	–	–	–46 ± 9
$E(Rb^+–MeCN)$ / kJ mol^{-1}	–10 ± 13	–54 ± 31	–35 ± 30
$E(Rb^+–MeCN_{incl})$ / kJ mol^{-1}	–	5 ± 1	–
$E(Rb^+–CH_2Cl_2)$ / kJ mol^{-1}	–7 ± 5	–6 ± 5	–4 ± 6
$E(Rb^+–CH_2Cl_{2incl})$ / kJ mol^{-1}	–	–	3 ± 1
t / t_{tot}	0.055	0.877	0.068
N(coordinated nitrogen atoms)	2.15	2.42	2.48
$N(SOLV_{incl})$	–	2	6
$\bar{d}$ / Å	6.72 8.52	7.82 7.88	7.69 8.13
$\sigma(\bar{d})$ / Å	0.56 0.39	0.30 0.30	0.36 0.30

[a] Average distance between the opposing aromatic carbon atoms directly bound to *tert*-butyl groups.

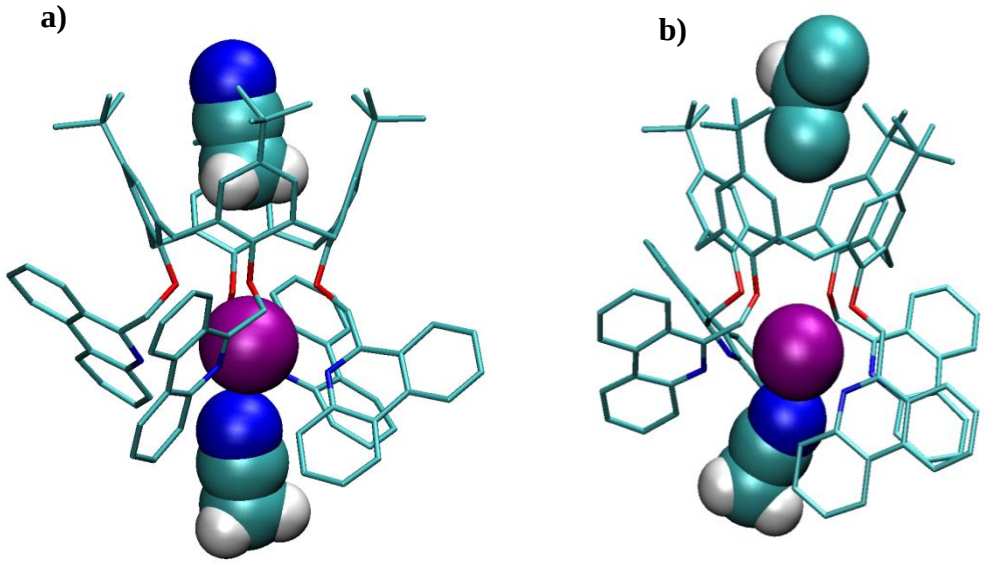

Figure S55. Molecular structures of a) Rb**1**$(MeCN)_2^+$ and b) Rb**1**$(CH_2Cl_2)(MeCN)^+$ adducts obtained by MD simulation of Rb**1**$^+$ in $MeCN/CH_2Cl_2$ mixture ($\varphi = 0.5$) at 25 °C. Hydrogen atoms bound to carbon atoms of **1** have been omitted for clarity.

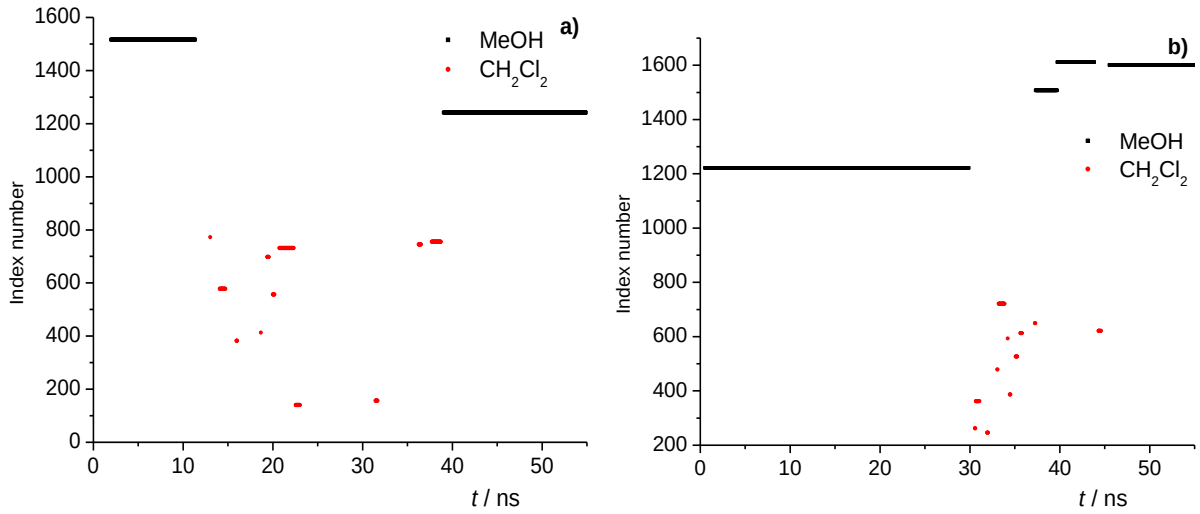

Figure S56. Index numbers of methanol and dichloromethane molecules that occupied hydrophobic cavity of **a)** ligand **1** and **b)** ligand **3** during MD simulations in MeOH/CH_2Cl_2 mixture (φ = 0.5) at 25 °C.

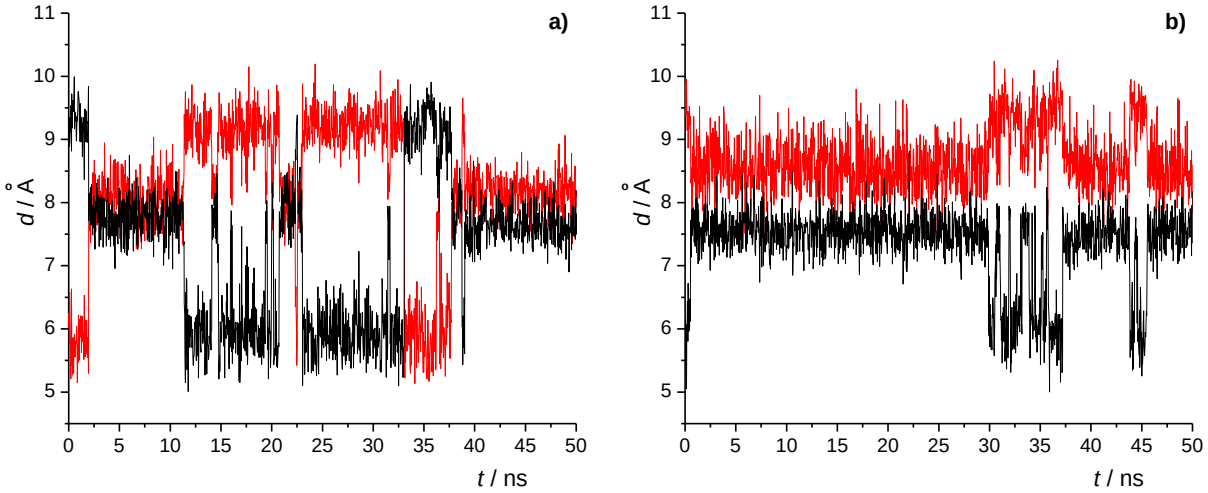

Figure S57. Distances between the opposing phenyl carbon atoms that are directly connected to the *tert*-butyl group during the MD simulations of **a)** ligand **1** and **b)** ligand **3** in MeOH/CH_2Cl_2 mixture (φ = 0.5) at 25 °C.

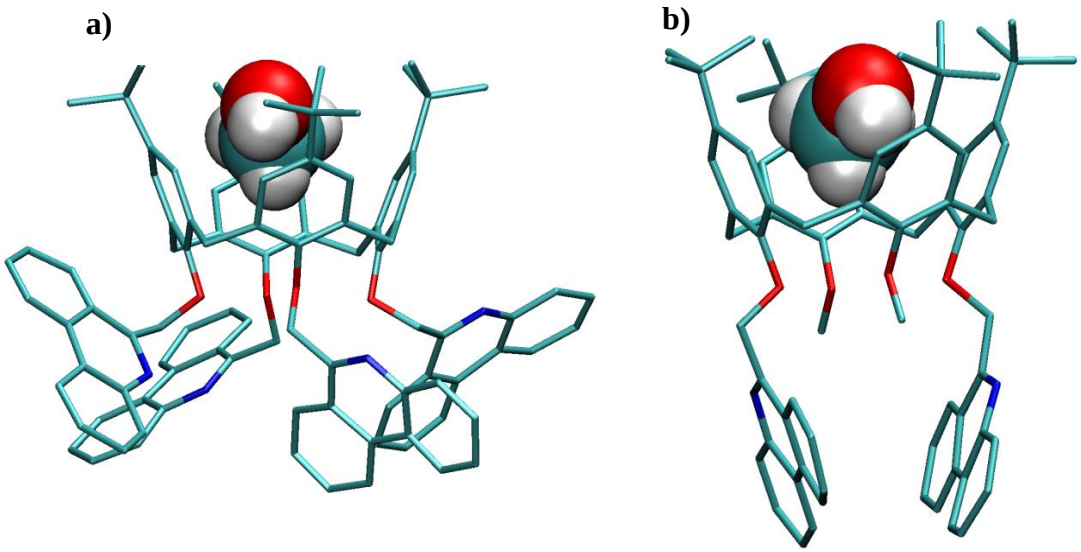

Figure S58. Molecular structures of **a) 1**MeOH and **b) 3**MeOH adducts obtained by MD simulation of **1** and **3** in MeOH/CH_2Cl_2 mixture ($\varphi = 0.5$) at 25 °C. Hydrogen atoms bound to carbon atoms of **1** and **3** have been omitted for clarity.

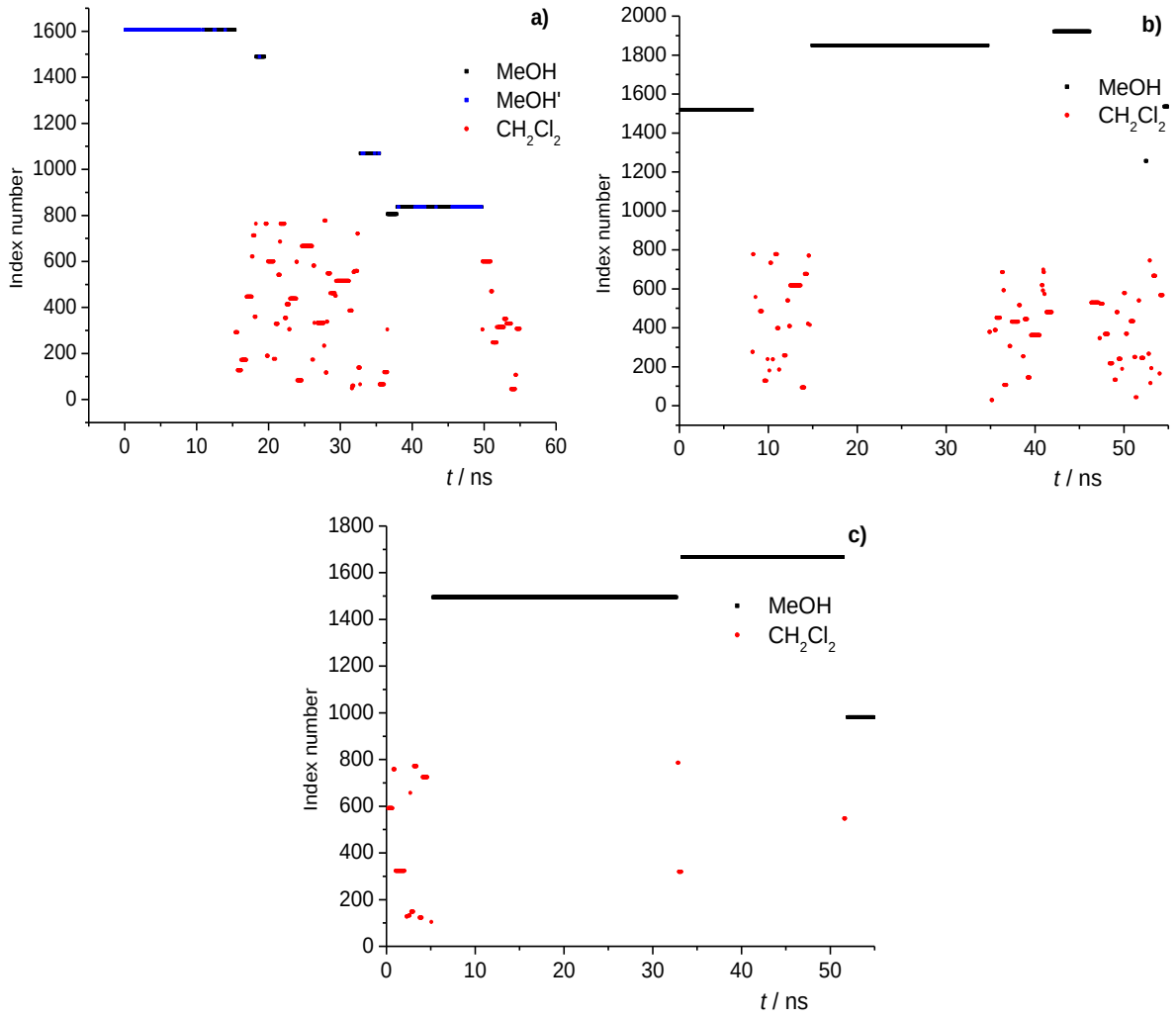

Figure S59. Index numbers of methanol and dichloromethane molecules that occupied hydrophobic cavity of **a)** Na**1**$^+$, **b)** K**1**$^+$, and **c)** Rb**1**$^+$ complexes during MD simulations in MeOH/CH_2Cl_2 mixture (φ = 0.5) at 25 °C.

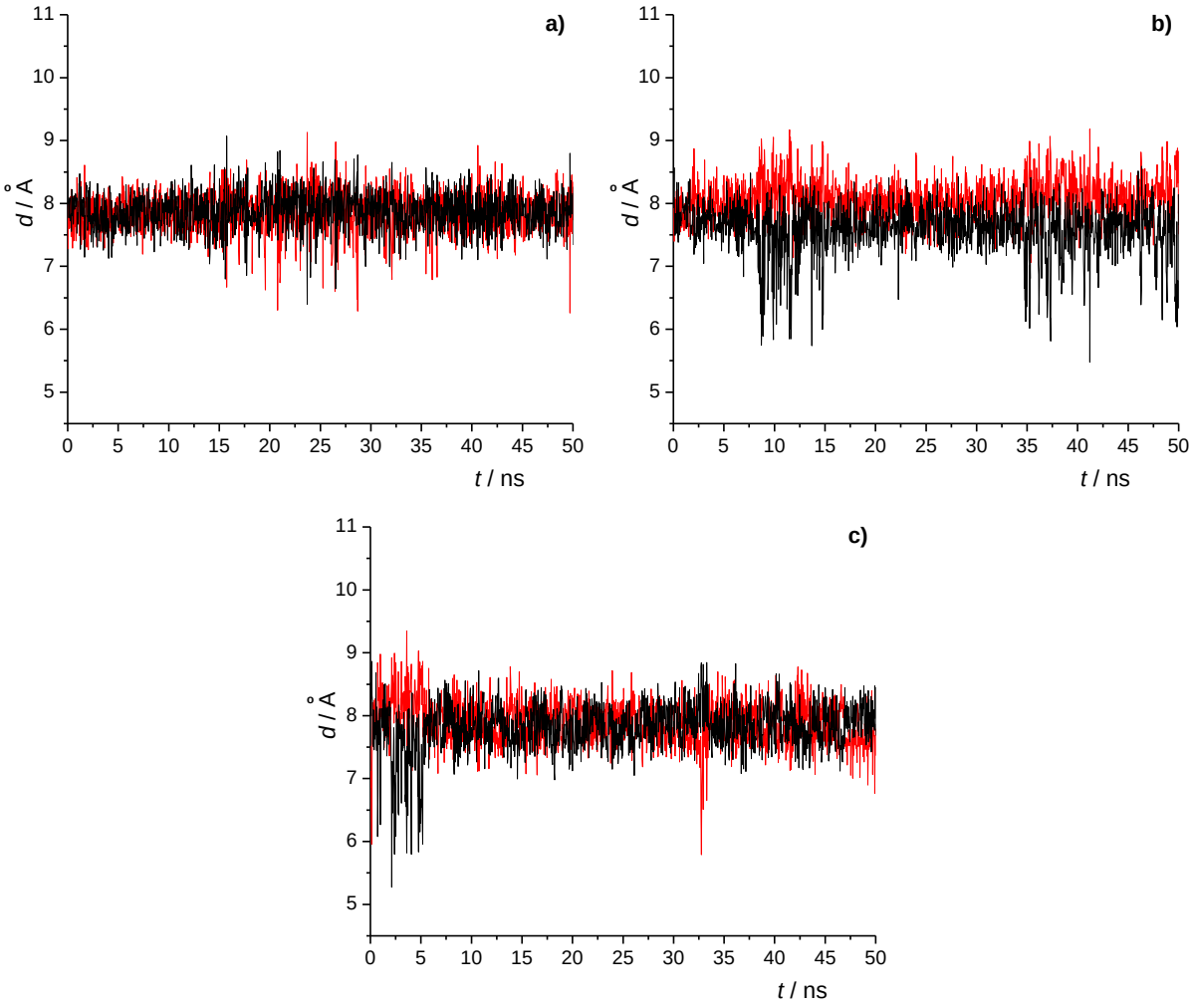

Figure S60. Distances between the opposing phenyl carbon atoms that are directly connected to the *tert*-butyl group during the MD simulations of **a)** Na**1**$^+$, **b)** K**1**$^+$ and **c)** Rb**1**$^+$ in MeOH/CH_2Cl_2 mixture (φ = 0.5) at 25 °C.

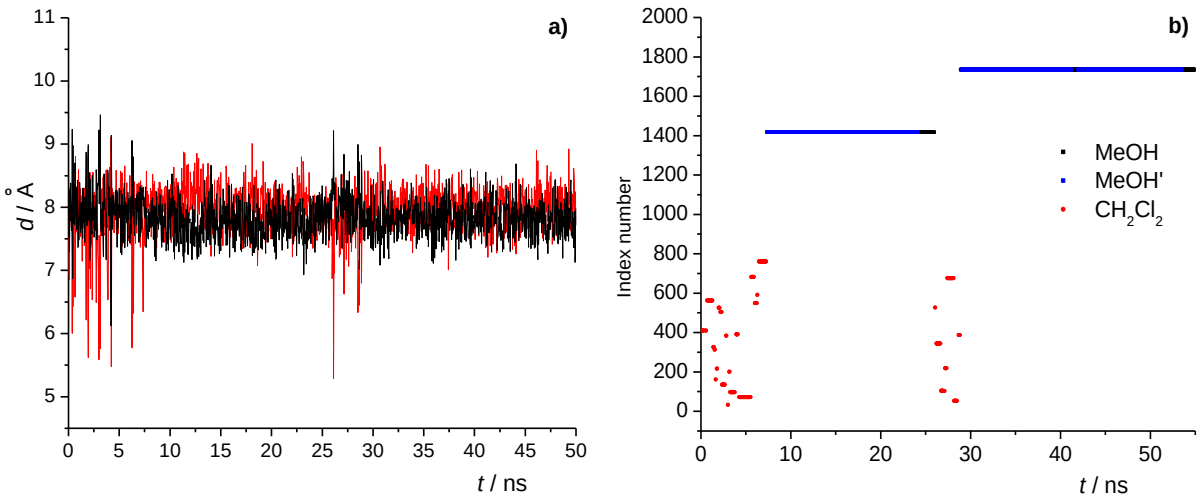

Figure S61. a) Distances between the opposing phenyl carbon atoms that are directly connected to the *tert*-butyl group during the MD simulations of Na**3**$^+$ in MeOH/CH_2Cl_2 mixture (φ = 0.5) at 25 °C. **b)** Index numbers of methanol and dichloromethane molecules that occupied hydrophobic cavity of Na**3**$^+$ complex.

Table S20. Energies of interactions of **1** with sodium cation, methanol, and dichloromethane, occurrence time ratio of different chemical species, and the number of phenanthridine nitrogen atoms which coordinate metal cation in the complexes obtained by MD simulations in $MeOH/CH_2Cl_2$ mixture (φ = 0.5) at 25 °C; t_{tot} = 50 ns.

	$Na\mathbf{1}^+$	$Na\mathbf{1}MeOH^+$	$Na\mathbf{1}MeOH'^+$	$Na\mathbf{1}CH_2Cl_2^+$
$E(Na^+–\mathbf{1})$ / kJ mol^{-1}	–307 ± 11	–307 ± 14	–247 ± 16	–287 ± 11
$E(\mathbf{1}–MeOH)$ / kJ mol^{-1}	–157 ± 46	–214 ± 48	–183 ± 44	–167 ± 27
$E(\mathbf{1}–MeOH_{incl})$ / kJ mol^{-1}	–	–47 ± 7	–64 ± 15	–
$E(\mathbf{1}–CH_2Cl_2)$ / kJ mol^{-1}	–434 ± 58	–415 ± 58	–416 ± 54	–333 ± 34
$E(\mathbf{1}–CH_2Cl_{2incl})$ / kJ mol^{-1}	–	–	–	–47 ± 7
$E(Na^+–MeOH)$ / kJ mol^{-1}	–3 ± 5	1 ± 15	–66 ± 15	–36 ± 14
$E(Na^+–MeOH_{incl})$ / kJ mol^{-1}	–	7 ± 4	–13 ± 9	–
$E(Na^+–CH_2Cl_2)$ / kJ mol^{-1}	–9 ± 6	–11 ± 6	–6 ± 4	–5 ± 7
$E(Na^+–CH_2Cl_{2incl})$ / kJ mol^{-1}	–	–	–	4 ± 2
t / t_{tot}	0.088	0.332	0.264	0.316
N(coordinated nitrogen atoms)	1.96	1.94	0.68	1.99
$N(SOLV_{incl})$	–	2	5	51
$\bar{d}$ / Å	7.64	7.85	7.83	7.91
	7.90	7.85	7.88	7.92
$\sigma(\bar{d})$ / Å	0.59	0.27	0.27	0.31
	0.52	0.27	0.27	0.30

[a] Average distance between the opposing aromatic carbon atoms directly bound to *tert*-butyl groups.

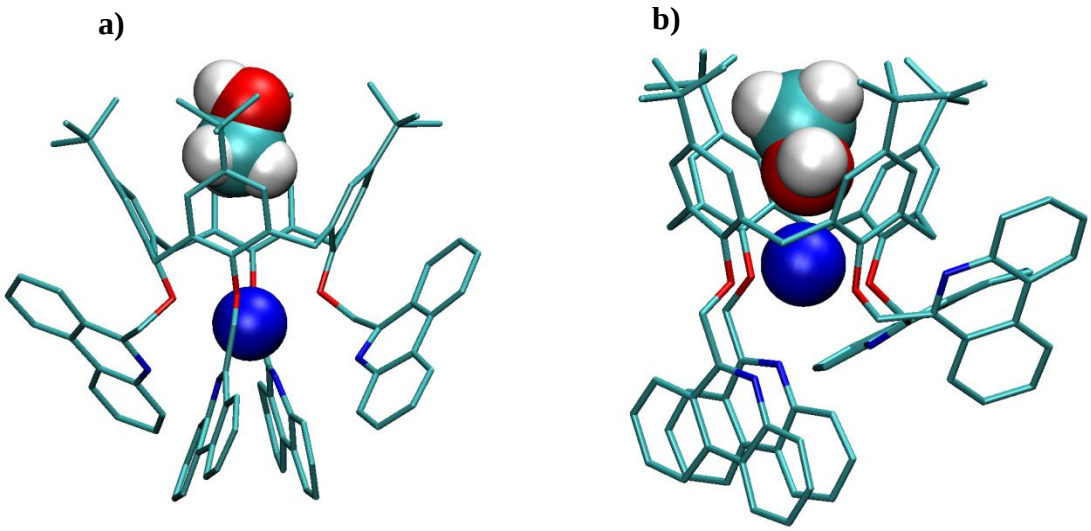

Figure S62. Molecular structure of **a)** Na**1**MeOH$^+$ and **b)** Na**1**MeOH**'**$^+$ adducts obtained by MD simulation of Na**1**$^+$ in MeOH/CH_2Cl_2 mixture ($\varphi = 0.5$) at 25 °C. Hydrogen atoms bound to carbon atoms of **1** have been omitted for clarity.

Table S21. Energies of interactions of **3** with sodium cation, methanol, and dichloromethane, occurrence time ratio of different chemical species, and the number of phenanthridine nitrogen atoms which coordinate metal cation in the complexes obtained by MD simulations in $MeOH/CH_2Cl_2$ mixture (φ = 0.5) at 25 °C; t_{tot} = 50 ns.

	$Na\mathbf{3}^+$	$Na\mathbf{3}MeOH^+$	$Na\mathbf{3}MeOH'^+$	$Na\mathbf{3}CH_2Cl_2^+$
$E(Na^+$–**3**) / kJ mol^{-1}	–290 ± 12	–288 ± 11	–230 ± 18	–286 ± 12
E(**3**–MeOH) / kJ mol^{-1}	–134 ± 39	–205 ± 38	–157 ± 39	–140 ± 38
E(**3**–$MeOH_{incl}$) / kJ mol^{-1}	–	–47 ± 7	–11 ± 5	–
E(**3**–CH_2Cl_2) / kJ mol^{-1}	–355 ± 54	–323 ± 43	–329 ± 46	–381 ± 48
E(**3**–CH_2Cl_{2incl}) / kJ mol^{-1}	–	–	–	–44 ± 10
$E(Na^+$– MeOH) / kJ mol^{-1}	–9 ± 10	–7 ± 14	–75 ± 15	–14 ± 13
$E(Na^+$– $MeOH_{incl}$) / kJ mol^{-1}	–	7 ± 6	–75 ± 7	–
$E(Na^+$– CH_2Cl_2) / kJ mol^{-1}	–18 ± 8	–19 ± 8	–9 ± 5	–15 ± 10
$E(Na^+$– CH_2Cl_{2incl}) / kJ mol^{-1}	–	–	–	4 ± 2
t / t_{tot}	0.048	0.067	0.762	0.123
N(coordinated nitrogen atoms)	1.94	1.95	0.21	1.92
N($SOLV_{incl}$)	–	2	2	27
$\bar{d}$ / Å	7.29	7.83	7.78	7.92
	8.18	7.88	8.02	7.97
$\sigma(\bar{d})$ / Å	0.76	0.28	0.28	0.32
	0.53	0.27	0.29	0.30

[a] Average distance between the opposing aromatic carbon atoms directly bound to *tert*-butyl groups.

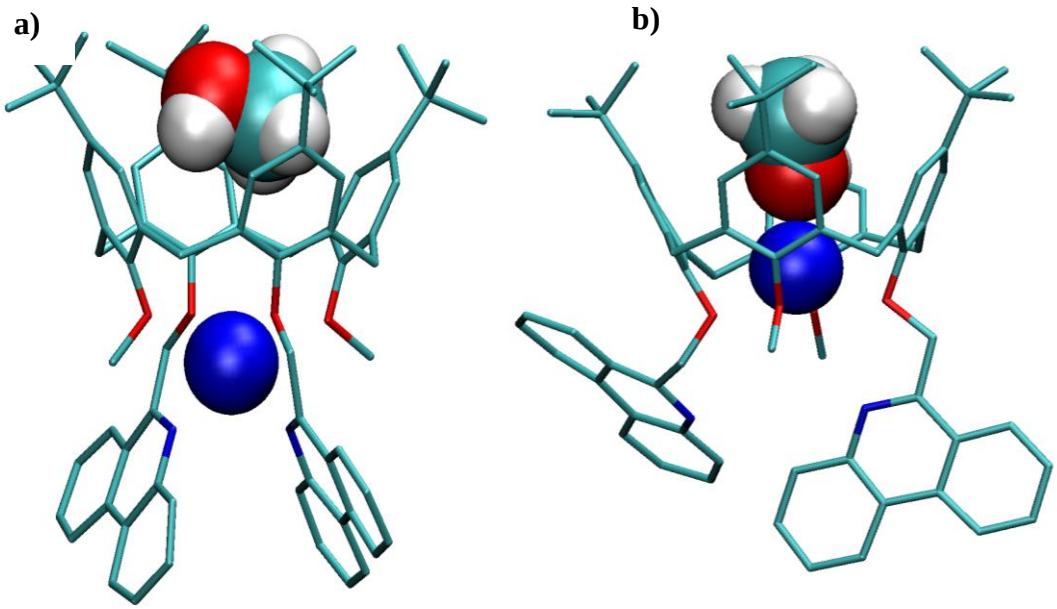

Figure S63. Molecular structures of **a)** Na**3**MeOH^{+} and **b)** Na**3**MeOH'$^{+}$ adducts obtained by MD simulation of Na**3**$^{+}$ in MeOH/CH_2Cl_2 mixture ($\varphi = 0.5$) at 25 °C. Hydrogen atoms bound to carbon atoms of **3** have been omitted for clarity.

Table S22. Energies of interactions of **1** with potassium cation, methanol, and dichloromethane, occurrence time ratio of different chemical species, and the number of phenanthridine nitrogen atoms which coordinate metal cation in the complexes obtained by MD simulations in $MeOH/CH_2Cl_2$ mixture (φ = 0.5) at 25 °C; t_{tot} = 50 ns.

	$K\mathbf{1}^+$	$K\mathbf{1}MeOH^+$	$K\mathbf{1}CH_2Cl_2^+$
$E(K^+–\mathbf{1})$ / kJ mol^{-1}	–244 ± 9	–208 ± 39	–244 ± 8
$E(\mathbf{1}–MeOH)$ / kJ mol^{-1}	–167 ± 40	–208 ± 39	–160 ± 39
$E(\mathbf{1}–MeOH_{incl})$ / kJ mol^{-1}	–	–48 ± 6	–
$E(\mathbf{1}–CH_2Cl_2)$ / kJ mol^{-1}	–414 ± 52	–425 ± 47	–459 ± 51
$E(\mathbf{1}–CH_2Cl_{2incl})$ / kJ mol^{-1}	–	–	–46 ± 9
$E(K^+–MeOH)$ / kJ mol^{-1}	–3 ± 7	–10 ± 26	–3 ± 5
$E(K^+–MeOH_{incl})$ / kJ mol^{-1}	–	5 ± 1	–
$E(K^+–CH_2Cl_2)$ / kJ mol^{-1}	–9 ± 5	–10 ± 5	–6 ± 6
$E(K^+–CH_2Cl_{2incl})$ / kJ mol^{-1}	–	–	3 ± 2
t / t_{tot}	0.196	0.587	0.217
N(coordinated nitrogen atoms)	2.00	1.85	2.01
$N(SOLV_{incl})$	–	5	60
$\bar{d}$ / Å	7.07 8.31	7.69 7.98	7.72 8.08
$\sigma(\bar{d})$ / Å	0.61 0.46	0.27 0.28	0.30 0.29

[a] Average distance between the opposing aromatic carbon atoms directly bound to *tert*-butyl groups.

Table S23. Energies of interactions of **1** with rubidium cation, methanol, and dichloromethane, occurrence time ratio of different chemical species, and the number of phenanthridine nitrogen atoms which coordinate metal cation in the complexes obtained by MD simulations in MeOH/CH_2Cl_2 mixture (φ = 0.5) at 25 °C; t_{tot} = 50 ns.

	Rb**1**$^+$	Rb**1**MeOH$^+$	Rb**1**$CH_2Cl_2^+$
E(Rb$^+$–**1**) / kJ mol^{-1}	–215 ± 14	–193 ± 22	–207 ± 19
E(**1**–MeOH) / kJ mol^{-1}	–162 ± 42	–234 ± 42	–178 ± 37
E(**1**–$MeOH_{incl}$) / kJ mol^{-1}	–	–48 ± 6	–
E(**1**–CH_2Cl_2) / kJ mol^{-1}	–421 ± 51	–394 ± 51	–440 ± 48
E(**1**–CH_2Cl_{2incl}) / kJ mol^{-1}	–	–	–47 ± 8
E(Rb$^+$– MeOH) / kJ mol^{-1}	–10 ± 20	–45 ± 32	–26 ± 28
E(Rb$^+$– $MeOH_{incl}$) / kJ mol^{-1}	–	5 ± 1	–
E(Rb$^+$– CH_2Cl_2) / kJ mol^{-1}	–9 ± 5	–8 ± 5	–6 ± 5
E(Rb$^+$– CH_2Cl_{2incl}) / kJ mol^{-1}	–	–	2 ± 1
t / t_{tot}	0.047	0.893	0.06
N(coordinated nitrogen atoms)	1.92	1.53	1.74
N($SOLV_{incl}$)	–	3	14
$\bar{d}$ / Å	6.96	7.83	7.77
	8.31	7.87	8.06
$\sigma(\bar{d})$ / Å	0.78	0.31	0.34
	0.67	0.31	0.32

[a] Average distance between the opposing aromatic carbon atoms directly bound to *tert*-butyl groups.

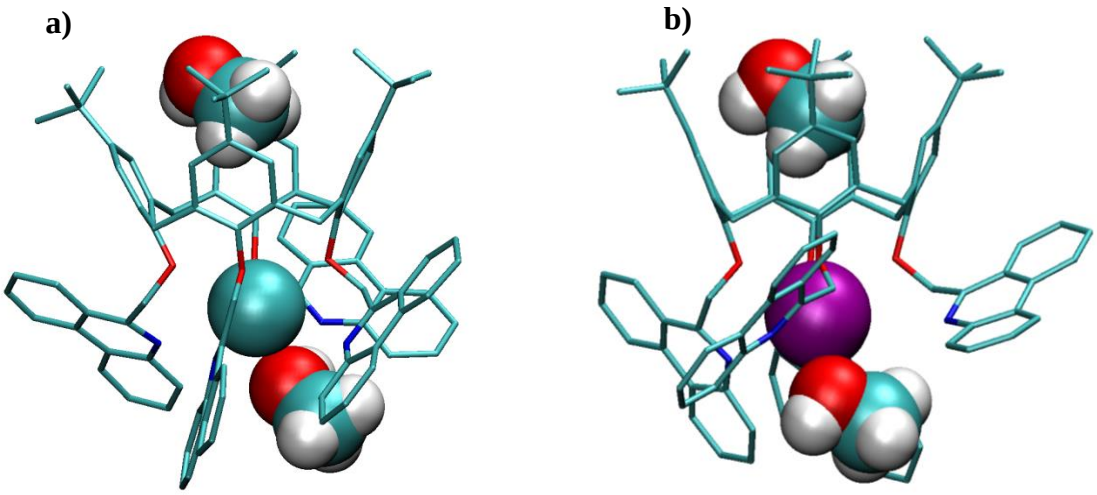

Figure S64. Molecular structures of **a)** K**1**$(MeOH)_2^+$ and **b)** Rb**1**$(MeOH)_2^+$ adducts obtained by MD simulation of K**1**$^+$ and Rb**1**$^+$ in MeOH/CH_2Cl_2 mixture ($\varphi = 0.5$) at 25 °C. Hydrogen atoms bound to carbon atoms of **1** have been omitted for clarity.

DFT results

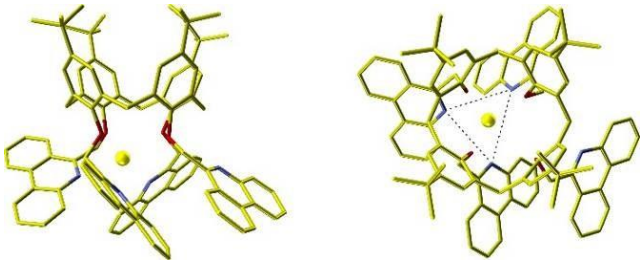

Figure S65. Conformer with the coordination number 7 (C_1 point group): complex of **1** with Na^+. The hydrogen atoms are omitted for clarity.

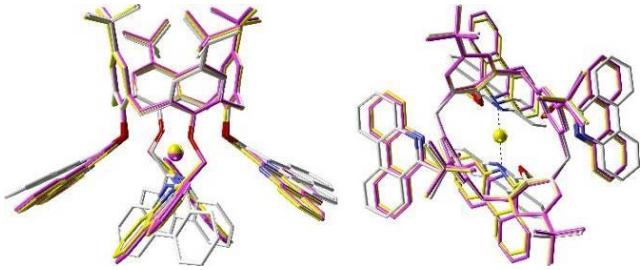

Figure S66. Conformer with the coordination number 6 (C_2 point group): complex of **1** with Li^+ (white), with Na^+ (yellow), with K^+ (purple). The hydrogen atoms are omitted for clarity.

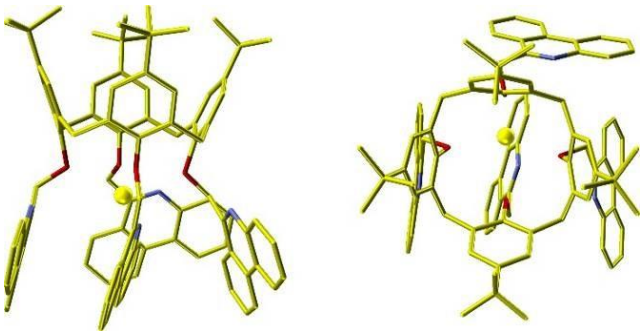

Figure S67. Conformer with the coordination number 5 (C_1 point group): complex of **1** with Na^+. The hydrogen atoms are omitted for clarity.

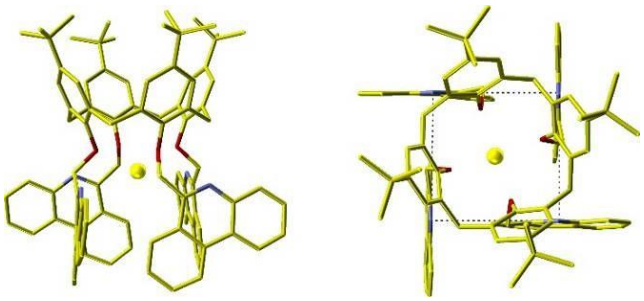

Figure S68. Conformer with the coordination number 4 (C_4 point group): complex of **1** with Na^+. The hydrogen atoms are omitted for clarity.

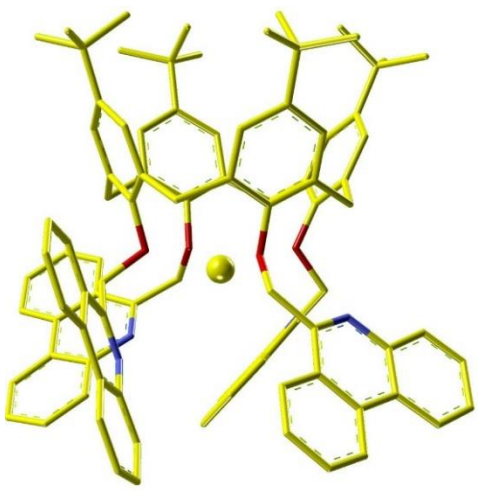

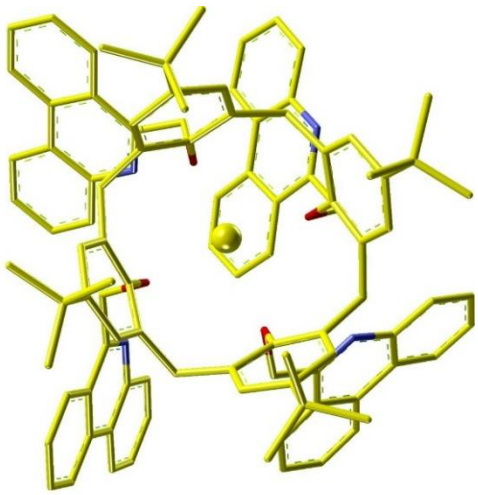

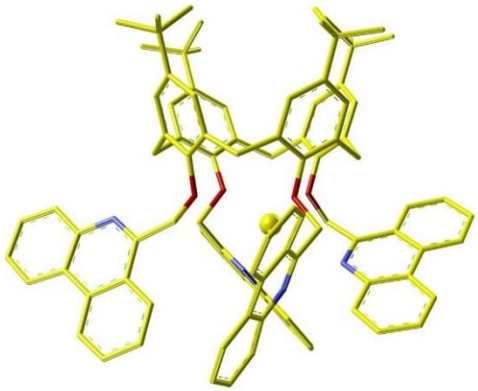

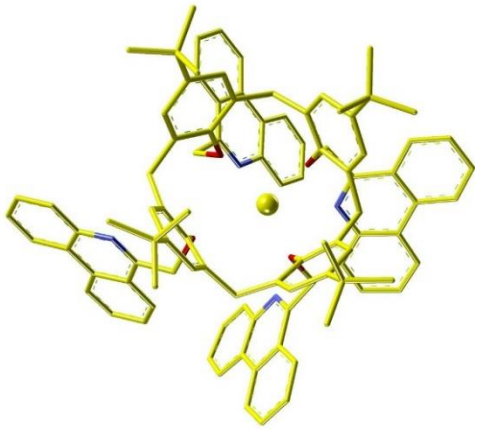

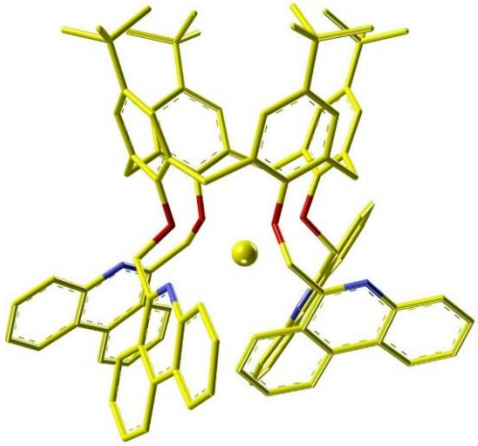

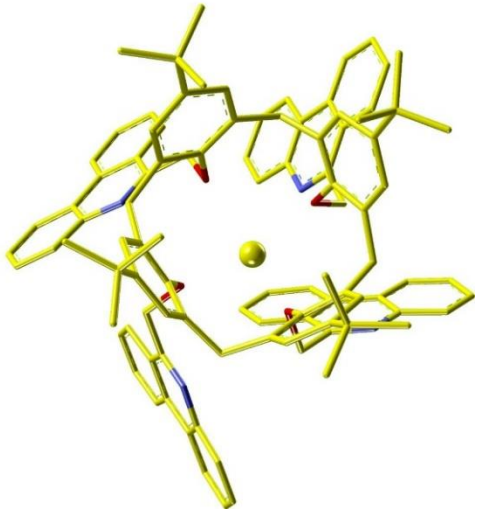

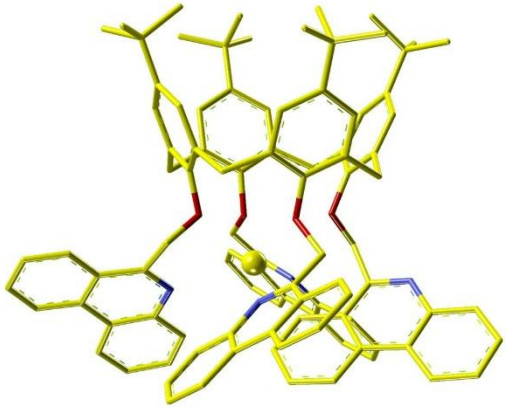

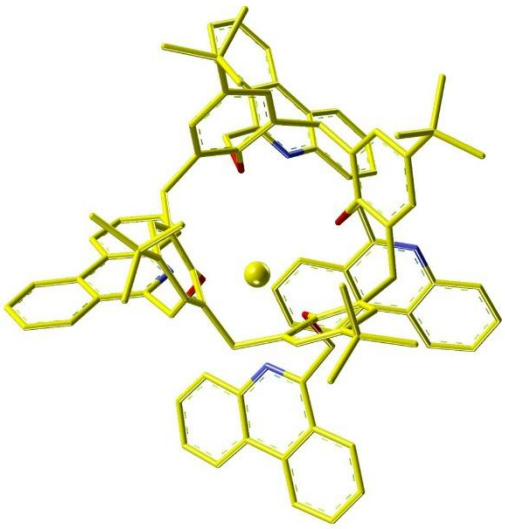

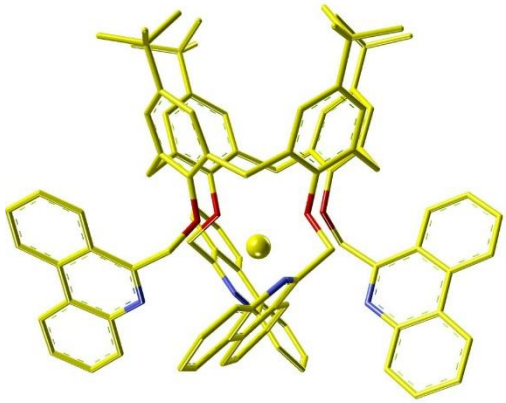

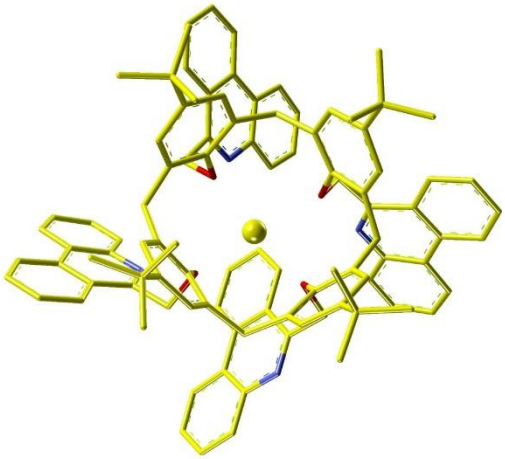

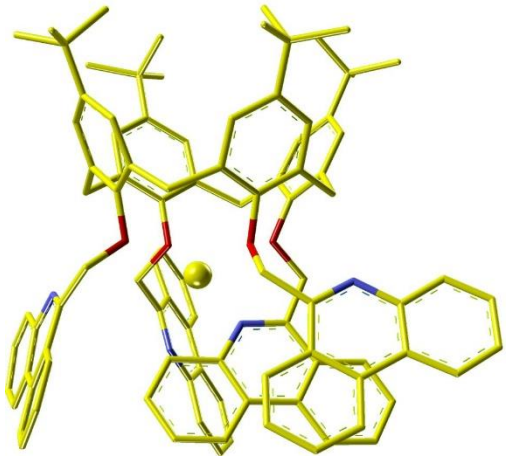

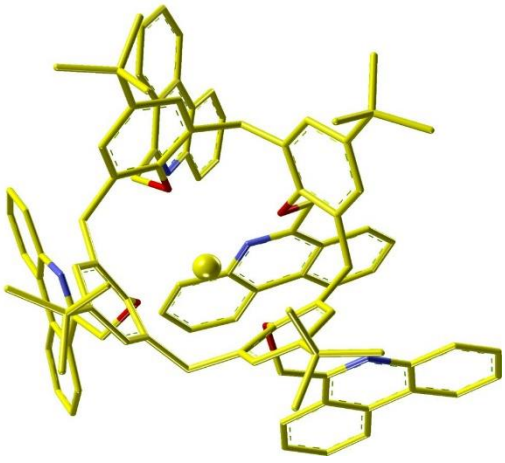

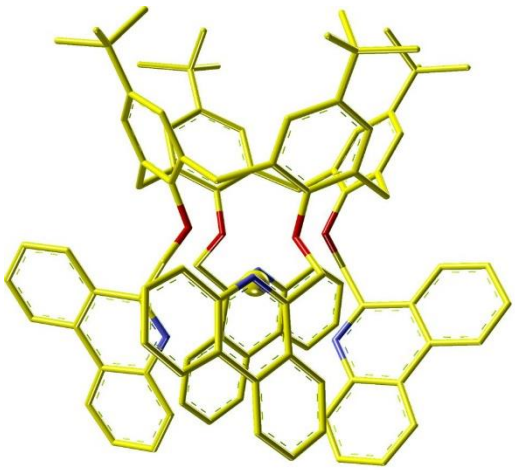
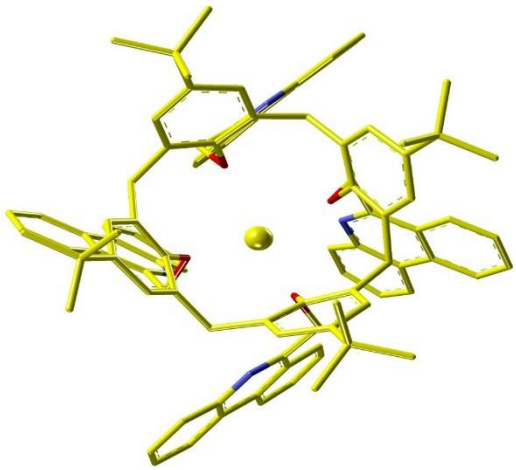
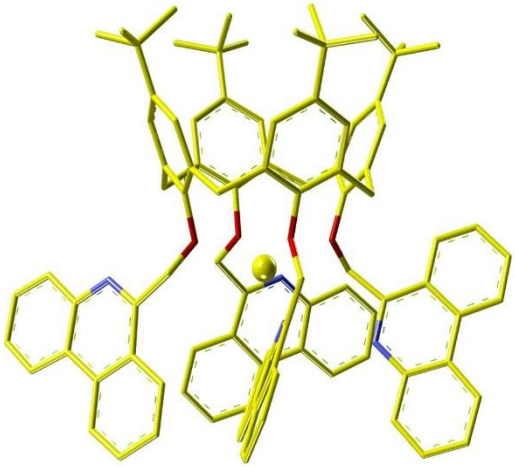
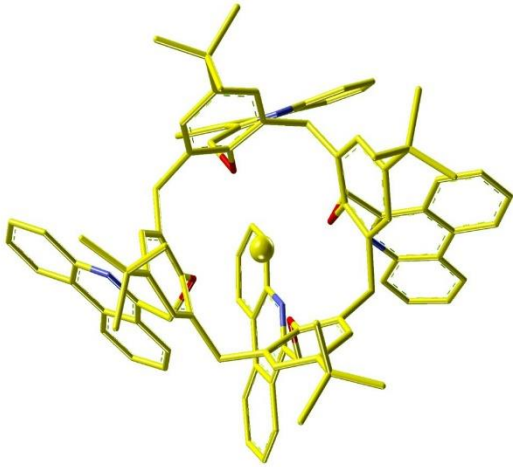
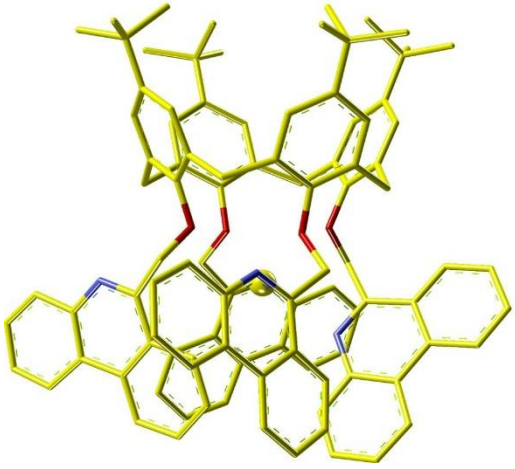
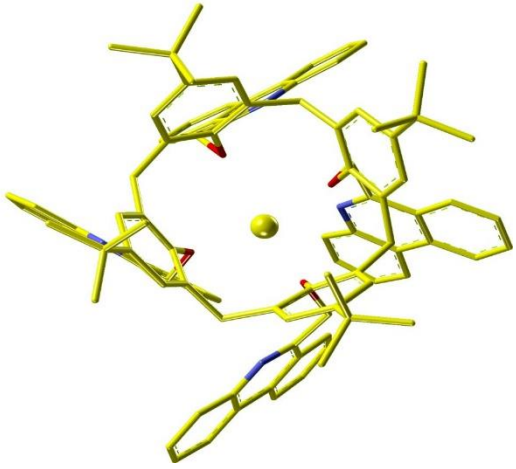

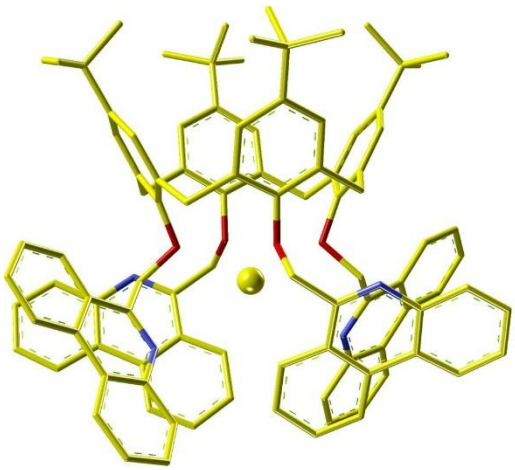
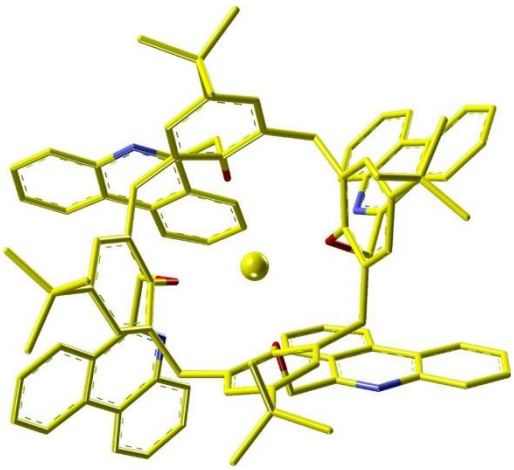
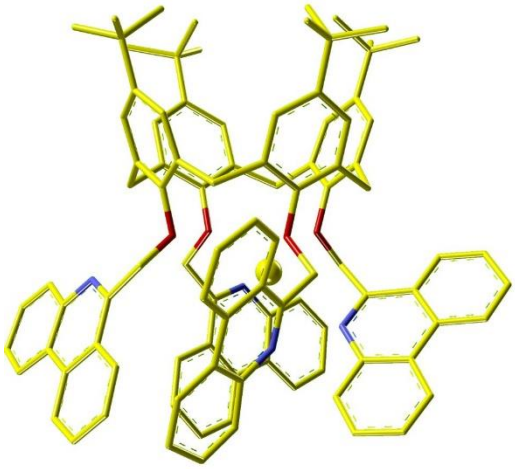
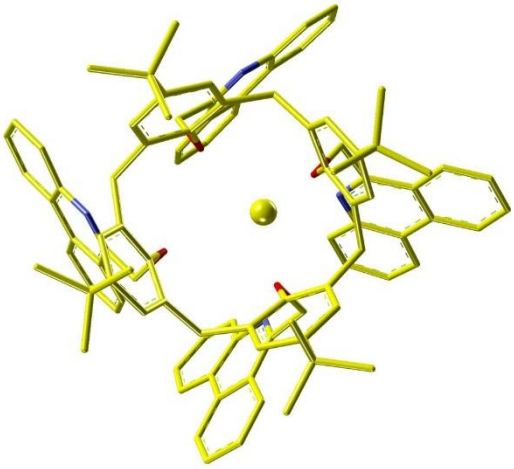
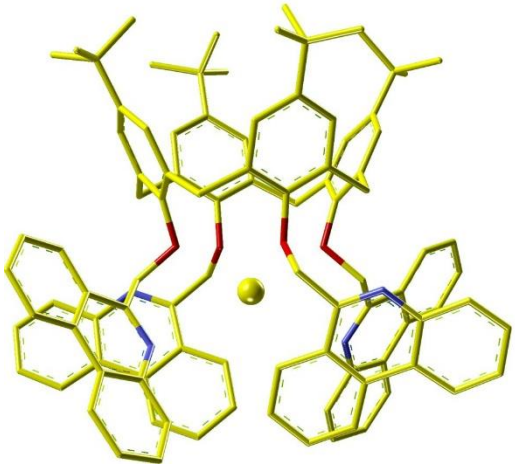
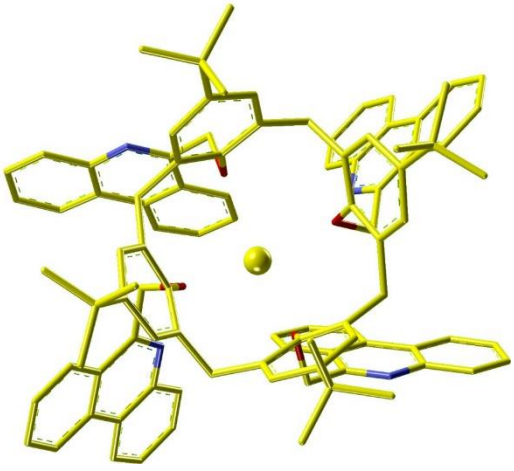

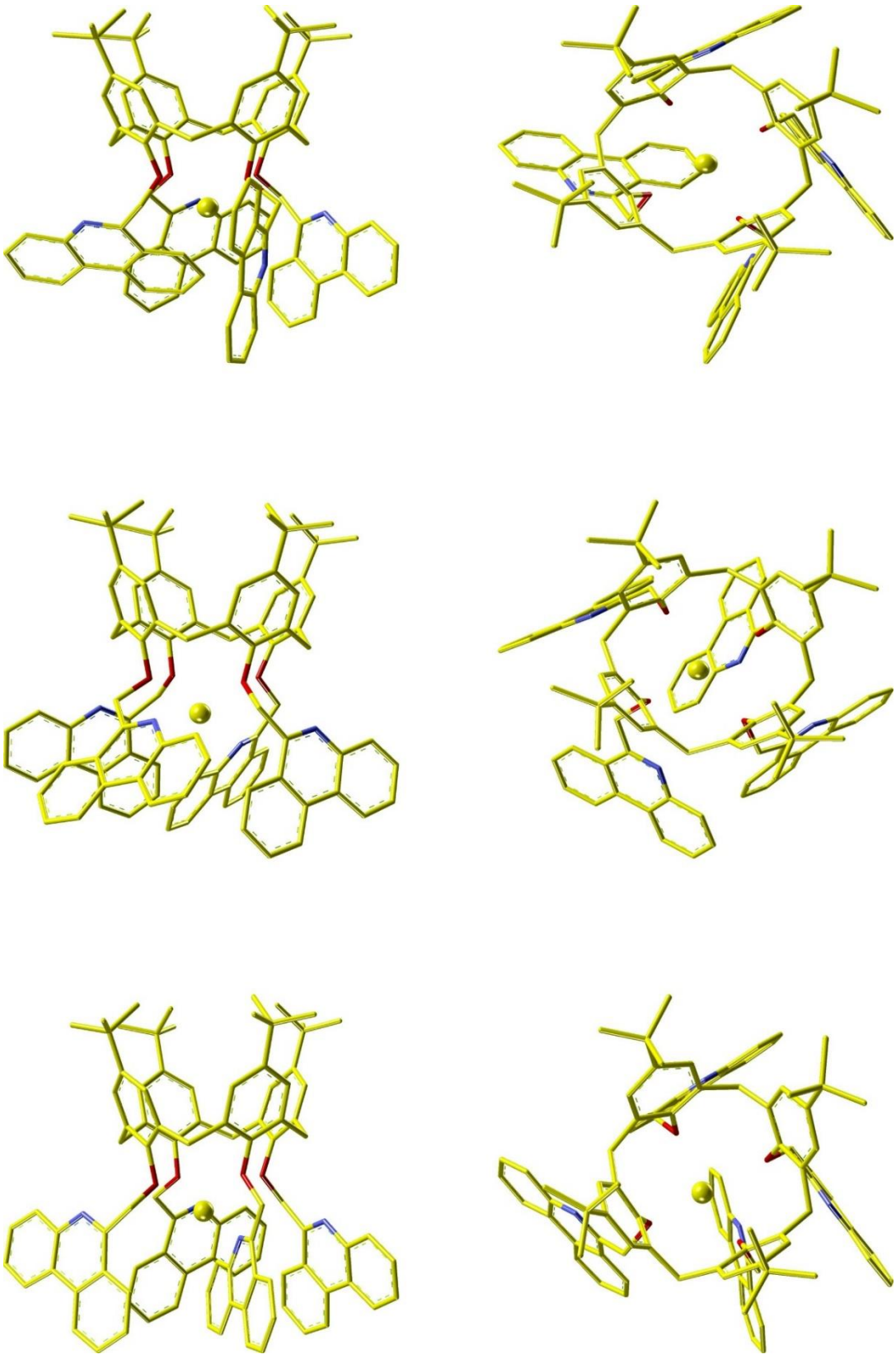

Figure S69. Other conformers of **1** with Na^+ obtained by 8D PES scan. Hydrogen atoms are omitted for clarity.